UNIVERSITY OF CALIFORNIA
Santa Barbara

Scalable Graph Algorithms in a High-Level Language Using Primitives Inspired by Linear Algebra

A Dissertation submitted in partial satisfaction
of the requirements for the degree of

Doctor of Philosophy

in

Computer Science

by

Adam Lugowski

Committee in Charge:

Professor John R. Gilbert, Chair

Professor Ben Zhao

Professor Xifeng Yan

September 2014

The Dissertation of
Adam Lugowski is approved:

Professor Ben Zhao

Professor Xifeng Yan

Professor John R. Gilbert, Committee Chairperson

September 2014

Scalable Graph Algorithms in a High-Level Language Using Primitives Inspired by Linear Algebra

by

Adam Lugowski

To my supportive parents and Nupur.

Acknowledgements

I'm very grateful to be able to do my dissertation work at a great institution like UCSB.

I'd especially like to thank my advisor, John Gilbert. His patience and superb mentorship taught me the art and science of research. His masterful command of the English language taught me the value of good presentation. I'm also grateful for his willingness to mark up endless drafts of papers and theses with his signature purple pen.

I also wish to thank my committee, Ben Zhao and Xifeng Yan. They have provided me with valuable feedback that helped guide my research in the right direction.

Many thanks also go to Aydın Buluç, who provided me with a great base to work from, and for his ongoing support in making the KDT project possible. Similarly, I want to thank Steve Reinhardt for his collaboration on KDT. His insights, patience, and skill were invaluable on the KDT project. I owe a debt to Shoaib Kamil and Armando Fox, for bringing their insights, direction, code, and ideas to make the KDT and SEJITS integration work possible.

I also wish to thank Leonid Oliker, Sam Williams, and Aydın Buluç for giving me the opportunity to intern at Lawrence Berkeley National Lab. It's an honor to work on our projects at that prestigious institution.

The help of David Mizell, Steve Reinhardt and my labmate Kevin Deweese were instrumental in making our iterative algorithm in SPARQL work possible.

Research is a group effort; in that vein the lab discussions, collaborations, and general support from my current and former lab mates proved invaluable. I thank Aydın, Varad Deshmukh, Kevin Deweese, Veronika Strnadova, Victor Amelkin, and Viral Shah for that.

Many people also helped with the less visible tasks that made my dissertation work possible. I wish to thank Paul Weakliem, Jason Riedy, Stefan Boeriu, and the staff at NERSC for help in getting access to the various machines that my work benefitted from. I'd also like to thank the fine staff from the Computer Science department office for making the administrative tasks so easy.

Finally I wish to thank my fellow graduate students for making these years such a joy.

Curriculum Vitæ

Adam Lugowski

Education

2012	Master of Science in Computer Science, UC Santa Barbara
2006	Bachelor of Science in Computer Science and Mathematics, Purdue University

Experience

2009-2014	Graduate Research Assistant, UC Santa Barbara
2012	Summer Intern, Lawrence Berkeley National Labs
2005	Interns for Indiana (IFI) intern, Seyet LLC
2005	Interns for Indiana (IFI) intern, Vasc-Alert LLC
2004	Intern, Caterpillar Inc.
2003-2004	Intern, Delphi-Delco Verification Lab
2003	Undergraduate TA, Purdue University
2001-2003	Intern, Micro Data Base Systems

Selected Publications

Adam Lugowski, David Alber, Aydõn BuluƆ, John R Gilbert, Steve Reinhardt, Yun Teng and Andrew Waranis: "A Flexible

Open-Source Toolbox for Scalable Complex Graph Analysis", In *Proceedings of the Twelfth SIAM International Conference on Data Mining (SDM12)*, April 2012.

Adam Lugowski, Aydõn BuluƆ, John Gilbert and Steve Reinhardt: "Scalable Complex Graph Analysis with the Knowledge Discovery Toolbox", In *IEEE International Conference on Acoustics, Speech, and Signal Processing (ICASSP)*, March 2012.

Aydõn BuluƆ, Erika Duriakova, Armando Fox, John R Gilbert, Shoaib Kamil, Adam Lugowski, Leonid Oliker and Samuel Williams: "High-Productivity and High-Performance Analysis of Filtered Semantic Graphs", In *27th IEEE International Symposium on Parallel and Distributed Processing (IPDPS 2013)*, May 2013.

Kevin Deweese, John R Gilbert, Adam Lugowski and Steve Reinhardt: "Graph Clustering in SPARQL", In *SIAM Workshop on Network Science*, 2013.

Robert W. Techentin, Barry K. Gilbert, Adam Lugowski, Kevin Deweese, John R. Gilbert, Eric Dull, Mike Hinchey, Steven P. Reinhardt: "Implementing Iterative Algorithms with SPARQL", In *EDBT/ICDT Workshops*, 2014.

Adam Lugowski, John R Gilbert: “Efficient Sparse Matrix-Matrix Multiplication on Multicore Architectures", In *Sixth SIAM Workshop on Combinatorial Scientific Computing (CSC14)*, July 2014.

Adam Lugowski, Shoaib Kamil, Aydõn BuluƋ, Samuel Williams, Erika Duriakova, Leonid Oliker, Armando Fox, John R. Gilbert: “Parallel Processing of Filtered Queries in Attributed Semantic Graphs", Accepted to *JPDC*.

Abstract

Scalable Graph Algorithms in a High-Level Language Using Primitives Inspired by Linear Algebra

Adam Lugowski

This dissertation advances the state of the art for scalable high-performance graph analytics and data mining using the language of linear algebra. Many graph computations suffer poor scalability due to their irregular nature and low operational intensity. A small but powerful set of linear algebra primitives that specifically target graph and data mining applications can expose sufficient coarse-grained parallelism to scale to thousands of processors.

In this dissertation we advance existing distributed memory approaches in two important ways. First, we observe that data scientists and domain experts know their analysis and mining problems well, but suffer from little HPC experience. We describe a system that presents the user with a clean API in a high-level language that scales from a laptop to a supercomputer with thousands of cores. We utilize a Domain-Specific Embedded Language with Selective Just-In-Time Specialization to ensure a negligible performance impact over the original distributed memory low-level code. The high-level language enables ease of use, rapid prototyping, and additional features such as on-the-fly filtering, runtime-defined objects, and exposure to a large set of third-party visualization packages.

The second important advance is a new sparse matrix data structure and set of algorithms. We note that shared memory machines are dominant both in stand-alone form and as nodes in distributed memory clusters. This thesis offers the design of a new sparse-matrix data structure and set of parallel algorithms, a reusable implementation in shared memory, and a performance evaluation that shows significant speed and memory usage improvements over competing packages. Our method also offers features such as in-memory compression, a low-cost transpose, and chained primitives that do not materialize the entire intermediate result at any one time. We focus on a scalable, generalized, sparse matrix-matrix multiplication algorithm. This primitive is used extensively in many graph algorithms such as betweenness centrality, graph clustering, graph contraction, and subgraph extraction.

Professor John R. Gilbert
Dissertation Committee Chair

Contents

List of Figures

List of Tables

Chapter 1

Introduction

Analysis of very large graphs has become indispensable in fields ranging from genomics and biomedicine to financial services, marketing, national security, and many others. In many applications the requirements are moving beyond relatively simple filtering and aggregation queries to complex graph algorithms involving clustering, shortest-path searches, centrality, and so on. These complex graph algorithms typically require high-performance computing resources to be feasible on large graphs. However, users and developers of complex graph algorithms are hampered by the lack of a flexible, scalable, reusable infrastructure for high-performance computational graph analytics.

In this thesis we show that high performance computation on very large graphs is enabled by efficient implementations of interfaces to algebraic primitives.

1.1 The Landscape of Graph Analytics

Many packages have answered the call for an HPC graph analysis toolkit. Their approaches, scalability, and applicability vary significantly.

Pregel [78] wraps the "think like a vertex" principle in a bulk synchronous model. In each iteration a vertex may send and receive messages to and from other vertices, perform computation, and vote whether to halt. Pregel is an internal Google project built with massive scale and fault-tolerance in mind. Giraph [7] is an open source counterpart.

GraphLab [69] also follows the "think like a vertex" style. Users write vertex code in a domain-specific language (DSL), while GraphLab handles the distribution between nodes and the parallelism. GraphLab is targeted at iterative sparse graph algorithms in the machine learning domain.

LEMON [33] is a C++ template library that supplies graph concepts, methods that operate on those concepts, and pre-made complete algorithms. LEMON is powerful and is easy to learn, but it is purely sequential.

Java Universal Network/Graph framework (JUNG) [87] is a very flexible Java graph library whose healthy set of algorithms and visualization tools make it a good prototyping platform.

The sequential Boost Graph Library (BGL) [100] takes its inspiration from the Standard Template Library. BGL recognizes that there is no one-size-fits-all graph data structure, so it provides a variety of containers and algorithms that work on abstract containers. The Parallel Boost Graph Library (PBGL) [50] is a distributed memory extension of BGL that retains the latter's large algorithm library by building distributed variants of BGL's containers.

Pegasus [55] is a package built on top of MapReduce that uses a primitive similar to matrix-vector multiplication, called `GIM-V`. This primitive expresses vertex-centered computations that combine data from neighboring edges and vertices. Pegasus is a good fit when the graph is extracted from a MapReduce cloud, at the cost of MapReduce's significant overhead.

The MultiThreaded Graph Library (MTGL) [14] follows a design similar to the PBGL, but with kernels written to take advantage of the massively multithreaded Cray ThreadStorm processors used in the Cray XMT and Urika systems. The MTGL introduces extremely parallel methods to traverse graphs which work very well on the XMT, but may not translate to more conventional machines.

YarcData's Urika [112] is a ThreadStorm-based dedicated SPARQL appliance that provides a SQL-like query interface to search for patterns in very large graphs. Urika takes advantage of the unique abilities of its processor to handle queries that are very inefficient on conventional hardware.

1.2 Graph Algorithms in the Language of Linear Algebra

Our work builds on the idea that linear-algebraic primitives provide a strong foundation for scalable parallel graph algorithms.

Many traditional approaches to graph description and computation result in algorithms that are limited by memory latency, with many cache misses and low computational intensity. In contrast, the definitions of linear algebraic operations provide natural paths to both partitioning of data and parallelizing computation. More importantly, the well-structured data access patterns of linear algebraic primitives allow code that is limited by bandwidth rather than latency [57].

The list of graph algorithms that have been implemented with linear algebraic primitives is long. It includes breadth first search [57], betweenness centrality [24], shortest paths and spanning trees [57], peer pressure clustering [57], PageRank [88], maximal independent set [57] (by variation of Luby's algorithm [71]), graph contraction [57], triangle counting [44], and triangle enumeration [45].

Formally, matrix and vector operations involve linear algebra over a semiring [46]. The most familiar semiring is the field of real numbers with the operations $(+, \times)$, but there are many others. The choice of semiring is important to the implemen-

tation of graph algorithms in linear algebra. Some formulations use the $(+, \times)$ semiring, some use the tropical $(min, +)$, some use others.

Since graphs are rarely complete, *sparse* data structures and algorithms are used to represent what is abstractly a 2-D adjacency array. We distinguish between a sparse *matrix* (which is an algebraic object) and a sparse *array* (which is a data structure). A sparse matrix algorithm can be implemented using a sparse array, but a sparse array does not require existence of an explicit identity element and allows mixing different semirings on the same data structure.

1.3 Outline of Thesis

The remaining chapters cover five significant contributions.

In Chapter 2, we describe the motivation for and architecture of the Knowledge Discovery Toolbox (KDT) [72]. KDT's main goal is to expose a scalable high-performance infrastructure to *Domain Experts*, that is, people familiar with a particular applied problem but who are not skilled high-performance computing (HPC) programmers. Thus KDT has three main layers targeted at three distinct groups. The foundation is laid by *HPC Experts* who are able to write scalable and flexible primitives in a high-performance language. *Algorithm Experts* craft

algorithms using the exposed primitives in a high-productivity language. Finally, *Domain Experts* use the algorithms to solve their problems.

Attributed semantic graphs are important in many workloads [**?**], but are difficult to express in traditional linear algebraic packages. In Chapter 3 we describe KDT's support for user-defined attributes, and the design of a powerful, flexible, and computationally inexpensive on-the-fly graph filtering system built on predicates.

KDT's primitive functions are customizable through a callback mechanism that enables user-defined semirings and filter predicates, among many other uses. Like the rest of KDT user code, these callbacks are written in a high-productivity language. In Chapter 4 we describe our method to ensure that callbacks are not a performance bottleneck.

In Chapter 5 we describe a new sparse matrix data structure called QuadMat, and a shared-memory parallel sparse matrix-sparse matrix multiplication algorithm. Sparse matrix multiplication forms the foundation of many graph algorithms, but this work also has applications that go beyond graph algorithms.

SPARQL, as implemented in the Urika appliance, provides a very effective way to perform local queries, while linear algebraic algorithms are particularly well suited to calculating global metrics. In Chapter 6 we explore a method to compute a global metric, PeerPressure clustering, using SPARQL as the underlying engine.

Chapter 2

Basic Architecture of the Knowledge Discovery Toolbox

This chapter is based on a paper published in SDM'12 [72].

2.1 Introduction

This chapter provides an introduction to the Knowledge Discovery Toolbox, its architecture, and how it is meant to be used.

In many applications, the requirements for analysis of large graphs are moving beyond relatively simple filtering and aggregation queries to complex graph algorithms involving clustering (which may depend on machine learning methods), shortest-path computations, and so on. These complex graph algorithms typically require high-performance computing resources to be feasible on large graphs. However, users and developers of complex graph algorithms are hampered by the lack

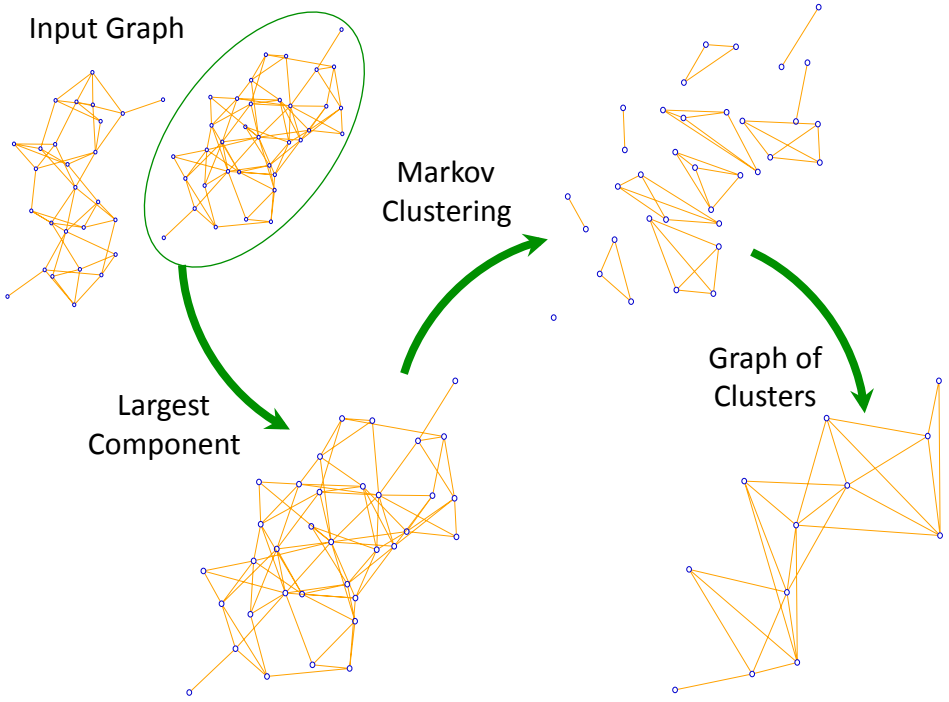

Figure 2.1: An example graph analysis mini-workflow in KDT.

of a flexible, scalable, reusable infrastructure for high-performance computational graph analytics.

Our Knowledge Discovery Toolbox (KDT) is the first package that combines ease of use for domain (or subject-matter) experts, scalability on large HPC clusters where many domain scientists run their large scale experiments, and extensibility for graph algorithm developers. KDT addresses the needs both of graph analytics users (who are not expert in algorithms or high-performance computing) and of graph analytics researchers (who are developing algorithms and/or tools for graph analysis). KDT is an open-source, flexible, reusable infrastructure that

implements a set of key graph operations with excellent performance on standard computing hardware.

The principal contribution of this chapter is the introduction of a graph analysis package which is useful to domain experts and algorithm designers alike. Graph analysis packages that are entirely written in very-high level languages such as Python perform poorly. On the other hand, simply wrapping an existing high-performance package into a higher level language impedes user productivity because it exposes the underlying package's lower-level abstractions that were intentionally optimized for speed.

KDT uses high-performance kernels from the Combinatorial BLAS [24]; but KDT is a great deal more than just a Python wrapper for a high-performance backend library. Instead it is a higher-level library with real graph primitives that does not require knowledge of how to map graph operations to a low-level high performance language (linear algebra in our case). It uses a distributed memory framework to scale from a laptop to a supercomputer consisting of hundreds of nodes. It is highly customizable to fit users' problems.

Our design activates a virtuous cycle between algorithm developers and domain experts. High-level domain experts create demand for algorithm implementations while lower-level algorithm designers are provided with a user base for their code. Domain experts use graph abstractions and existing routines to develop new ap-

```
# the variable bigG contains the input graph
# find and select the giant component
comp = bigG.connComp()
giantComp = comp.hist().argmax()
G = bigG.subgraph(mask=(comp==giantComp))

# cluster the graph
clus = G.cluster('Markov')

# get per-cluster stats, if desired
clusNvert = G.nvert(clus)
clusNedge = G.nedge(clus)

# contract the clusters
smallG = G.contract(clusterParents=clus)
```

Figure 2.2: KDT code implementing the mini-workflow illustrated in Figure 2.1.

plications quickly. Algorithm researchers build new algorithm implementations based on a robust set of primitives and abstractions, including graphs, dense and sparse vectors, and sparse matrices, all of which may be distributed across the memory of multiple nodes of an HPC cluster.

Figure 2.1 is a snapshot of a sample KDT workflow (described in more detail in Section 2.4.7). First we locate the largest connected component of the graph; then we divide this "giant" component of the graph into clusters of closely-related vertices; we contract the clusters into supervertices; and finally we perform a detailed structural analysis on the graph of supervertices. Figure 2.2 shows the actual KDT Python code that implements this workflow.

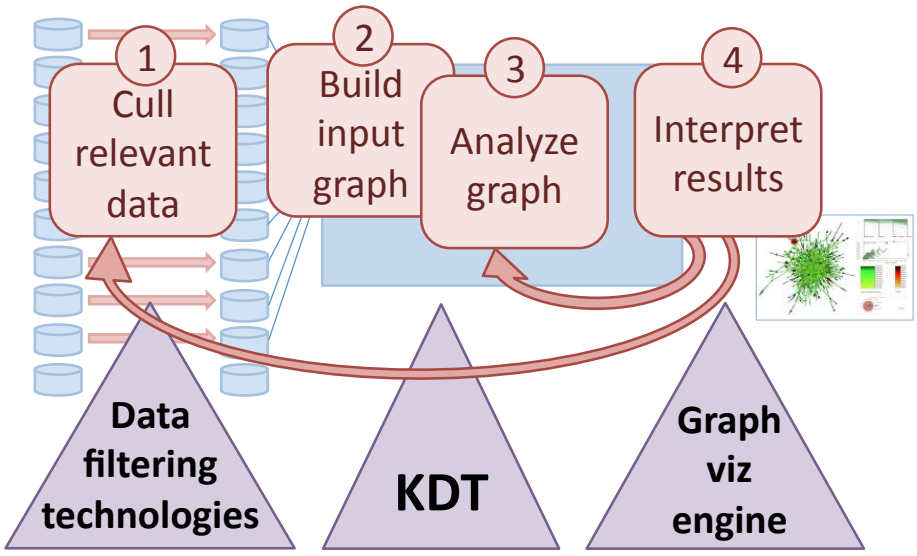

Figure 2.3: A notional iterative analytic workflow, in which KDT is used to build the graph and perform the complex analysis at steps 2 and 3.

The remainder of this chapter is organized as follows. Section 2.2 highlights KDT's goals and how it fits into a graph analysis workflow. Section 2.3 covers projects related to our work. We provide examples and performance comparisons in Section 2.4. The high-level language interface is described in Section 2.5 followed by an overview of our back-end in Section 2.6. Finally we summarize our contribution in Section 2.7.

2.2 Architecture and Context

A repeated theme in discussions with likely user communities for complex graph analysis is that the domain expert analyzing a graph often does not know in advance exactly what questions he or she wants to ask of the data. Therefore, support for interactive trial-and-error use is essential.

Figure 2.3 sketches a high-level analytical workflow that consists of (1) culling possibly relevant data from a data store (possibly disk files, a distributed database, or streaming data) and cleansing it; (2) constructing the graph; (3) performing complex analysis of the graph; and (4) interpreting key portions or subgraphs of the result graph. Based on the results of step 4, the user may finish, loop back to step 3 to analyze the same data differently, or loop back to step 1 to select other data to analyze.

KDT introduces only a few core concepts to ease adoption by domain experts. The top layer in Figure 2.4 shows these; a central graph abstraction and high-level graph methods such as `cluster` and `centrality`. Domain experts compose these to construct compact, expressive workflows via KDT's Python API. Exploratory analyses are supported by a menu of different algorithms for each of these core methods (*e.g.*, Markov and eventually spectral and k-means algorithms for clustering). Good characterizations of each algorithm's fitness for various types of

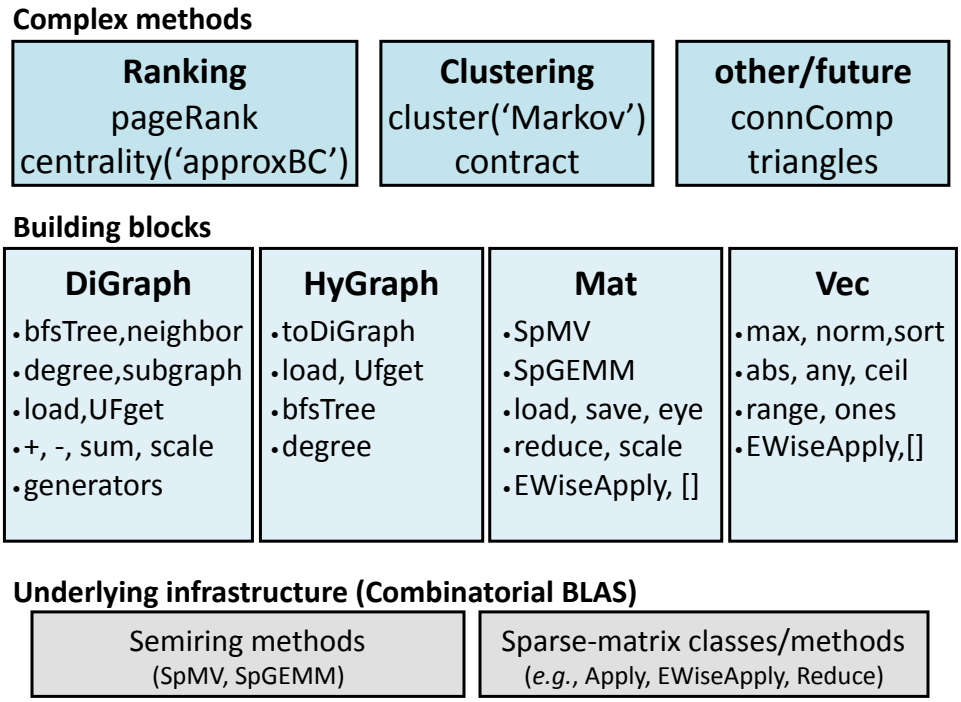

Figure 2.4: The architecture of Knowledge Discovery Toolbox. The top-layer methods are primarily used by domain experts, and include `centrality` and `cluster` for semantic graphs. The middle-layer methods are primarily used by graph-algorithm developers to implement the top-layer methods. KDT is layered on top of Combinatorial BLAS.

very large data are rare and so most target users will not know in advance which algorithms will work well for their data. We expect the set of high-level methods to evolve over time.

The high-level methods are supported by a small number of carefully chosen building blocks. KDT is targeted to analyze large graphs for which parallel execu-

tion in distributed memory is vital, so its primitives are tailored to work on entire collections of vertices and edges. As the middle layer in Figure 2.4 illustrates, these include directed graphs (`DiGraph`), hypergraphs (`HyGraph`), and matrices and vectors (`Mat`, `Vec`). The building blocks support lower-level graph and sparse matrix methods (for example, `degree`, `bfsTree`, and `SpGEMM`). This is the level at which the graph algorithm developer or researcher programs KDT.

Our current computational engine is Combinatorial BLAS [24] (shortened to CombBLAS), which gives excellent and highly scalable performance on distributed-memory HPC clusters. It forms the bottom layer of our software stack.

Knowledge discovery is a new and rapidly changing field, so KDT's architecture fosters extensibility. For example, a new clustering algorithm can easily be added to the `cluster` routine, reusing most of the existing interface. This makes it easy for the user to adopt a new algorithm merely by changing the `algorithm` argument. Since KDT is open-source (available at `http://kdt.sourceforge.net`), algorithm researchers can look at existing methods to understand implementation details, to tweak algorithms for their specific needs, or to guide the development of new methods.

2.3 Related Work

KDT combines a high-level language environment, to make both domain users and algorithm developers more productive, with a high-performance computational engine to allow scaling to massive graphs. Several other research systems provide some of these features, though we believe that KDT is the first to integrate them all.

Titan [103] is a component-based pipeline architecture for ingestion, processing, and visualization of informatics data that can be coupled to various high-performance computing platforms. Pegasus [55] is a graph-analysis package that uses MapReduce [31] in a distributed-computing setting. Pegasus uses a generalized sparse matrix-vector multiplication primitive called `GIM-V`, much like KDT's `SpMV`, to express vertex-centered computations that combine data from neighboring edges and vertices. This style of programming is called "think like a vertex" in Pregel [78], a distributed-computing graph API. In traditional scientific computing terminology, these are all BLAS-2 level operations; neither Pegasus nor Pregel currently includes KDT's BLAS-3 level `SpGEMM` "friends of friends" primitive. BLAS-3 operations are higher level primitives that enable more optimizations and generally deliver superior performance. Pregel's C++ API targets efficiency-

layer programmers, a different audience than the non-parallel-computing-expert domain experts (scientists and analysts) targeted by KDT.

Libraries for high-performance computation on large-scale graphs include the Parallel Boost Graph Library [50], the Combinatorial BLAS [24], and the Multithreaded Graph Library [14]. All of these libraries target efficiency-layer programmers, with lower-level language bindings and more explicit control over primitives.

GraphLab [69] is an example of an application-specific system for parallel graph computing, in the domain of machine learning algorithms. Unlike KDT, GraphLab runs only on shared-memory architectures.

2.4 Examples of use

In this section, we describe experiences using the KDT abstractions as graph-analytic researchers, implementing complex algorithms intended as part of KDT itself (breadth-first search, betweenness centrality, PageRank, Gaussian belief propagation, and Markov clustering), and as graph-analytic users, implementing a mini-workflow.

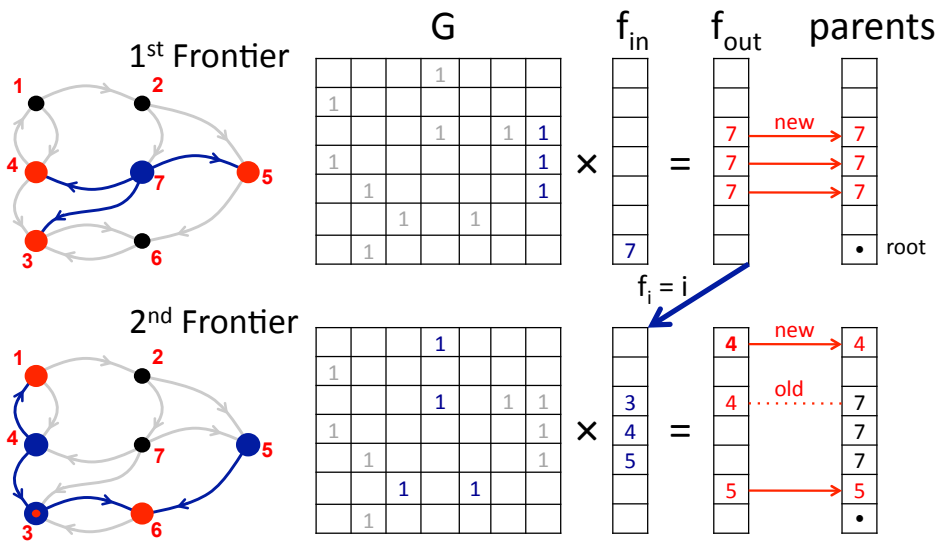

Figure 2.5: Two steps of breadth-first search, starting from vertex 7, using sparse matrix-sparse vector multiplication with "max" in place of "+".

2.4.1 Breadth-First Search

An algebraic implementation of BFS

Breadth-first search (BFS) is a building block of many graph computations, from connected components to maximum flows, route planning, and web crawling and analysis [47, 86]. BFS explores a graph starting from a specific vertex, identifying the "frontiers" consisting of vertices that can be reached by paths of 1, 2, 3, ... edges. BFS also computes a spanning tree, in which each vertex in one frontier has a parent vertex from the previous frontier.

In computing the next frontier from the current one, BFS explores all the edges out of the current frontier vertices. For a directed simple graph this is the same computational pattern as multiplying a sparse matrix (the transpose of the graph's adjacency matrix) by a sparse vector (whose nonzeros mark the current frontier vertices). The example in Figure 2.5 discovers the first two frontiers `f` from vertex 7 via matrix-vector multiplication with the transposed adjacency matrix G, and computes the parent of each vertex reached. `SpMV` is KDT's matrix-vector multiplication primitive.

Notice that while the structure of the computation is that of matrix-vector multiplication, the actual "scalar" operations are selection operations not addition and multiplication of real numbers. Formally speaking, the computation is done in a semiring different from $(+, \times)$. The `SpMV` user specifies the operations used to combine edge and vertex data; the computational engine then organizes the operations efficiently according to the primitive's well-defined memory access pattern.

It is often useful to perform BFS from multiple vertices at the same time. This can be accomplished in KDT by "batching" the sparse vectors for the searches into a single sparse matrix and using the sparse matrix-matrix multiplication primitive `SpGEMM` to advance all searches together. Batching exposes three levels of potential parallelism: across multiple searches (columns of the batched matrix);

across multiple frontier vertices in each search (rows of the batched matrix or columns of the transposed adjacency matrix); and across multiple edges out of a single high-degree frontier vertex (rows of the transposed adjacency matrix). The Combinatorial BLAS `SpGEMM` implementation exploits all three levels of parallelism when appropriate.

The Graph500 Benchmark

The intent of the Graph500 benchmark [49] is to rank computer systems by their capability for basic graph analysis just as the Top500 list [83] ranks systems by capability for floating-point numerical computation. The benchmark measures the speed of a computer performing a BFS on a specified input graph in *traversed edges per second* (TEPS). The benchmark graph is a synthetic undirected graph with vertex degrees approximating a power law, generated by the RMAT [66] algorithm. The size of the benchmark graph is measured by its *scale*, the base-2 logarithm of the number of vertices; the number of edges is about 16 times the number of vertices. The RMAT generation parameters are $a = 0.59, b = c = 0.19, d = 0.05$, resulting in graphs with highly skewed degree distributions and a low diameter. We symmetrize the input to model undirected graphs, but we only count the edges traversed in the original graph for TEPS calculation, despite visiting the symmetric edges as well.

We have implemented the Graph500 code in KDT, including the parallel graph generator, the BFS itself, and the validation required by the benchmark specification. Per the spec, the validation consists of a set of consistency checks of the BFS spanning tree. The checks verify that the tree spans an entire connected component of the graph, that the tree has no cycles, that tree edges connect vertices whose BFS levels differ by exactly one, and that every edge in the connected component has endpoints whose BFS levels differ by at most one. All of these checks are simple to perform with KDT's elementwise operators and `SpMV`.

Figure 2.6 gives Graph500 TEPS scores for both KDT and for a custom C++ code that calls the Combinatorial BLAS engine directly. Both runs are performed on the Hopper machine at NERSC, which is a Cray XE6. Each XE6 node has two twelve-core 2.1 Ghz AMD Opteron processors, connected to the Cray Gemini interconnect. The C++ portions of KDT are compiled with GNU C++ compiler v4.5, and the Python interpreter is version 2.7. We utilized all the cores in each node during the experiments. In other words, an experiment on p cores ran on $\lceil p/24 \rceil$ nodes. The two-dimensional parallel BFS algorithm used by Combinatorial BLAS is detailed elsewhere [26].

We see that KDT introduces negligible overhead; its performance is identical to CombBLAS, up to small discrepancies that are artifacts of the network partition granted to the job. The absolute TEPS scores are competitive; the purpose-built

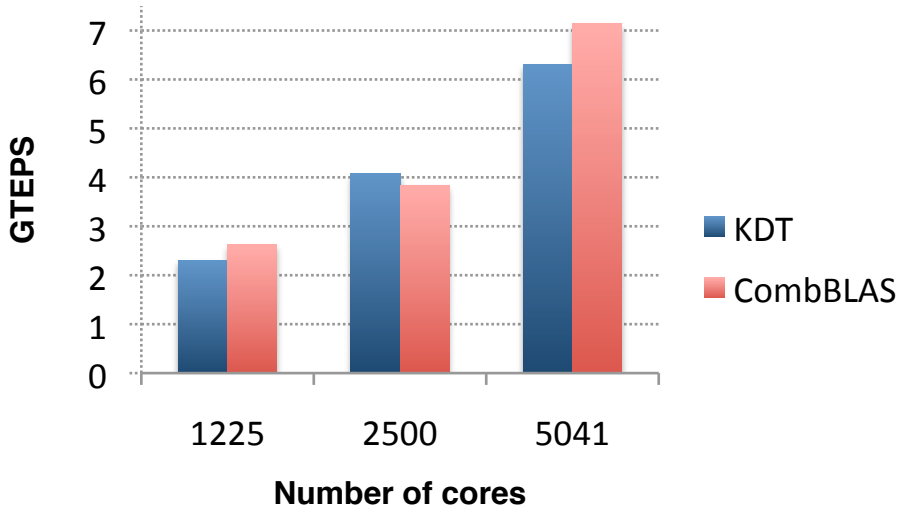

Figure 2.6: Speed comparison of the KDT and pure CombBLAS implementations of Graph500. BFS was performed on a scale 29 input graph with 500M vertices and 8B edges. The units on the vertical axis are GigaTEPS, or 10^9 traversed edges per second. The small discrepancies between KDT and CombBLAS are largely artifacts of the network partition granted to the job. KDT's overhead is negligible.

application used for the official June 2011 Graph500 submission for NERSC's Hopper has a TEPS rating about 4 times higher (using 8 times more cores), while KDT is reusable for a variety of graph-analytic workflows.

We compare KDT's BFS against a PBGL BFS implementation in two environments. Neumann is a shared memory machine composed of eight quad-core AMD Opteron 8378 processors. It used version 1.47 of the Boost library, Python 2.4.3, and both PBGL and KDT were compiled with GCC 4.1.2. Carver is an IBM iDataPlex system with 400 compute nodes, each node having two quad-core Intel Nehalem processors. Carver used version 1.45 of the Boost library, Python 2.7.1, and both codes were compiled with Intel C++ compiler version 11.1. The test data consists of scale 19 to 24 RMAT graphs. We did not use Hopper in these experiments as PBGL failed to compile on the Cray platform.

The comparison results are presented in Figure 2.7. We observe that on this example KDT is significantly faster than PBGL both in shared and distributed memory, and that in distributed memory KDT exhibits robust scaling with increasing processor count.

2.4.2 Betweenness Centrality

Betweenness centrality (BC) [39] is a widely accepted importance measure for the vertices of a graph, where a vertex is "important" if it lies on many shortest

Core Count (Machine)	Code	Problem Size		
		Scale 19	Scale 22	Scale 24
4 (Neumann)	PBGL	3.8	2.5	2.1
	KDT	8.9	7.2	6.4
16 (Neumann)	PBGL	8.9	6.3	5.9
	KDT	33.8	27.8	25.1
128 (Carver)	PBGL		25.9	39.4
	KDT		237.5	262.0
256 (Carver)	PBGL		22.4	37.5
	KDT		327.6	473.4

Figure 2.7: Performance comparison of KDT and PBGL breadth-first search. The reported numbers are in MegaTEPS, or 10^6 traversed edges per second. The graphs are Graph500 RMAT graphs as described in the text.

paths between other vertices. BC is a major kernel of the HPCS Scalable Synthetic Compact Applications graph analysis benchmark [9].

The definition of the betweenness centrality $C_B(v)$ of a vertex v is

$$C_B(v) = \sum_{s \neq v \neq t \in V} \frac{\sigma_{st}(v)}{\sigma_{st}}, \tag{2.1}$$

where σ_{st} is the number of shortest paths between vertices s and t, and $\sigma_{st}(v)$ is the number of those shortest paths that pass through v. Brandes [19] gave a sequential algorithm for BC that runs in $O(ne)$ time on an unweighted graph with n vertices and e edges. This algorithm uses a BFS from each vertex to find the frontiers and all shortest paths from that source, and then backtracks through the frontiers to update a sum of importance values at each vertex.

The quadratic running time of BC is prohibitive for large graphs, so one typically computes an approximate BC by performing BFS only from a sampled subset of vertices [10].

KDT implements both exact and approximate BC by a batched Brandes' algorithm. It constructs a batch of k BFS trees simultaneously by using the `SpGEMM` primitive on $n \times k$ matrices rather than k separate `SpMV` operations. The value of k is chosen based on problem size and available memory. The straightforward KDT code is able to exploit parallelism on all three levels: multiple BFS starts, multiple frontier vertices per BFS, and multiple edges per frontier vertex.

Figure 2.8 shows KDT's performance on calculating BC on RMAT graphs. Our inputs are RMAT matrices with the same parameters and sparsity as described in Graph500 experiments (Section 2.4.1). Since the running time of BC on undirected graphs is quadratic, we ran our experiments on smaller data sets, presenting strong scaling results up to 256 cores. We observe excellent scaling up to 64 cores, but speedup starts to degrade slowly after that. For 256 cores, we see speedup of 118 times compared to a serial run. For all the runs, we used an approximate BC with starting vertices composed of a 3% sample, and a batchsize of 768. This experiment was run on Hopper, utilizing all 24 cores in each node.

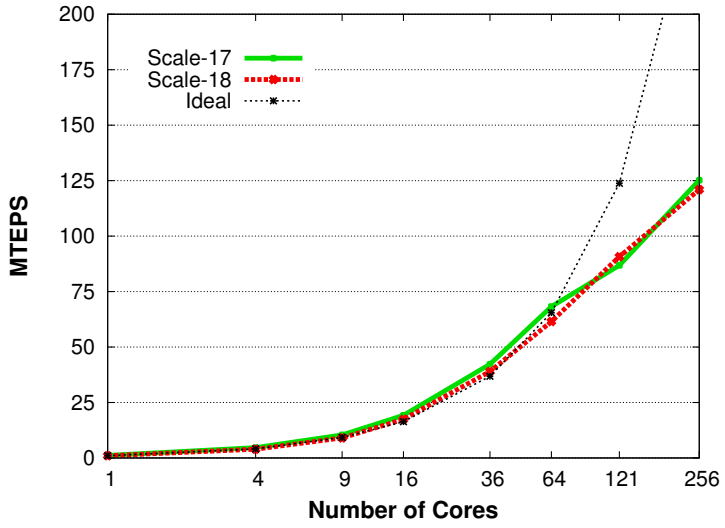

Figure 2.8: Performance of betweenness centrality in KDT on synthetic power-law graphs (see Section 2.4.1). The units on the vertical axis are MegaTEPS, or 10^6 traversed edges per second. The black line shows ideal linear scaling for the scale 18 graph. The x-axis is in logarithmic scale. Our current backend requires a square number of processors.

2.4.3 PageRank

PageRank [88] computes vertex relevance by modeling the actions of a "random surfer". At each vertex (*i.e.*, web page) the surfer either traverses a randomly-selected outbound edge (*i.e.*, link) of the current vertex, excluding self loops, or the surfer jumps to a randomly-selected vertex in the graph. The probability that the surfer chooses to traverse an outbound edge is controlled by the *damping factor*, d. A typical damping factor in practice is 0.85. The output of the algorithm is the probability of finding the surfer visiting a particular vertex at any moment, which is the stationary distribution of the Markov chain that describes the surfer's moves.

KDT computes PageRank by iterating the Markov chain, beginning by initializing vertex probabilities $P_0(v) = 1/n$ for all vertices v in the graph, where n is the number of vertices and the subscript denotes the iteration number. The algorithm updates the probabilities iteratively by computing

$$P_{k+1}(v) = \frac{1-d}{n} + d \sum_{u \in \mathrm{Adj}^-(v)} \frac{P_k(u)}{|\mathrm{Adj}^+(u)|}, \tag{2.2}$$

where $\mathrm{Adj}^-(u)$ and $\mathrm{Adj}^+(u)$ are the sets of inbound and outbound vertices adjacent to u. Vertices with no outbound edges are treated as if they link to all vertices.

After removing self loops from the graph, KDT evaluates (2.2) simultaneously for all vertices using the `SpMV` primitive. The iteration process stops when the

1-norm of the difference between consecutive iterates drops below a default or, if supplied, user-defined stopping threshold ϵ.

We compare the PageRank implementations which ship with KDT and Pegasus in Figure 2.9. The dataset is composed of scale 19 and 21 directed RMAT graphs with isolated vertices removed. The scale 19 graph contains 335K vertices and 15.5M edges, the scale 21 graph contains 1.25M vertices and 63.5M edges and the convergence criteria is $\epsilon = 10^{-7}$. The test machine is Neumann (a 32-core shared memory machine, same hardware and software configuration as in Section 2.4.1). We used Pegasus 2.0 running on Hadoop 0.20.204 and Sun JVM 1.6.0_13. We directly compare KDT core counts with maximum MapReduce task counts despite this giving Pegasus an advantage (each task typically shows between 110%-190% CPU utilization). We also observed that mounting the Hadoop Distributed Filesystem in a ramdisk provided Pegasus with a speed boost on the order of 30%. Despite these advantages we still see that KDT is two orders of magnitude faster.

Both implementations are fundamentally based on an SpMV operation, but Pegasus performs it via a MapReduce framework. MapReduce allows Pegasus to be able to handle huge graphs that do not fit in RAM. However, the penalty for this ability is the need to continually touch disk for every intermediate operation, parsing and writing intermediate data from/to strings, global sorts, and spawning

Core Count	Task Count	Code	Problem Size	
			Scale 19	Scale 21
–	4	Pegasus	2h 35m 10s	6h 06m 10s
4	–	KDT	55s	7m 12s
–	16	Pegasus	33m 09s	4h 40m 08s
16	–	KDT	13s	1m 34s

Figure 2.9: Performance comparison of KDT and Pegasus PageRank ($\epsilon = 10^{-7}$). The graphs are Graph500 RMAT graphs as described in Section 2.4.1. The machine is Neumann, a 32-core shared memory machine with HDFS mounted in a ramdisk.

and killing VMs. Our result illustrates that while MapReduce is useful for tasks that do not fit in memory, it suffers an enormous overhead for ones that do.

A comparison of the two codes also demonstrates KDT's user-friendliness. The Pegasus PageRank implementation is approximately 500 lines long. It is composed of three separate MapReduce stages and job management code. The Pegasus algorithm developer must be proficient with the MapReduce paradigm in addition to the GIM-V primitive. The KDT implementation is 30 lines of Python consisting of input checks and sanitization, initial value generation, and a loop around our SpMV primitive.

2.4.4 Belief Propagation

Belief Propagation (BP) is a so-called "message passing" algorithm for performing inference on graphical models such as Bayesian networks [113]. Graphical models are used extensively in machine learning, where each random variable is represented as a vertex and the conditional dependencies among random variables are represented as edges. BP calculates the approximate marginal distribution for each unobserved vertex, conditional on any observed vertices.

Gaussian Belief Propagation (GaBP) is a version of the BP algorithm in which the underlying distributions are modeled as Gaussian [15]. GaBP can be used to iteratively solve symmetric positive definite systems of linear equations $Ax = b$, and thus is a potential candidate for solving linear systems that arise within KDT. Although BP is applicable to much more general settings (and is not necessarily the method of choice for solving a linear equation system), GaBP is often used as a performance benchmark for BP implementations.

We implemented GaBP in KDT and used it to solve a steady-state thermal problem on an unstructured mesh. The algorithm converged after 11 iterations on the Schmid/thermal2 problem that has 1.2 million vertices and 8.5 million edges [29].

We demonstrate strong scaling using steady-state 2D heat dissipation problems in Figure 2.10. The $k \times k$ 2D grids yield graphs with k^2 vertices and $5k^2$ edges.

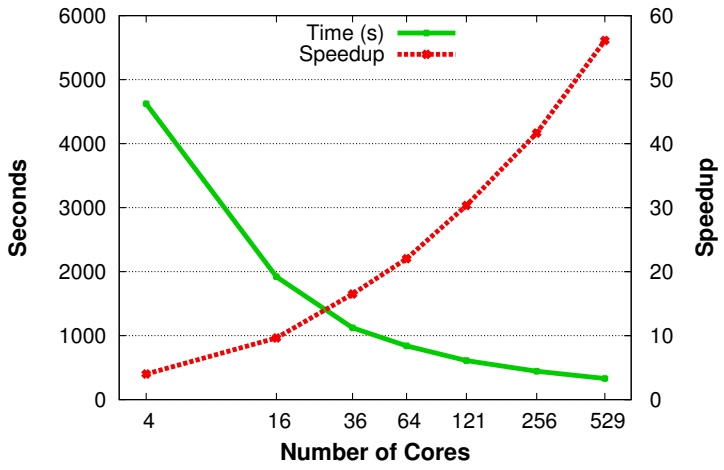

Figure 2.10: Performance of GaBP in KDT on solving a 500×500 structured mesh, steady-state, 2D heat dissipation problem (250K vertices, 1.25M edges). The algorithm took 400 iterations to converge to a relative norm $\leq 10^{-3}$. The speedup and timings are plotted on separate y-axes, and the x-axis is in logarithmic scale.

We observed linear scaling with increasing problem size and were able to solve a $k = 4000$ problem in 31 minutes on 256 cores. Parallel scaling is sub-linear because GaBP is an iterative algorithm with low arithmetic intensity which makes it bandwidth (to RAM) bound. The above experiments were run on Hopper, but we observed similar scaling on the Neumann shared memory machine.

We compared our GaBP implementation with GraphLab's GaBP on our shared memory system. The problem set was composed of structured and unstructured meshes ranging from hundreds of edges to millions. KDT's time to solution compared favorably with GraphLab on problems with more than 10,000 edges.

2.4.5 Markov Clustering

Markov Clustering (MCL) [105] is used in computational biology to discover the members of protein complexes [35, 20], in linguistics to separate the related word clusters of homonyms [34], and to find circles of trust in social network graphs [89, 82]. MCL finds clusters by postulating that a random walk that visits a dense cluster will probably visit many of its vertices before leaving.

The basic algorithm operates on the graph's adjacency matrix. It iterates a sequence of steps called expansion, inflation, normalization and pruning. The expansion step discovers friends-of-friends by raising the matrix to a power (typically 2). Inflation separates low- and high-weight edges by raising the individual matrix

elements to a power which can vary from about 2 to 20, higher values producing finer clusters. This has the effect of both strengthening flow inside clusters and weakening it between clusters. The matrix is scaled to be column-stochastic by a normalization step. The pruning step is one key to MCL's efficiency because it preserves sparsity. Our implementation prunes elements which fall below a threshold though other pruning strategies are possible. These steps are repeated until convergence, then the clusters are identified. The standard, and KDT's default, method is to identify the connected components of the pruned graph as clusters. The KDT Markov clustering method provides sensible defaults for all parameters and options, but allows the user to override them if desired.

2.4.6 Peer-Pressure Clustering

Peer Pressure is a clustering algorithm based on the observation that for a given graph clustering the cluster assignment of a vertex will be the same as that of most of its neighbors.

The algorithm starts with a base case of an initial cluster assignment, such as each vertex being in its own cluster. Each iteration performs an election at each vertex to select which cluster that vertex should belong to at the end of the iteration. The votes are the cluster assignments of its neighbors. Ties are settled by selecting the lowest cluster ID to maintain determinism, but can be

settled arbitrarily. The algorithm converges when two consecutive iterations have a (tunably) small difference between them.

This algorithm can take up to $O(\#\ of\ vertices)$ iterations in pathological cases, however it typically converges in a small number of iterations (on the order of five to ten) on well-clustered graphs.

This algorithm is also known by the name *Label Propagation* [92] in the physics literature. Boldi et. al. [16] extend that work with *Layered Label Propagation* which accepts a parameter γ which selects between large relatively sparse clusters and small relatively dense clusters.

RDF/SPARQL Implementation

Chapter **??** is about our Peer Pressure implementation in RDF/SPARQL for YarcData's uRiKA appliance.

2.4.7 Mini-workflow Example

End-to-end graph analysis workflows vary greatly between domains, between problems, and likely even between individual analysts; we do not attempt to describe them here. However, we can identify some smaller mini-workflows as being close enough to real workflows to serve as examples. One mini-workflow,

which users say is often applied to power-law graphs resulting from relationship analysis data, has the following steps:

1. Identify the "giant" or largest component
2. Extract the giant component from the graph
3. Find the clusters in the giant component
4. Collapse each cluster into a supervertex
5. Visualize the resulting graph of supervertices

For example, this mini-workflow could analyze Twitter data about politics starting with all people who subscribe to a set of political hash-tags, identifying those people who care strongly about an upcoming election, as evidenced by both sending and receiving political tweets (the giant component), and then clustering them into which candidate they associate with most closely. In KDT this is expressed by the Python code in Figure 2.2. This mini-workflow illustrates how the KDT methods are designed to work together in sequence. For example, the output of `cluster` (a vector of length equal to the number of vertices in the graph, with each element denoting the cluster in which that vertex resides) is in the same format expected by the `contract` function (which contracts all vertices with the same cluster-ID into a single vertex) and the vertex-partition form of the `nedge`

function. The output of this example workflow for a tiny input graph is illustrated in Figure 2.1.

2.5 High Level Language Interface

2.5.1 High Productivity for Graph Analysis

KDT targets a demanding environment – domain experts exploring novel very large graphs with hard-to-specify goals. Today this requires knowledge in so many domains that only the most talented, cross-disciplinary, and well-funded groups succeed. KDT aims not only to enable these (non-graph-expert) domain experts to analyze very large graphs quickly but also to accelerate the work of graph-algorithm researchers developing the next generation of algorithms attacking the inherent combinatorial wall of graph analysis.

KDT delivers high productivity to domain experts by limiting the number of new concepts and by providing powerful abstractions for both data and methods. For instance, the `DiGraph` class implements directed graphs for distributed memory, hiding the details of how the directed graph is represented in distributed memory. Similarly, KDT users use the `cluster` method to cluster a graph's vertices by an (initially brief) menu of algorithms. Detailed algorithm-specific options such as the expansion and inflation factors for Markov clustering default

to appropriate values for the typical user but enable more knowledgeable users to exercise more control if needed. Those wanting even more control are provided with methods that are too detailed for many domain experts. These include access to well optimized linear algebraic methods and additional graph methods such as `bfsTree` and `normalizeEdgeWeights`

Our experience implementing the primary methods of KDT may illustrate the productivity of this approach. One of us implemented exact betweenness centrality in Python using serial SciPy. Moving that code to run in a distributed parallel manner with KDT required changing the initial definitions of (*e.g.* variable arrays), but much of the core code (*e.g.* multiplying and adding intermediate matrices) did not change. The changes took only 11 hours of programming time for the BC routine itself. The resulting code runs correctly and scales effectively to hundreds of cores. Similarly, after initial explorations to understand the Markov Clustering algorithm and KDT well, an undergraduate student produced our Markov Clustering routine in only six hours.

2.5.2 Organization of the Fundamental Classes

KDT's productivity benefits extend beyond simply providing an opaque set of built-in graph algorithms. The provided set of algorithms also serve as guides for

users who want to implement their own graph algorithms based on our extensible primitives.

As Figure 2.4 illustrates, the `kdt` Python module exposes two types of classes: graph objects and their supporting linear algebraic objects. It includes classes representing directed graphs (`DiGraph`), hypergraphs (`HyGraph`), as well as sparse matrices (`Mat`) and sparse and dense vectors (`Vec`). Computation is performed using a set of pre-defined patterns:

- Matrix-Matrix multiplication (SpGEMM), Matrix-Vector multiplication (SpMV)
- Element-wise (EWiseApply)
- Querying operations (Count, Reduce, Find)
- Indexing and Assignment (SubsRef, SpAsgn)

These operations are the key to KDT's scalability. Each one is implemented for parallel execution and accepts user-defined callbacks that act similarly to visitors. The pre-defined access patterns allow considerable scalability and account for the bulk of processing time. This allows KDT code to appear serial yet have parallel semantics.

The sparse matrix and vector classes that support the graph classes are exposed to allow complex matrix analysis techniques (*e.g.*, spectral methods). Directed graphs are represented using an $n \times n$ sparse adjacency matrix. Hypergraphs

use an $n \times m$ rectangular incidence matrix. Note that bipartite graphs can also be represented with a hypergraph. A graph's edge attributes are represented as the matrix's element values while vertex attributes are stored in vectors of length matching the matrix dimension. KDT's matrices and vectors can be of several types including boolean for connectivity only, floating point, and custom objects.

User-defined callbacks can take several forms. KDT operations accept unary, binary and n-ary operations, predicates, and semiring functions. Each one may be a built-in function or a user-written Python callback or wrapped C routine for speed.

Taken together, these building blocks and finished algorithms provide KDT with a high degree of power and flexibility.

2.5.3 Semantic Graphs

Users found that the initial release of KDT lacked support for semantic graphs, *i.e.* graphs whose vertices and edges have types. Semantic graphs are valuable when data is of disparate types (*e.g.* link data about communication via email, Twitter, and Facebook) and considering different types of data together delivers better insight. The KDT semantic graph interface enables on the fly selection of vertices and edges via user-defined callbacks. Computations are only performed on selected vertices and edges. In some situations the graph is very large and the

user wants to select most of the graph, in which case materializing the selected graph is wasteful of memory; in other cases the user wants to select only a small portion of the graph, in which case materializing the smaller graph may be more efficient. The KDT semantic graph operations appear to be a dual for SQL's ability to push certain computations onto the database.

The subsequent KDT release (v0.2) defines the notion of a *filter*. A filter determines whether or not a particular vertex or edge is included in the computation. Our filter design relies on three basic principles.

1. A user-defined predicate determines whether or not a vertex or edge exists in the filtered graph.

2. Multiple user-defined predicates can be stacked and the filters they define are applied in the order they are added to the graph. Thus, both users and algorithm developers can use filters.

3. All graph operations respect the filter. This ensures that algorithms can be written without taking filters into consideration at all, thus greatly easing their design.

For example, assume that a graph contains link data about communication between employees via email, Twitter, and Facebook, and that a user wants to

```
def onlyEngineers(self):
    return self.position == Engineer

def onlyEmailTwitter(self):
    return self.type == email
        or self.type == Twitter

# the variable G contains the graph
G.addVFilter(onlyEngineers)
G.addEFilter(onlyEmailTwitter)
clus = G.cluster('Markov')
```

Figure 2.11: Clustering of a filtered semantic graph in KDT. The vertex- and edge-filters consist of predicates which are attached to the graph. They are invoked whenever the graph is traversed.

find clusters in the graph of engineers based on email and Twitter links. This could be implemented with filtered KDT semantic graphs using the code in Figure 2.11.

We expect the semantic-graph interface to evolve as we continue gathering feedback from KDT users.

2.6 HPC Computational Engines

2.6.1 Combinatorial BLAS

The Combinatorial BLAS [24] is a proposed standard for combinatorial computational kernels. It is a highly-templated C++ library which serves as the cur-

rent KDT backend. It offers a small set of linear algebraic kernels that can be used as building blocks for the most common graph-analytic algorithms. Graph abstractions can be built on top of its sparse matrices, taking advantage of its existing best practices for handling parallelism in sparse linear algebra. Its flexibility comes from the arbitrary operations that it supports. The user, or in this case the KDT implementor, specifies the `add` and `multiply` routines in matrix-matrix and matrix-vector operations, or unary and binary functions for element-wise operations. The main data structures are distributed sparse matrices and vectors, which are distributed in a two-dimensional processor grid for scalability.

We use the publicly available MPI reference implementation of the Combinatorial BLAS as our computational engine. We extended its interface in order to provide further capabilities, such as fully-distributed (to all the processors) sparse vectors, sparse matrix-sparse vector multiplication, and routines akin to MATLAB®'s `sparse` and `find`.

The primary KDT abstractions are different from Combinatorial BLAS abstractions. CombBLAS exposes distributed-memory dense and sparse vectors and sparse matrices and key operations on them, mostly linear algebra, required to implement combinatorial problems. KDT exposes graph abstractions such as directed graphs, and graph operations such as ranking vertices (e.g., betweenness centrality or PageRank), clustering, and finding neighbors within k hops of a set

of vertices; the underlying linear algebraic implementation is not immediately visible. This shift in abstractions between the linear-algebra worldview and the graph worldview is one of the primary contributions of KDT. It creates usability for domain experts while retaining performance and customizability.

2.6.2 Evolution of KDT

The design of KDT intentionally separates its user-level language and interface from its computational engine. This allows us to extend KDT easily along at least two axes: an architectural axis, and a capability axis.

On the architectural axis, we intend KDT to map readily to computational engines that provide the functionality of Combinatorial BLAS on different platforms. We and our collaborators are currently working on two such engines: one for manycore shared-address-space architectures, and one for more loosely coupled distributed-computing cloud architectures. We are also contemplating engines that will be able to use more specialized hardware, including GPUs, FPGAs, and massively multithreaded architectures like Cray XMT [58].

On the capability axis, we are extending the set of algorithms and primitives that underlie KDT in various ways. Numerical computational primitives such as linear equation solvers and spectral analysis (computing eigenvalues, singular values, eigenvectors, etc.) are useful in many data analysis settings, and fit naturally

into KDT's parallel sparse matrix paradigm. We are also exploring some other classes of graph primitives—for example, the visitor paradigm of the Boost Graph Library and its relatives [100, 62, 50, 14].

In many cases, enhancing KDT's capabilities means interfacing KDT to existing high-performance computational libraries; for example, an upcoming release of KDT is planned to include the numerical PARPACK library [79, 63] in its computational engine, and high-quality high-performance libraries for other numerical computations exist [68, 52, 56].

One of our goals is to use the KDT API as a high-level interface to other existing high-performance graph libraries (such as The MultiThreaded Graph Library [14] and Parallel Boost Graph Library [50]) and representations (such as STINGER [8]). We expect that KDT's high-level language interface will evolve to permit different graph libraries to be used as back ends; we view the current high-level Python specification as a starting point and we are actively soliciting feedback from users and developers to help us guide its evolution.

2.7 Conclusion

The Knowledge Discovery Toolbox makes truly scalable graph analysis accessible in a high-level language to both domain experts and developers of graph

analytics. The two key ingredients are a core set of graph abstractions (and accompanying Python API) providing flexibility and simplicity, and a high-performance computational back end providing scalable performance for graphs in excess of 10 billion edges on HPC clusters. KDT version 0.2, released in 2012, implements the core architecture, which are shown here to enable rapid development of both highly performant graph-analytic workflows and the underlying graph-analytic operations themselves. The performance of KDT approaches that of efficiency-level applications while being reusable for a variety of graph-analytic workflows. In current work, we are extending both KDT's capabilities and the range of hardware and software platforms on which it can be used.

Chapter 3

Attributed Semantic Graphs and Filters

This chapter is based on a paper published in ICASSP'12 [73].

3.1 Introduction

This chapter describes features of KDT that support graphs with attributes on both edges and vertices (so-called *semantic* graphs), the design of KDT's filtering mechanism, and how these changes meet the criteria of customizability and performance.

3.2 Semantic Graph Example

Consider the example of a social network where information is known about cell-phone calls and text messages. To understand the patterns of communication

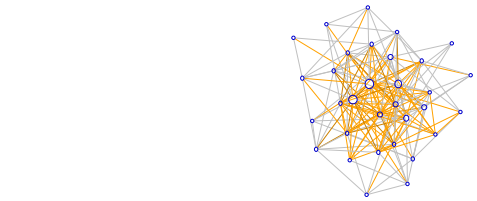

(a) all communications

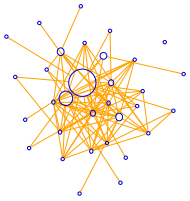

(b) only text messages

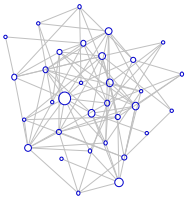

(c) only phone calls

Figure 3.1: Example of placing a filter on a graph. We compute betweenness centrality on a graph of communications consisting of both text messages and cell phone calls, then filter to only text messages or cell phone calls. A vertex's size indicates its normalized centrality score. Each filtered graph highlights different central nodes, leading to better understanding of communication patterns.

in the social network, an analyst may want to explore the graph by looking at each mode of communication separately, with any of the algorithms supported in KDT. For example, betweenness centrality [39] often gives insight into those people (vertices) who most connect the whole graph. Calculating betweenness centrality considering only phone calls, and then only text messages may give deeper insight than calculating betweenness centrality considering both communication modes

```
# the variable bigG contains the graph
# define the edge selection filter
def eFilter(self):
    return self.eType == eType

# for each edge type, calculate
# betweenness centrality
mList=(PhoneCall,TextMessage)
bigG.addEFilter(eFilter)
for eType in mList:
    bc = bigG.rank('approxBC')
    #visualize vertex centrality in graph composed of edges of only a single
        type

bigG.delEFilter(eFilter)
bc = bigG.rank('approxBC')
#visualize vertex centrality based on all edges
```

Figure 3.2: KDT code implementing the semantic-graph example described in Section 3.2. All filtering is done dynamically without creating any intermediaries.

simultaneously. Note that the latter is not simply a linear combination of the former two. Figure 3.1 provides an illustration. This can be implemented in KDT v0.2 with the code in Figure 3.2.

An important aspect of this example is that the filtered graphs (*e.g.* the graph of only text messages) are never materialized. The predicates used to filter the edges are applied on the fly, thus eliminating the need to create intermediaries. The edge filter predicate `eFilter` is attached to the graph by the `addEFilter` method, and then executed whenever edge traversing operations are invoked.

This example has analogues in life sciences, where the different edges might be protein-protein or protein-DNA interactions.

3.3 KDT Design

We build on our previous work on the Combinatorial BLAS (or CombBLAS for short) [24] by utilizing it as our initial backend. The CombBLAS is a proposed standard for combinatorial computational kernels. It is a highly-templated C++ library. It offers a small set of linear algebraic kernels that can be used as building blocks for the most common graph-analytic algorithms. Graph abstractions can be built on top of its sparse matrices, taking advantage of its existing best practices for handling parallelism in sparse linear algebra. Its flexibility comes from the arbitrary operations that it supports. The user, or in this case the KDT implementor, specifies the `add` and `multiply` routines in matrix-matrix and matrix-vector operations, or unary and binary functions for element-wise operations. The main data structures are distributed sparse matrices and vectors, which are distributed in a two-dimensional processor grid for scalability.

KDT transforms the linear algebra primitives into graph primitives. The graph's edges are collectively stored in a matrix, and vertex attributes are stored in a vector. Sparse matrix-vector multiplication (SpMV) and sparse matrix-matrix

multiplication (SpGEMM) become KDT's graph traversal primitives, where user code in the `add` and `multiply` semiring routines defines the function of the traversal. Element-wise operations become edge and vertex visitors. The main benefit of this approach is that traditional graph frameworks are latency-bound whereas linear algebra primitives are bandwidth bound. The latter is far more scalable.

Our first KDT release (described in Chapter 2) focused on providing key abstractions on data structures and algorithms (*e.g.* digraphs, rank, cluster) and the supporting infrastructure (vectors, matrices, Python bindings). Our goal was to be able to deliver our world-class CombBLAS performance with conceptual simplicity and user-friendly design. We did not focus on extending the graph abstractions; instead we supported only floating-point attributes on both vertices and edges.

The progression of capabilities of CombBLAS and KDT is illustrated in Figure 3.3.

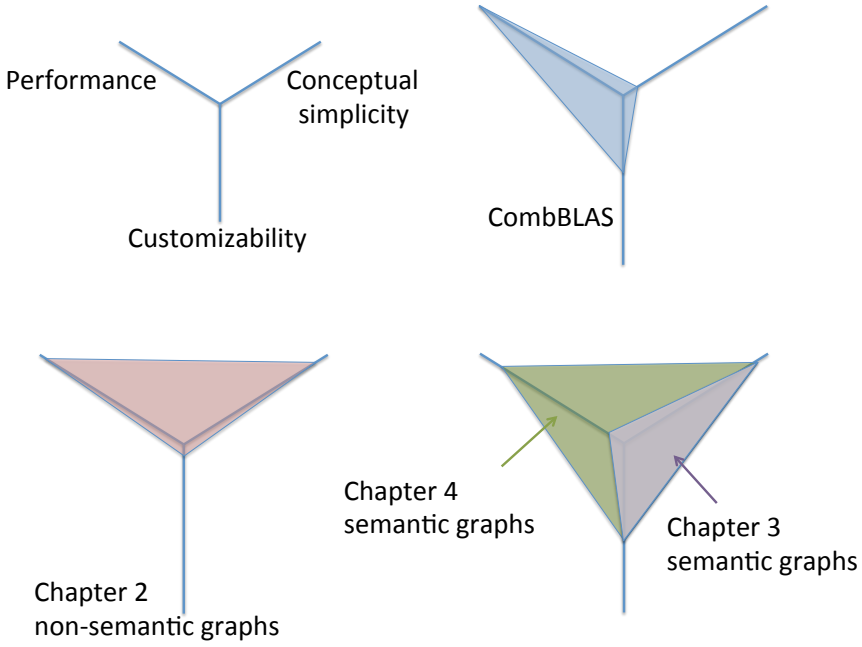

Figure 3.3: A high-level comparison of advances in CombBLAS and KDT. Our current semantic graph implementation has high simplicity and customizability. In Chapter 4 we build on that by adding the performance of our current non-semantic graphs.

3.4 Customizability: Supporting Attributes for Vertices and Edges

3.4.1 Datatypes

The primary feedback we received from potential KDT users on our initial release was the need to support semantic graphs, *i.e.*, graphs whose edges and

vertices have attributes on them. The needed support consisted of two primary changes to KDT: the ability to create graphs with edge objects more complex than the single 64-bit data element of our first release (and similarly vectors with vertex objects more complex than the 64-bit element), and the ability to customize KDT operations to filter or compute on elements of the edge and vertex objects. These changes must be made balanced with the conceptual simplicity and performance requirements.

Our filter design relies on three basic principles.

1. A user-defined predicate determines whether or not a vertex or edge exists in the filtered graph

2. Multiple user-defined predicates can be stacked and the filters they define are applied in the order they are added to the graph. Thus, both users and algorithm developers can use filters.

3. All graph operations respect the filter. This ensures that algorithms can be written without taking filters into consideration at all, thus greatly easing their design.

Two performance issues constrain the semantic-graph design in KDT. First, KDT is targeted at complex graph analytics, which usually traverse the graph more than simple analytics. These traversals are time-consuming, so to avoid

a catastrophic performance decrease when using semantic graphs in KDT, the semantic-graph mechanisms must support computations that require only minimally (and ideally no) more passes over the graph than the non-semantic case. Second, because of the traversal-intensive nature of complex graph analytics and the fact that in-memory operation is typically much faster than on-disk operation, frugal memory use will enable much larger problems to be solved. Specifically, when a user filters a graph to operate on only certain types of edges or vertices, avoiding the materialization of the intermediate graph will typically be a large saving in memory consumption. KDT's semantic-graph mechanisms strive to achieve this.

Given that KDT interfaces are via Python, a natural target for customizable data structures would be a fully general Python object. Unfortunately, Python objects are so general that even their size might not remain constant during their lifetime. KDT's dependence on the Combinatorial BLAS, a C++ package, requires a set of statically-typed and statically-sized objects known at compile time, which does not lend itself to straightforward support of general run-time definable Python objects. In practice, less-general structures targeted at semantic graphs provide the support needed for many semantic-graph problems; *e.g.*, STINGER [8] has been proposed as a common graph data structure.

We are continually relaxing our requirements for what an attribute can be. Our original implementation used simple 64-bit floating point scalar values as the only supported attribute types.

KDT v0.2 provides two statically-defined object types, `Obj1` and `Obj2`, which are motivated by STINGER. Unlike STINGER, however, our users may modify the object types, albeit in C++ at KDT compile time. Each object type, as well as scalars, can be used for either edge or vertex attributes. With this data-structure flexibility comes some additional user responsibility in defining how the elements of the objects are used, *i.e.*, how the `load` function will fill the members of the object from data values in an input file, overload operators if desired, etc.

As described in Chapter 4, a later version of KDT supports arbitrary object types defined by the user in Python. These objects are subject to the restriction that they do not change structure (size or makeup) during execution and that all elements of a matrix or vector (i.e. any particular graph) must have all attributes of the same type. These restrictions allow us to keep our high-performance communication methods, and are common in high-performance Python packages.

3.4.2 Computation

Computations on the edge and vertex objects consist of three types: *semirings* that perform the elemental calculation that occurs at each position of a dot prod-

uct corresponding to a single step in a graph traversal (such as `+` or `min`), *element-wise* functions that define the behavior of elemental operations on edges or vertices, and *filter predicates* that return a Boolean True value for each vertex or edge to be retained in the computation.

KDT's breadth-first search function is an illustrative example. For a graph with no attributes, at each step the *fringe* vertices that were newly encountered on the previous step have their out-edges examined. If a previously unvisited vertex is encountered, the source vertex of the edge to the new vertex is remembered as the *parent* (in case of multiple edges from fringe vertices to the new vertex, the highest-numbered source vertex is remembered).

The semiring multiply operation visits an edge; the add operation consolidates multiple edges coming into a single vertex (using a *max* operation in our example). Element-wise operations are used to determine if a vertex is newly discovered, for updates to the parents, and for pruning the frontier of discovered vertices.

Applying a filter to either the edges or vertices effectively removes the filtered elements from the graph. For example, a user may want to calculate a time-dependent path operation for just CellPhone edges, and the time-dependent operation itself may filter edges based on their start times.

3.4.3 In-place Graph Filtering

In addition to the three filter principles listed in Section 3.4.1, we take the step of implementing filters at a high level. Our backend can thus be designed without explicit support for filtering, greatly simplifying its implementation. Our backend supports operations that fall into three basic categories. We have element-wise operations of the form $e_i = f(e_i)$, operations to select elements based on a predicate (*eg.* Count), and semiring operations (SpMV, SpGEMM). Each operation supports filters without altering its basic implementation.

The element-wise operations can be filtered by introducing a "shim" function $s(x)$ that traverses the filter predicate stack and determines if the element x is kept or not. If not, $s(x)$ returns x and the result is a no-op. If x passes the filter then the user's operation is called and $s(x) = f(x)$.

The predicate operations can be filtered with a similar shim. The filter stack essentially prepends additional logical AND terms to the user's predicate.

SpMV and SpGEMM operations using semirings are both filtered in the multiply step. If either element is filtered out then the multiply becomes a no-op, as if it didn't happen at all. The SpGEMM case can again be implemented with a simple shim in the multiply operation. The SpMV case is more complex because of the semantics of the vector's filter. A filter on the vector means that vertices of the graph are filtered. If a vertex is filtered out then all edges incident to it

must also be filtered out. In the SpMV data pattern, the multiply operation only has the values of vertices at the tails of the edges, but not the heads. A naïve application of the vertex filter would not filter out edges whose heads are incident to a vertex which is filtered out. A solution is to turn the vertex filter into an edge filter by adding a boolean flag to each edge. The vertex filter is applied once to the vector, and its result is broadcast along the rows and columns of the matrix. The SpMV's multiply operation can now filter on just an edge filter.

3.5 Performance

A key performance aspect is the ability to run user code efficiently in the most inner loops of the framework. The ideal solution is to efficiently execute code written by the user in the high level language (Python). This, however, introduces the performance penalty of calling into an interpreter for every operation.

An alternative solution is to pre-define a set of composable primitives which are implemented in the fast low-level language but exposed in the high level one. The user then composes their operation from these primitives. We found this approach to provide near hard-coded speed and approximately 80X performance benefits over calling Python code because the callback into the interpreter is eliminated. The price is reduced ease of use.

A superior approach is to run code written in Python at C speeds. This is the goal of SEJITS [27], which provides a translation and compilation framework for Python which automatically accelerates repeated operations. It translates the operation to C++, compiles it, then calls the native code instead of the original Python code. The heavy-lifting task of optimization is left to the C++ compiler so the SEJITS framework itself is very lightweight. Chapter 4 describes our work on using SEJITS to accelerate KDT.

3.6 Conclusion

We demonstrated KDT's increasing flexibility in the types of graphs it can represent and operations it supports. Namely we described arbitrary attributes on vertices and edges, and custom user-defined operations for writing graph algorithms using high-performance patterns. We also introduced the ability to filter graphs in-place without incurring additional storage requirements. We also showed that despite their customizability and user-friendliness, these operations can still be efficiently performed.

Chapter 4

Eliminating Python Callback Overhead with JIT Specialization

This chapter is based on a paper submitted to JPDC [77]. It is an extension of papers published in IPDPS'13 [21] and PACT'12 [23].

4.1 Introduction

Large-scale graph analytics is a central requirement of bioinformatics, finance, social network analysis, national security, and many other fields that deal with "big data". Going beyond simple searches, analysts use high-performance computing systems to execute complex graph algorithms on large corpora of data. Often, a large semantic graph is built up over time, with the graph vertices representing entities of interest and the edges representing relationships of various kinds—

for example, social network connections, financial transactions, or interpersonal contacts.

In a semantic graph, edges and/or vertices are labeled with *attributes* that might represent a timestamp, a type of relationship, or a mode of communication. An analyst (i.e. a user of graph analytics) may want to run a complex workflow over a large graph, but wish to only use those graph edges whose attributes pass a filter defined by the analyst.

In this chapter we expand KDT's semantic graph facilities as outlined in Chapter 3. We develop support for arbitrary object types and improve KDT's callback performance.

Filters act to enable or disable KDT's action (the semiring operations) based on the attributes that label individual edges or vertices. The programmer's ability to specify custom filters and semirings directly in a high-level language like Python is crucial to ensure high-productivity and customizability of graph analysis software. This chapter presents new work that allows KDT users to define filters and semirings in Python without paying the performance penalty of upcalls to Python.

Filters raise performance issues for large-scale graph analysis. In many applications it is prohibitively expensive to run a filter across an entire graph data corpus, and produce ("materialize") a new filtered graph as a temporary object

for analysis. In addition to the obvious storage problems with materialization, the time spent during materialization is typically not amortized by many graph queries because the user modifies the query (or just the filter) during interactive data analysis. The alternative is to filter edges and vertices "on the fly" during execution of the complex graph algorithm. A graph algorithms expert can implement an efficient on-the-fly filter as a set of primitive Combinatorial BLAS operations coded in C/C++ and incur a significant productivity hit. Conversely, filters written at the KDT level, as predicate callbacks in Python, are productive, but incur a significant performance penalty.

Our solution to this challenge is to apply Selective Just-In-Time Specialization (SEJITS) techniques [27]. We define two semantic-graph-specific domain-specific languages (DSL): one for filters and one for the user-defined scalar semiring operations for flexibly implementing custom graph algorithms. Both DSLs are subsets of Python, and they use SEJITS to implement the specialization necessary for filters and semirings written in that subset to execute efficiently as low-level C++ code. Unlike writing a compiler for the full Python language, implementing our DSLs requires much less effort due to their domain-specific nature. On the other hand, our use of existing SEJITS infrastructure preserves the high-level nature of expressing computations in Python without forcing users to write C++ code.

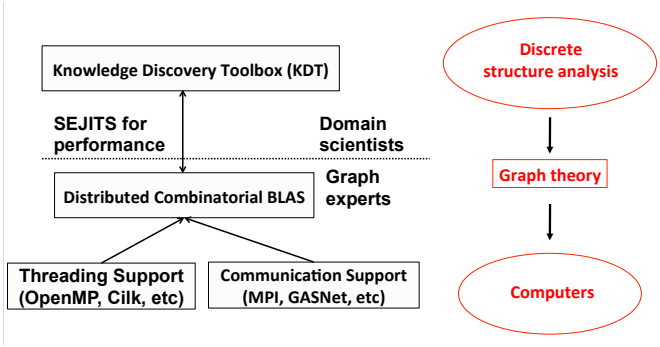

Figure 4.1: Overview of the high-performance graph-analysis software architecture described in this chapter. KDT has graph abstractions and uses a very high-level language. Combinatorial BLAS has sparse linear-algebra abstractions, and is geared towards performance.

We demonstrate that SEJITS technology significantly accelerates Python graph analytics codes written in KDT, running on clusters and multicore CPUs. An overview of our approach is shown in Figure 4.1. SEJITS specialization allows our graph analytics system to bridge the gap between the performance-oriented Combinatorial BLAS and and usability-oriented KDT.

The primary new contributions of this chapter are:

1. A domain-specific language implementation that enables flexible filtering and customization of graph algorithms without sacrificing performance, using SEJITS selective compilation techniques.

2. A new Roofline performance model [107] for high-performance graph exploration, suitable for evaluating the performance of filtered semantic graph operations.

3. Experimental demonstration of excellent performance scaling to graphs with tens of millions of vertices and hundreds of millions of edges.

4. Demonstration of the generality of our approach by specializing two different graph algorithms: breadth-first search (BFS) and maximal independent set (MIS). In particular, the MIS algorithm requires multiple programmer-defined semiring operations beyond the defaults that are provided by KDT.

Figure 4.2 summarizes the work implemented in this chapter, by comparing the performance of three on-the-fly filtering implementations on a breadth-first search query in a graph with 4 million vertices and 64 million edges. The chart shows time to perform the query as we synthetically increase the portion of the graph that passes the filter on an input R-MAT graph [67] of scale 22. The top, red, line is the method implemented in the v0.2 release of KDT as described in Chapter 2, with filters and semiring operations implemented as Python callbacks. The second, blue, line is our new KDT+SEJITS implementation where filters and semiring operations implemented in our DSLs are specialized using SEJITS.

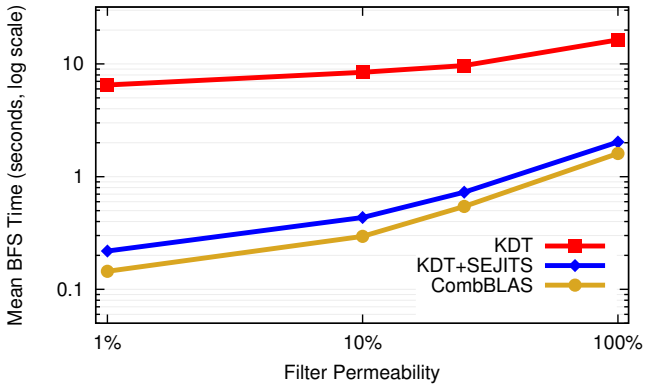

Figure 4.2: Performance of a filtered BFS query, comparing three methods of implementing custom semiring operations and on-the-fly filters. The vertical axis is running time in seconds on a log scale; lower is better. From top to bottom, the methods are: high-level Python filters and semiring operations in KDT; high-level Python filters and semiring operations specialized at runtime by KDT+SEJITS (this chapter's main contribution); low-level C++ filters implemented as customized semiring operations and compiled into Combinatorial BLAS. The runs use 36 cores (4 sockets) of Intel Xeon E7-8870 processors.

This new implementation shows minimal overhead and comes very close to the performance of native Combinatorial BLAS, which is in the third, gold line.

The rest of the chapter is organized as follows. Section 4.2 gives background on the graph-analytical systems our work targets and builds upon. Section 4.3 is the technical heart of the chapter, which describes how we meet performance challenges by using selective, embedded, just-in-time specialization. Section 4.4

presents Python-defined objects that enable the user to declare attribute types directly in Python, enabling a broad set of applications. Section 4.6 proposes a theoretical model that can be used to evaluate the performance of our implementations, giving "Roofline" bounds on the performance of breadth-first search in terms of architectural parameters of a parallel machine, and the permeability of the filter (that is, the percentage of edges that pass the filter). Section 4.5 gives details about the experimental setting and Section 4.7 presents our experimental results. In Section 4.8, we precisely analyze the performance implications of selective just-in translation using hardware performance counters. We survey related work in Section 4.9. Section 4.10 gives our conclusions and some remarks on future directions and problems.

4.2 Background

Running Example: Throughout the chapter, we will use a running example query to show how different implementations of filters and semiring operations express the query and compare their performance executing it. We consider a graph whose vertices are Twitter users, and whose edges represent two different types of relationships between users. In the first type, one user "follows" another; in the second type, one user "retweets" another user's tweet. Each retweet edge carries

as attributes a timestamp and a count. The example query is a breadth-first search (BFS) through vertices reachable from a particular user via the subgraph consisting only of "retweet" edges with timestamps earlier than June 30. The pseudocode for the full BFS implementation is given in Algorithm 1. This is a classical top-down BFS as opposed to the recently developed direction-optimizing algorithm that incorporates a bottom-up step [12, 13].

Algorithm 1 Pseudocode of breadth-first search algorithm used in our running example.

Require: Graph G with transposed adjacency matrix $G.edges$ and $root$
Ensure: BFS parent vector $parents$

```
parents ← dense vector length nvert(G), initialized to −1
frontier ← empty sparse vector length nvert(G)
parents[root] ← root                          ▷ The root is its own parent.
frontier[root] ← root
while frontier is not empty do
    frontier[i] ← i
    frontier ← G.edges.SpMV(frontier, semiring=SR)
    prune frontier[i] if parents[i] ≠ −1      ▷ Remove already discovered vertices from the frontier.
    for all non-null frontier[i] do           ▷ Update the parent vector with vertices discovered in this iteration.
        parents[i] = frontier[i]
    end for
end while
```

4.2.1 Filters As Scalar Semiring Operations

In this section, we show how a filter can be implemented below the KDT level, as a user-specified semiring operation in the C++/MPI Combinatorial BLAS library that underlies KDT. This is a path to high performance at the cost of usability: the analyst must translate the graph-attribute definition of the filter into low-level C++ code for custom semiring scalar operations in Combinatorial BLAS.

The Combinatorial BLAS (CombBLAS for short) views graph computations as sparse matrix computations using various algebraic semirings, such as the tropical (min,+) semiring for shortest paths, or the real (+,*) semiring/field for numerical computation. A semiring consists of a set of 'scalars', and two operations called 'addition' and 'multiplication'. The semiring additive identity (SAID for short) is also the multiplicative annihilator. The addition operation is commutative, and both multiplication and addition are associative. Speaking generally about graph algorithms, the 'scalars' are the edge and vertex data (attributes), 'multiplication' determines how the data on a sequence of edges are combined to represent a path, and 'addition' determines how to combine two or more parallel paths. The scalar multiply function is called for each edge examination, making it a suitable candidate to embed the filtering logic. Two fundamental kernels in CombBLAS, sparse matrix-vector multiplication (SpMV) and sparse matrix-matrix multiplica-

tion (SpGEMM), both use semirings to explore the graph by expanding existing frontier(s) by a single hop.

The expert user can define new semirings and operations on them in C++ at the CombBLAS level, but most KDT users do not have the expertise for this. Figure 4.3 shows the semiring for our running example of BFS on a Twitter graph. The usual semiring multiply for BFS is `select2nd`, which returns the second value it is passed; the multiply operation is modified to only return the second value if the filter succeeds. At the lowest levels of SpMV, SpGEMM, and the other CombBLAS primitive, the return value of the scalar multiply is checked against SAID (in this example, the default constructed ParentType object is the additive identity), and the returned object is retained only if it does not match the SAID.

Filters written as semiring operations in C++ can have high performance because the filter itself is a local operation that uses only the data on one edge, and the number of calls to the filter operations is asymptotically the same as the minimum necessary calls to the semiring scalar multiply, which itself is called once per edge examination. The filtered multiply returns SAID if the predicate is not satisfied.

```
struct TwitterBFSSemiring
{
  ParentType multiply( const TwitterEdge & arg1, const
     ParentType & arg2)
  {
    if (arg1.isRetweet() && arg1.latest(sincedate))
      return arg2;  // unfiltered multiply returns normal value
    else
      return ParentType(); // filtered multiply yields SAID
  }
  ParentType add(const ParentType & arg1, const ParentType &
     arg2)
  {
    return ((arg2 == ParentType()) ? arg1: arg2); // select
       non-SAID
  }
  time_t sincedate = stringtotime("2009/06/30");
}
```

Figure 4.3: An example of a filtered scalar semiring operation in Combinatorial BLAS. This semiring would be used in the SpMV primitive in Algorithm 1. The multiply operation only traverses edges that represent a retweet before June 30, and the add operation returns one of the operands that is not SAID (if any).

4.2.2 KDT Filters in Python

The Knowledge Discovery Toolbox is a flexible open-source toolkit for complex graph algorithms on high-performance parallel computers. KDT targets two classes of users. Domain-expert analysts, who are not graph experts, invoke the algorithms built by graph-algorithm developers. KDT algorithms are composed in

```
# define the semiring
class select2nd(kdt.KDTBinaryFunction):
  def __call__(self, x, y):
    return y

SR = kdt.sr(select2nd(), select2nd())
```

Figure 4.4: An example semiring definition in KDT. This semiring would be used in the SpMV primitive in Algorithm 1. In KDT, the semiring and filter definitions are independent; a filtered semiring operation is achieved by using an unfiltered semiring operation on a graph that has had a filter added to it. A filter is added to a graph in Figure 4.5.

Python from primitives supplied by the CombBLAS. This subsection describes the high-level filtering facility in KDT, in which filters are specified as simple Python predicates [74]. This approach yields easy customization, and scales to many queries from many analysts without demanding correspondingly many graph programming experts; however, it poses challenges to achieving high performance.

Filter semantics: In KDT, any graph algorithm can be performed in conjunction with an edge filter. A filter is a unary predicate that returns true if the edge is to be considered, or false if it should be ignored. KDT users write filter predicates as Python functions or lambda expressions of one input that return a boolean value.

Using a filter does not require any change in the code for the graph algorithm. For example, KDT code for betweenness centrality or for breadth-first search is the same whether or not the input semantic graph is filtered. Instead, the filtering occurs in the low-level primitives. Our design allows all current and future KDT algorithms to support filters without additional effort on the part of algorithm designers. To implement our running example we define the semiring in Figure 4.4. In Figure 4.5 we define an edge filter and add it to the graph.

It is possible in KDT to add multiple filters to a graph. The result is a nested filter whose predicate is a lazily-evaluated "logical and" of the individual filter predicates. Filters are evaluated in the order they are added. Multiple filter support allows both end users and algorithm designers to use filters for their own purposes.

Filtering approaches: KDT supports two approaches for filtering semantic graphs:

- *Materializing filter:* When a filter is placed on a graph (or matrix or vector), the entire graph is traversed and a copy is made that includes only edges that pass the filter. We refer to this approach as *materializing* the filtered graph.

- *On-the-fly filter:* No copy of the graph/matrix/vector is made. Rather, every primitive operation (e.g. semiring scalar multiply and add) applies the filter to its inputs when called. Roughly speaking, every primitive operation accesses the graph through the filter and behaves as if the filtered-out edges were not present.

Both materializing and on-the-fly filters have their place; neither is superior in every situation. For example, materialization may be more efficient when running many analyses on a well-defined small subset of a large graph. On the other hand, materialization may be impossible if the graph already fills most of memory; and materialization may be much more expensive than on-the-fly filtering for a query whose filter restricts it to a localized neighborhood and thus does not even touch most of the graph. Indeed, an analyst who needs to modify and fine-tune a filter while exploring data may not be willing to wait for materialization at every step.

A key focus of this chapter is on-the-fly filtering and making it more efficient. Our experiments demonstrate that materializing the subgraph can take as much as 18 times the time of performing a single BFS on the largest of the real twitter datasets. In this comparison, both materialization (an embarrassingly parallel task) and the BFS are run in parallel using 36 cores of Intel Xeon E7-8870.

Implementation details: Filtering a semiring operation requires the semiring scalar multiply to be able to return "null", in the sense that the result should

```
# G is a kdt.DiGraph
class TwitterFilter(kdt.KDTUnaryPredicate):
  def __call__(self, e):
    return (e.count > 0 and e.latest <
        str_to_date("2009/06/30"))

earlyRetweetsOnly = TwitterFilter()

G.addEFilter(earlyRetweetsOnly)
G.e.materializeFilter() # omit this line for on-the-fly filtering

# perform some operations or queries on G, such as BFS

G.delEFilter(earlyRetweetsOnly)
```

Figure 4.5: Adding and removing an edge filter in KDT, with or without materialization.

be the same as if the multiply never occurred. In semiring terms, the multiply operation must return the SAID. CombBLAS treats SAID the same as any other value. However, CombBLAS uses a sparse data structure to represent the graph as an adjacency matrix—and, formally speaking, SAID is the implicit value of any matrix entry not stored explicitly.

CombBLAS ensures that SAID is never stored as an explicit value in a sparse structure. This corresponds to Matlab's convention that explicit zeros are never stored in sparse matrices [42], and differs from the convention in the CSparse sparse matrix package [28]. Note that SAID need not be "zero": for example, in

the min-plus semiring used for shortest path computations, SAID is ∞. Indeed, it is possible for a single graph or matrix to be used with different underlying semirings whose operations use different SAIDs.

We benchmarked several approaches to representing, manipulating, and returning SAID values from semiring scalar operations. It is crucial for usability to allow filters to be ignorant of the semiring they are applied to; therefore, returning a SAID needs to be an out-of-band signal. We pair each basic semiring scalar operation with a `returnedSAID()` predicate which is called after the scalar operation. We use a predicate instead of a flag because the predicate can be optimized out by the compiler for unfiltered operations.

The result is a clean implementation of on-the-fly filters: filtering a semiring simply requires a small adapter code in the semiring `multiply()` function that calls the filter predicate on both operands. If the predicate returns false for either operand then the adapter causes `returnedSAID()` to return true. Otherwise the semiring's callback is called and its value returned.

4.3 SEJITS Translation of Filters and Semiring Operations

Defining semirings and filters in Python results in one or more serialized upcalls from the low-level Combinatorial BLAS into Python for both semiring operations and filtering. In order to mitigate this slowdown, we use the Selective Embedded Just-In-Time Specialization (SEJITS) approach [27]. We define embedded DSLs for semiring and filter operations which are subsets of Python. As shown in Figure 4.6, callbacks written in these DSLs are translated at runtime to C++ to eliminate performance penalties while still allowing users the flexibility to specify filters and semirings in Python. We use the Asp[1] framework to implement our DSLs.

We allow users to write their filters and semirings in our embedded DSLs. The languages are defined as proper subsets of Python with normal Python syntax, but they restrict the kinds of operations and constructs that users can utilize in filters and semiring operations. At instantiation, source code of filters and semirings is introspected to get the Abstract Syntax Tree (AST), and then is translated into low-level C++. Subsequent applications of the filter use this low-level implementation, sidestepping the serialization and cost of upcalling into Python.

[1] Asp is SEJITS for Python, http://sejits.com

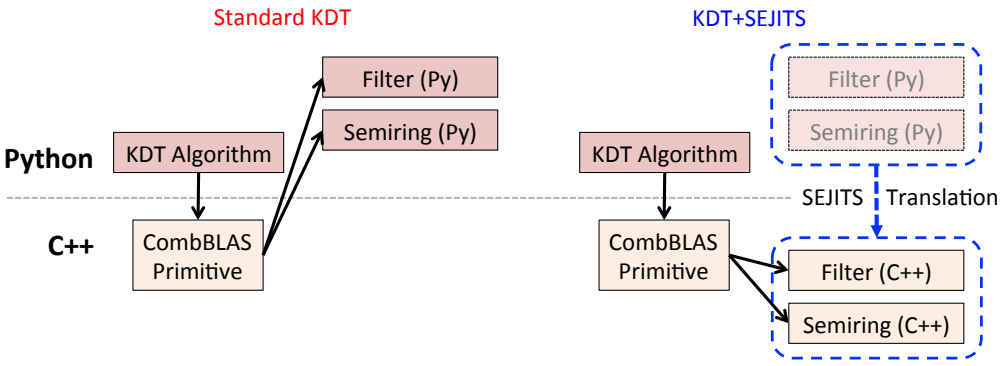

Figure 4.6: **Left:** Calling process for filter and semiring operations in KDT. For each edge, the C++ infrastructure must upcall into Python to execute the callback. **Right:** Using our DSLs, the C++ infrastructure calls the translated version of the operation, eliminating the upcall overhead.

Although KDT is our target platform in this work, our specialization approach can be used to accelerate other graph processing systems with similar performance challenges. In the next sections, we define our domain-specific languages and show several examples of using them from Python.

4.3.1 Python Syntax for the DSLs

We choose to implement two separate DSLs to clearly express and restrict the kinds of computations that can be done with each; for example, filters require boolean return values, while semiring operations require return values that are one of the vertex or edge types. Separating out the languages and their forms allows

us to more easily ensure correctness of each. An alternative approach would build a single language but enforce restrictions using typechecking; we forgo the complexity involved in building a typechecker and instead enforce that filters are correct by construction. We do share internal abstract syntax tree node types between the two DSLs.

Consider the filter embedded DSL. Informally, we specify the language by stating what a filter can do: namely, a filter takes in one input (whose type is predefined), must return a boolean, and is allowed to do comparisons, accesses, and arithmetic on immediate values and edge/filter instance variables. In addition, to facilitate translation, we require that a filter be an object that inherits from the `PcbFilter` Python class, and that the filter function itself use Python's usual interface for callable objects, requiring the class define a function `__call__`.

Binary operations used in semirings and other operations in KDT are similarly defined, but must inherit from the `PcbFunction` class and must return one of the inputs or a numeric value that corresponds to the KDT built-in numeric type. Binary predicates resemble filters but accept two arguments and return a boolean.

The example KDT filter from Figure 4.5 is presented in the filter embedded DSL syntax in Figure 4.7. It defines a fully-valid Python class that can be translated into C++ since it only uses constructs that are part of our restricted subset of Python.

```
class MyFilter(PcbFilter):
  def __init__(self, ts):
    self.ts = ts
  def __call__(self, e):
    # if it is a retweet edge
    if (e.isRetweet and
        # and it is before our initialized timestamp
        e.latest < self.ts):
      return True
    else:
      return False
```

Figure 4.7: Example of an edge filter that the translation system can convert from Python into fast C++ code. Note that the timestamp in question is passed in at filter instantiation time.

4.3.2 Translating User-Defined Filters and Semiring Operations

In the Asp framework for SEJITS embedded DSLs, the most important mechanism for ensuring correct translations is to create an intermediate representation, called the *semantic model*, which defines the semantics of valid translatable objects. AST nodes from parsing Python are translated into this intermediate form as a first step of translation, and most of the logic for checking whether the definition is translatable is executed in this first phase. To be clear, this representation

```
UnaryPredicate(input=Identifier, body=BoolExpr)

Expr = Constant | Identifier | BinaryOp | BoolExpr

Identifier(name=types.StringType)

BoolExpr = BoolConstant | IfExp | Attribute | BoolReturn |
          Compare | BoolOp

Compare(left=Expr, op=(ast.Eq | ast.NotEq | ast.Lt |
       ast.LtE | ast.Gt | ast.GtE), right=Expr)

BoolOp(op=(ast.And | ast.Or | ast.Not), operands=BoolExpr*)
    check assert len(self.operands)<=2

Constant(value = types.IntType | types.FloatType)

BinaryOp(left=Expr, op=(ast.Add | ast.Sub), right=Expr)

BoolConstant(value = types.BooleanType)

IfExp(test=BoolExpr, body=BoolExpr, orelse=BoolExpr)

Attribute(value=Identifier, attr=Identifier)

BoolReturn(value = BoolExpr)
```

Figure 4.8: Semantic Model for KDT filters using SEJITS.

is not the syntax of a language, but rather is the intermediate state that defines semantics based on user-supplied Python syntax.

In filters and semirings, the user may wish to inspect fields of the input data types, do comparisons, and perhaps perform arithmetic with fields. Consequently our semantic model allows these operations.

On the other hand, we want to (as much as possible) prevent users from writing code that does not conform to our assumptions; although we could use analysis for this, it is much simpler to construct the languages in a manner that prevents users from writing non-conformant code in either embedded DSL. If the filter or semiring operation does not fit into our language, we run it in the usual fashion, by doing upcalls into pure Python, after outputting a warning. Thus, if the user writes their code correctly, they achieve fast performance, otherwise the user experience is no worse than before— the code still runs, just not at fast speed.

The semantic models are shown in Figures 4.8 and 4.9. We have defined it to make it easy to write filters and operations that are "correct by construction"; that is, if they fit into the semantic model, they follow the restrictions of what can be translated. For example, for filters, we require that the return be provably a boolean (by forcing the BoolReturn node to have a boolean body), and that there be either a single input or two inputs (either UnaryPredicate or BinaryPredicate). The semantic model for semiring operations ensures the returned item is one of the inputs or an elemental type understood by KDT.

We define tree transformations that dictate how Python AST nodes are translated into semantic model nodes. For example, the Python function definition for `__call__` is translated into a UnaryPredicate node in the case of the filter embedded DSL. Similarly, in the filter embedded DSL, the transformation checks whether the body of the return statement is provably a boolean and returns a BooleanReturn node.

After the code is translated into instances of the semantic model, the rest of the translation is straightforward, utilizing Asp's infrastructure for converting semantic models into backend code. For many of these transformations, defaults built into Asp are sufficient; for example, we leverage the default translation for constant numbers and therefore do not need to define the transform. The end result of conversion is source code containing the function in a private namespace plus some glue code, described in the next section. This source is passed to CodePy, which compiles it into a small dynamically linked library that is then automatically loaded into the running interpreter.

4.3.3 Implementation in C++

We modify the C++ portion of KDT's callback mechanism which is based on pointers to Python functions. We add an additional function pointer that is checked before executing the upcall to Python. This function pointer is set

Table 4.1: Overheads of using the filtering DSL.

	First Run	Subsequent
Codegen	$0.0545s$	$0.0s$
Compile	$4.21s$	$0.0s$
Import	$0.032s$	$0.032s$

by our translation machinery to point to the translated function in C++. When executing a filter predicate, the pointer is first checked, and if it is non-null, the appropriate function is called directly. We similarly modify KDT's C++ function objects used for binary operations, which are used to implement semirings. For both kinds of objects, the functions or filters are type-specialized using user-provided information. Future refinements will allow inferred type-specialization.

Compared to Combinatorial BLAS, at runtime we have additional sources of overhead relating to the null check and function pointer call into a shared library, which usually is more expensive than a plain function call. However, these costs are trivial relative to the non-translated KDT machinery, particularly compared to the penalty of upcalling into Python.

Overheads of code generation are shown in Table 4.1 on an Intel Xeon E7-8870 machine. On first run of a particular specialized operation, the DSL infrastructure translates it to C++ and compiles it; most of the time here is spent calling the external C++ compiler, which is not optimized for speed. CodePy's built-in caching support ensures that subsequent runs only incur the penalty of Python's `import`

statement. On a multi-processor machine, only one process performs the compilation; the remaining ones load the cached version when that single compilation finishes.

4.4 Attributes defined in Python and exposed to C++

4.4.1 Motivation

The attribute types of vertices and edges should ideally be declared in Python, especially when the application requires several graphs with different edge and/or vertex datatypes. Consider the analysis of multi-modal brain networks (also known as connectomes). In this application, data from multiple modalities, such as fMRI, DTI, EEG, and PET, are collected for the patient's brain. Representing these data sources as graphs and using graph analysis has been instrumental in characterizing neurodegenerative diseases. The co-registration of these modalities requires the application to handle multiple graphs with different edge/vertex types. For example, the temporal and spatial resolution of fMRI and EEG data are incompatible [84], requiring different vertex types. Similarly, the voxel correlations in fMRI and DTI are defined differently, requiring different edge types.

The ability to declare edge and vertex types dynamically in Python allows co-analysis of different brain networks and overcomes the limitations of using a single modality [64], and we plan to leverage our described methodology for forthcoming investigations of computational neuropathology.

4.4.2 Challenge

We wish to enable the user to declare attribute types in Python. However, in order to obtain high-performance we must meet some CombBLAS and MPI requirements. CombBLAS's architecture requires that all elements of a matrix or vector must have the same type and size. These elements, or Python-Defined Objects (PDOs), must have the following properties:

- Self contained: no external references, object must be able to be copied by value (i.e. with `memcpy`).
- Object is declared and accessed in Python, memory is allocated in C++.
- Python-defined structure must be able to be operated on in C++

KDT 0.3 introduces just such a scheme. We declare a structure in Python that is then placed within a buffer of raw bytes. In other words, we turn C++ objects `Obj1` and `Obj2` into `void*` buffers which are in effect typecast to the Python-defined type at runtime.

4.4.3 Structure Declaration

Python's `ctypes` interface is used to call into C libraries. Since some C functions operate on `struct` datatypes, `ctypes` includes mechanisms to declare a C `struct` in Python. `ctypes` exposes C primitive datatypes such as `c_int` or `c_double` which can be composed together into a `struct` which is binary compatible with compiled C code on that particular system. We expose a subset of `ctypes`'s datatypes to the KDT user to use to declare a Python-Defined Object's data members.

Python access to the PDO is handled via `ctypes`'s hooks, which enable the structure to behave like any Python object. Python operators can be declared using Python's standard operator definition machinery.

A simple example of a custom edge type is a PDO version of the structure in Figure 4.10, as follows:

```
class TwitterEdge(Structure):
    _fields_ = [("follower", c_bool),
                ("latest", c_uint64), # time_t
                ("count", c_short)]
```

4.4.4 Memory Handling

CombBLAS is not aware that it is working with a Python-Defined Object; instead, what it sees is a byte buffer of a fixed size. Therefore, all memory for

PDOs is allocated by CombBLAS. Pointers to this memory are passed to the callbacks, which then use `ctypes`'s mechanisms to create a Python object backed by the CombBLAS buffer. The PDO is then accessible in the Python callback.

4.4.5 PDOs and SEJITS

For SEJITS to support the PDO it must be able to access the PDO's memory in the same way as the Python operations would. Luckily `ctypes` declares the structure in precisely such a way. We translate all PDO structs used by a specialized callback into C and add the declarations to the SEJITS-generated C++ module. The callback's parameters are the buffer objects, `Obj1` and/or `Obj2`. We add code to extract the buffers and typecast them to references to the particular structs that the buffers correspond to.

The rest of the C++ specialized callback can now operate on the buffer as if it were a `struct`.

4.4.6 Limitations

Our approach has some limitations, namely that we can only support the intersection of Python and C++ language features. In particular, data members and their types must be declared ahead of time. The declaration is decidedly

C-style, and any duck-typed definitions will be lost. The PDO must not contain any pointers or references.

CombBLAS requires that the datatypes must be copyable by value for MPI communication, so no copy constructors are called. In addition, the size of the buffers must be declared at compile time. Our scheme allows an unlimited number of different PDO types to be declared in a single program, but each one must fit into one of a handful different buffer sizes.

4.5 Experimental Design

This section describes the graph algorithms used in our experiments, the benchmark matrices we used to test the algorithms, and the machines on which we ran our tests. KDT version 0.3 is enabled with the SEJITS techniques described in this chapter, and is freely available at http://kdt.sourceforge.net.

4.5.1 Algorithms Considered

Our first algorithm is a filtered graph traversal. Given a vertex of interest, it determines the number of hops required to reach every other vertex using only those retweet edges timestamped earlier than a given date. The filter in this case is a boolean predicate on edge attributes that defines the types and timestamps

of the edges to be used. The query is a breadth-first search (BFS) on the graph that ignores edges that do not pass the filter.

Our second query is to find the maximal independent set (MIS) of this graph. MIS finds a subset of vertices such that no two members of the subset are connected to each other and all other vertices outside MIS are connected to at least one member of the MIS. Since MIS is defined on an undirected graph, we first ignore edge directions, then we execute Luby's randomized parallel algorithm [70] implemented in KDT. The filter is the same as in the first query.

4.5.2 Test Data Sets

We evaluate our techniques on both algorithms using synthetically-generated graphs and those that are based on real data sets. Our BFS experiments using the synthetic data are generated based on the R-MAT model [67] that can generate graphs with a highly skewed degree distribution. An R-MAT graph of scale N has 2^N vertices and approximately $edgefactor \cdot 2^N$ edges. In our tests, *edgefactor* is 16, and R-MAT seed parameters a, b, c, and d are $0.57, 0.19, 0.19$, and 0.05. After generating this non-semantic (boolean) graph, edge payloads are artificially introduced with timestamp values generated using the Mersenne Twister pseudo-random number generator [80]. A simple threshold controls filter permeability. We use a fixed seed so that the experiments are reproducible and all codes work

on the same problem. The edge type is the same as the Twitter edge type described in the next paragraph in order to be consistent between experiments on real and synthetic data. Our MIS experiments use Erdős-Rényi graphs [37] with an *edgefactor* of 4 because the MIS algorithm on R-MAT graphs completes in very few steps due to high coupling and would not yield a meaningful performance analysis.

Our real data graphs are based on social network interactions, using anonymized Twitter data [60, 111]. In our Twitter graphs, edges can represent two different types of interactions. The first interaction is the "following" relationship, where an edge from vertex v_i to v_j implies that v_i is following v_j (note that these directions are consistent with the common authority-hub definitions in the World Wide Web). The second interaction encodes an abbreviated "retweet" relationship: an edge from v_i to v_j implies that v_i has mentioned v_j at least once in tweets. The edge also keeps the count of such tweets as well as the last tweet date if the count is larger than one.

The tweets occurred in the period of June-December of 2009. To allow scaling studies, we created subsets of these tweets based on the date they occur. The *small* dataset contains tweets from the first two weeks of June, the *medium* dataset contains tweets from June and July, the *large* dataset contains tweets dated June through September, and finally the *huge* dataset contains all the tweets from June

Table 4.2: Sizes (vertex and edge counts) of different combined twitter graphs.

Label	Vertices (millions)	Edges (millions)		
		Tweet	Follow	Tweet&follow
Small	0.5	0.7	65.3	0.3
Medium	4.2	14.2	386.5	4.8
Large	11.3	59.7	589.1	12.5
Huge	16.8	102.4	634.2	15.6

Table 4.3: Statistics about the largest strongly connected components of the twitter graphs

	Vertices	Edges traversed	Edges processed
Small	78,397	147,873	29.4 million
Medium	55,872	93,601	54.1 million
Large	45,291	73,031	59.7 million
Huge	43,027	68,751	60.2 million

through December. These partial sets of tweets are then induced upon the graph that represents the follower/followee relationship. If a person tweeted someone or was tweeted by someone, then the vertex is retained in the tweet-induced combined graph.

More details for these four different (small-huge) combined graphs are listed in Table 4.2. Unlike the synthetic data, the real twitter data is directed and we only report breadth-first searches that hit the largest strongly connected component of the filter-induced graphs. More information on the statistics of the largest strongly

connected components of the graphs can be found in Table 4.3. Processed edge count includes both the edges that pass the filter and the edges that are filtered out.

4.5.3 Architectures

To evaluate our methodology, we examine graph analysis behavior on Mirasol, an Intel Nehalem-based machine, as well as Hopper, a Cray XE6 supercomputer at NERSC. Mirasol is a single node platform composed of four Intel Xeon E7-8870 processors. Each socket has ten cores running at 2.4 GHz, and supports two-way simultaneous multithreading (20 thread contexts per socket). The cores are connected to a very large 30 MB L3 cache via a ring architecture. The sustained STREAM [81] bandwidth is about 30 GB/s per socket. The machine has 256 GB of DDR3-1066 DRAM. We utilize a flat MPI programming modeling using OpenMPI 1.4.3 with GCC C++ compiler version 4.4.5, and Python 2.6.6.

Hopper is a Cray XE6 massively parallel processing (MPP) system, built from dual-socket 12-core "Magny-Cours" Opteron compute nodes. Each socket (multi-chip module) has two 6-core chips, so a node can be viewed as a four-chip compute configuration with strong NUMA properties. Each Opteron chip contains six super-scalar, out-of-order cores capable of completing one (dual-slot) SIMD add and one SIMD multiply per cycle. Additionally, each core has private 64 KB

L1 and 512 KB low-latency L2 caches. The six cores on a chip share a 6MB L3 cache and dual DDR3-1333 memory controllers capable of providing an average STREAM bandwidth of 12GB/s per chip. Each pair of compute nodes shares one Gemini network chip that collectively form a 3D torus. We use Cray's MPI implementation, which is based on MPICH2, and compile our code with GCC C++ compiler version 4.6.2 and Python 2.7. Complicating our experiments, some compute nodes of this MPP do not contain a compiler. To remedy this, we ensured that a compute node with access to the requisite compilers was used to build the KDT+SEJITS filters, since the on-the-fly compilation mechanism requires at least one MPI process be able to call the compilation toolchain.

4.6 A Roofline model of BFS

The Roofline model [107] is a visually intuitive representation of the performance characteristics of a kernel on a specific machine. It uses bound and bottleneck analysis to delineate performance bounds arising from bandwidth or compute limits and has been demonstrated to show that performance of many HPC kernels is well-correlated with STREAM bandwidth. Unfortunately, the traditional HPC application characteristics (massive parallelism, streaming memory access) and even metrics (flops per byte) are often antithetical to the computational chal-

lenges found in linear algebra-based graph algorithms. To remedy this, we extend the Roofline model to quantify the performance bounds of BFS as a function of optimization and filter success rate. Doing so allowed us to separate the effects of computation from data movement and express performance as a function of *Filter Permeability* — the percentage of edges that pass the filter — and thus explain the performance benefit of the technology demonstrated in this paper.

In order to model BFS performance, we decouple in-core compute limits (filter and semiring performance as measured in processed edges per second) from memory access performance. The in-core filter performance limits were derived by extracting the relevant CombBLAS, KDT, and SEJITS+KDT versions of the kernels and applying them to arrays that fit in each core's cache. We run the edge processing inner kernels 10,000 times (as opposed to once) to amortize any memory system related effects to get the in-core compute limits. The compute limit decreases with increasing permeability because two operations must be performed for an edge that passes the filter as opposed to the one operation for an edge that does not.

Analogous to arithmetic intensity, we can quantify the average number of bytes we must transfer from DRAM per edge we process — bytes per processed edge. To do so, we must not only estimate data movement, but also effective bandwidth for each operation. In the following analysis, the indices are 8 bytes and the

edge payload is 16 bytes. BFS exhibits three memory access patterns which are illustrated in Figure 4.11. First, there is a unit-stride *streaming* access pattern arising from access of the vertex pointers (this is amortized by degree) as well as the creation of the sparse output vector that acts as the new frontier (the gather step in Figure 4.11). The latter incurs 32 bytes of traffic per traversed edge in write-allocate caches assuming the edge was not filtered. Second, access to the adjacency list follows a *stanza-like* memory access pattern. That is, small blocks (stanzas) of consecutive elements are fetched from effectively random locations in memory. These stanzas are typically less than the mean degree, due to two reasons. The first reason is the heavy-tailed degree distribution that is characteristic of many real world graph instances, which applies to both sequential and parallel settings regardless of the data decomposition. In heavy-tailed distributions, the median is smaller than mean. The second reason only applies to the parallel setting and it is due to per-processor subgraphs being sparser than the full graph for the 2D decomposition (also called hypersparsity [25]). The stanza related traffic corresponds to approximately 24 bytes (16 for payload and 8 for index) of DRAM traffic per processed edge. Finally, updates to the list of visited vertices (the scatter/accumulate step in Figure 4.11) and the indirections when accessing the graph data structure exhibit a memory access pattern in which effectively *random* 8 byte elements are updated (assuming the edge was not filtered). Similarly, each

visited vertex generates 24 bytes of random access traffic to follow indirections on the graph structure before being able to access its edges.

In order to quantify these bandwidths, which we expect to be quite different than STREAM, we wrote a custom micro-benchmark that provides stanza-like memory access patterns (read or update) with spatial locality varying from 8 bytes (random access) to the size of the array (i.e. asymptotically the STREAM benchmark).

The memory bandwidth requirements depend on the number of edges processed (examined), number of edges traversed (that pass the filter), and the number of vertices in the frontier over all iterations. For instance, an update to the list of visited vertices only happens if the edge actually passes the filter. Typically, the number of edges traversed is roughly equal to the permeability of the filter times the number of edges processed. To get a more accurate estimate, we collected statistics from one of the synthetically generated R-MAT graphs that are used in our experiments. These statistics are summarized in Table 4.4. Similarly, we quantify the volume of data movement by operation and memory access type (*random*, *stanza-like*, and *streaming*) noting the corresponding bandwidth on Mirasol, our Intel Xeon E7-8870 test system (see Section 4.5), in Table 4.5. Combining Tables 4.4 and 4.5, we calculate the average number of processed edges

Table 4.4: Statistics about the filtered BFS runs on the R-MAT graph of Scale 23 (M: million)

Filter permeability	Vertices visited	Edges processed	Edges traversed
1%	655,904	213 M	2.5 M
10%	2,204,599	250 M	25.8 M
25%	3,102,515	255 M	64.6 M
100%	4,607,907	258 M	258 M

Table 4.5: Breakdown of the volume of data movement by memory access pattern and operation.

Memory access type	Vertices visited	Edges traversed	Edges processed	Bandwidth on Mirasol
Random	24 bytes	8 bytes	0	9.09 GB/s
Stanza	0	0	24 bytes	36.6 GB/s
Stream	8 bytes	32 bytes	0	106 GB/s

per second as a function of filter permeability by summing data movement time by type and inverting.

Figure 4.12 presents the resultant Roofline-inspired performance model for Mirasol. The plots are upper bounds on the achievable performance and also include the effects of caching of Python objects. The underlying implementation might incur additional overheads. For example, it is common to locally sort the discovered vertices to efficiently merge them later in the incoming processor; we

do not account for this overhead as it is not an essential step of the algorithm. Neither access to MPI buffers nor MPI performance was taken into account.

The Roofline model selects ceilings by optimization, and bounds performance by their minimum. We select a filter implementation (pure Python KDT, KDT+SEJITS, or CombBLAS) and look for the minimum between that filter implementation's limit and the weighted DRAM bandwidth limit. We observe a pure Python KDT filter will be the bottleneck in a BFS computation as it cannot sustain performance (edges per second) at the rate the processor can move edges on-chip. Conversely, the DRAM bandwidth performance limit is about 5× lower than the CombBLAS in-core performance limit. Ultimately, the performance of a SEJITS specialized filter is sufficiently fast to ensure a BFS implementation will be bandwidth-bound. This crucial observation explains why KDT+SEJITS performance is so close to CombBLAS performance in practice (as shown later in Section 4.7) even though its in-core performance is about 2.6× slower.

This Roofline model serves as an excellent surrogate for the performance we observe in practice in Figure 4.2 and generally in Section 4.7. Specifically, it methodologically explains the smaller (≈40×) gap we observe between SEJITS and pure Python KDT performances for BFS as opposed to over 140× suggested by the in-core compute limits. The actual performance difference is the gap between the DRAM bandwidth limit and the KDT in-core compute limit because

the SEJITS Roofline is the lower of the bandwidth-bound and in-core compute-bound lines. Due to the aforementioned data movement effects that we did not account for (such as sorting and MPI buffers), the model suggests a slightly higher bandwidth-bound line, hence a slightly bigger gap than what we observe in practice.

4.7 Experimental Results

In this section we use [semiring implementation]/[filter implementation] notation to describe the various implementation combinations we compare. For example, Python/SEJITS means that only the filter is specialized with SEJITS but the semiring is in pure Python (not specialized).

4.7.1 Performance Effects of Permeability

Figure 4.13 shows the relative distributed-memory performance of four methods in performing breadth-first search on a graph with 32 million vertices and 512 million edges, with varying filter permeability. The structure of the input graph is an R-MAT of scale 25, and the edges are artificially introduced so that the specified percentage of edges pass the filter. These experiments are run on Hopper using 576 MPI processes with one MPI process per core. The figure shows

that the SEJITS/SEJITS KDT implementation (blue line) closely tracks CombBLAS performance (gold line), with the gap between it and the Python/Python KDT implementation (red line) shrinking as permeability increases. This is expected because as the permeability increases, both implementations approach the bandwidth bound regime as suggested by the Roofline model in Section 4.6.

A similar but more condensed figure, showing the performance effects of permeability on Mirasol (Figure 4.2) is in Section 4.1. There, KDT+SEJITS is the same as SEJITS/SEJITS. The effects of permeability on the MIS performance are shown in Figure 4.14 and reflect the BFS findings.

Since low permeability (1-10%) cases incur less memory traffic, Python overheads (KDT algorithms are implemented in Python) as well as the function pointer chasing of the SEJITS approach leave a noticeable overhead over CombBLAS. This is not the case for high-permeability filters where the extra memory traffic largely eliminates CombBLAS's advantage, as observed in the shrinking gap between the blue and the gold lines in Figures 4.13 and 4.14 as permeability increases.

4.7.2 Performance Effects of Specialization

Since SEJITS specializes both the filter and the semiring operations, we discuss the effects of each specialization separately in this section.

All of the performance plots show that the performance of SEJITS/SEJITS (where both the filter and the semiring is specialized with SEJITS) is very close to the CombBLAS performance, showing that our specialization approach successfully bridges the performance gap between Python and the low-level CombBLAS. The Python/SEJITS case is typically slower than the SEJITS/SEJITS case, with the gap depending on the permeability. More selective filters make semiring specialization less relevant because as the permeability increases, more edges pass the filter and more semiring operations are performed, making Python based semiring operations the bottleneck. In the BFS case, shown in Figure 4.15, Python/SEJITS is $3-4\times$ slower than SEJITS/SEJITS when permeability is 100% due to the high number of semiring operations, but only $20-30\%$ slower when permeability is 1%. By going from 1% (Figure 4.15a) to 100% (Figure 4.15d), the green line separates from the other blue and gold lines and approaches the red line.

The performance of the MIS case, shown in Figure 4.16, is more sensitive to semiring translation, even for low permeabilities. The semiring operation in the MIS application is more computationally intensive, because each vertex needs to find its neighbor with the minimum label as opposed to just propagating its value as in the BFS case. Therefore, specializing semirings becomes more important in MIS.

4.7.3 Parallel Scaling

Parallel scalability is key to enabling analysis of very large graphs in a reasonable amount of time. The parallel scaling of our approach is shown in Figures 4.15 and 4.16 for lower concurrencies on Mirasol. CombBLAS achieves remarkable scaling with increasing process counts, while SEJITS translated filters and semirings closely track its performance and scaling.

Parallel scaling studies of BFS at higher concurrencies is run on Hopper, using the scale 25 synthetic R-MAT data set. Figure 4.17 shows the comparative performance of KDT on-the-fly filters (Python/Python), SEJITS filter translation only (Python/SEJITS), SEJITS translation of both filters and semirings (SEJITS/SEJITS), and CombBLAS, with 1% and 100% filter permeability. The SEJITS/SEJITS result tracks CombBLAS closely, except for the largest core counts with 1% permeability. This difference is because the BFS time is so short that the small fixed overhead of importing the SEJITS-compiled filter predicates and semirings is not amortized.

Finally, we show weak scaling results on Hopper using 1% filter permeability (other cases experienced similar performance). In this run, shown in Figure 4.18, each MPI process is responsible for approximately 11 million original edges (hence 22 million edges after symmetrization). More concretely, 121-concurrency runs are obtained on a scale 23 R-MAT graph, 576-concurrency runs are obtained on scale

25 R-MAT graph, and 2025-concurrency runs are obtained on scale 27 R-MAT graph (1 billion edges). The KDT curve is mostly flat (only 9% deviation) due to its in-core computational bottlenecks, while SEJITS+KDT and CombBLAS shows higher deviations (54% and 62%, respectively) from a perfect flat line. However, these deviations are expected on a large scale BFS run and are experienced on similar architectures [26]. The results demonstrate that our SEJITS approach does not impede scalability to thousands of processors, compared to a high-performance library like CombBLAS.

```
UnaryFunction(input=Identifier, body=Expr)

BinaryFunction(inputs=Identifier*, body=Expr)
    check assert len(self.inputs)==2

Expr = Constant
          | Identifier
          | BinaryOp
          | BoolConstant
          | IfExp
          | Attribute
          | FunctionReturn
          | Compare

Identifier(name=types.StringType)

Compare(left=Expr, op=(ast.Eq | ast.NotEq | ast.Lt |
       ast.LtE | ast.Gt | ast.GtE), right=Expr)

Constant(value = types.IntType | types.FloatType)

BinaryOp(left=Expr, op=(ast.Add | ast.Sub | ast.And), right=Expr)

BoolConstant(value = types.BooleanType)

IfExp(test=(Compare | Attribute | Identifier| BoolConstant |
           BinaryOp),
      body=Expr, orelse=Expr)

# this if for a.b
Attribute(value=Identifier, attr=Identifier)

FunctionReturn(value = Expr)
```

Figure 4.9: Semantic Model for KDT binary and unary functions, used in semirings and related vector-vector operations.

```
struct TwitterEdge {
        bool follower;
        time_t latest; // set if count>0
        short count; // number of tweets
};
```

Figure 4.10: The edge data structure used for the combined Twitter graph in C++

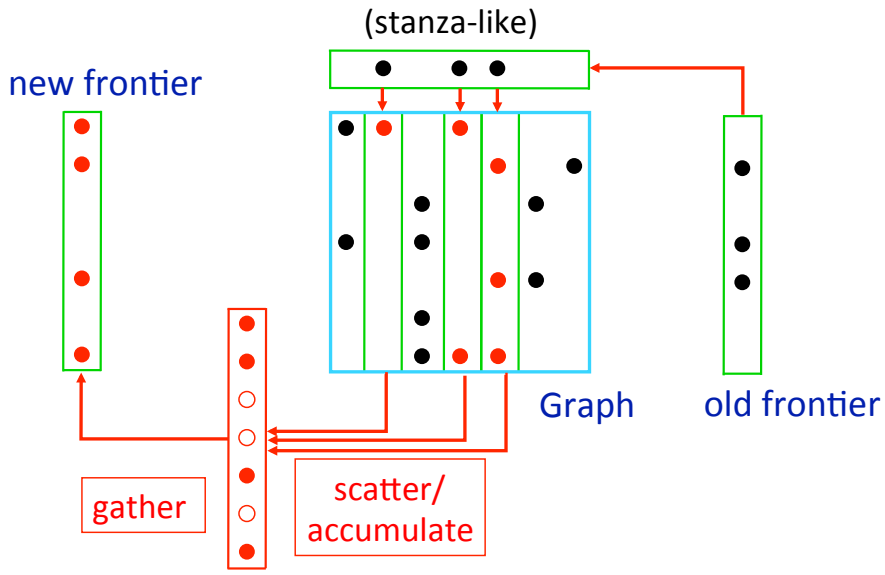

Figure 4.11: Memory access pattern of one BFS iteration. The graph is represented by the transpose of its sparse adjacency matrix. Each column in the matrix as well as each vector is stored in the compressed form of index-value pairs. In the case of frontier vectors, the pair represents (vertex index, parent's index).

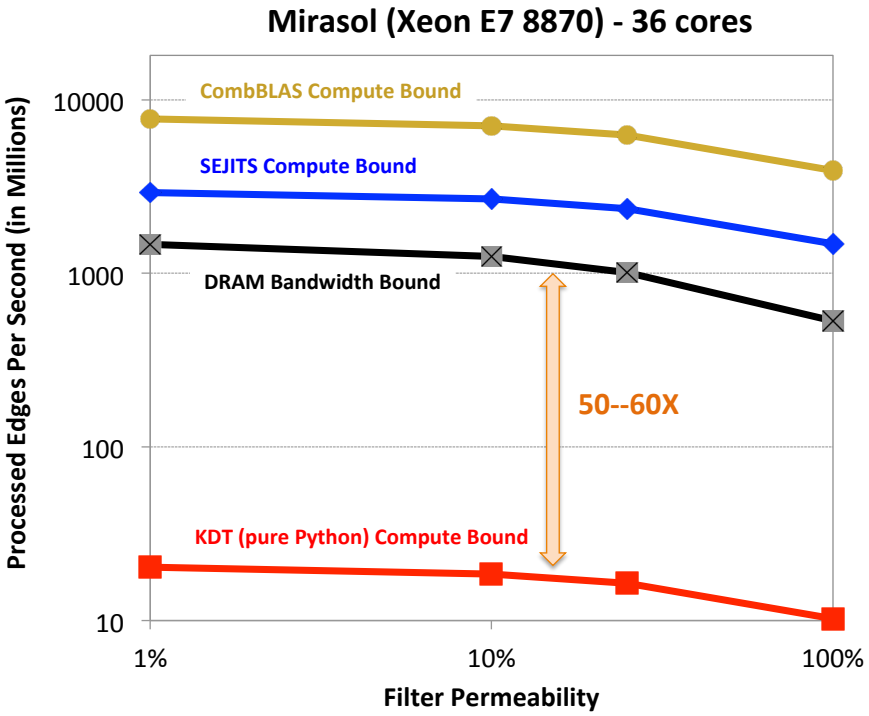

Figure 4.12: Roofline-inspired performance model for filtered BFS computations. Performance bounds arise from bandwidth, CombBLAS, KDT, or KDT+SEJITS filter performance, and filter success rate. The performance axis is in log-10 scale.

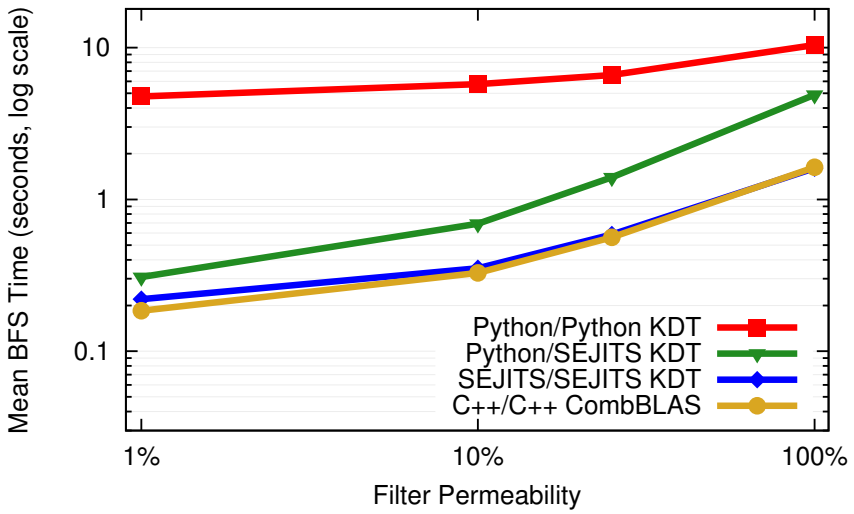

Figure 4.13: Relative breadth-first search performance of four methods on synthetic data (R-MAT scale 25). Both axes are in log scale. The experiments are run using 24 nodes of Hopper, where each node has two 12-core AMD processors. Time is mean of 16 BFS runs from different starting vertices. Notation: [semiring implementation]/[filter implementation].

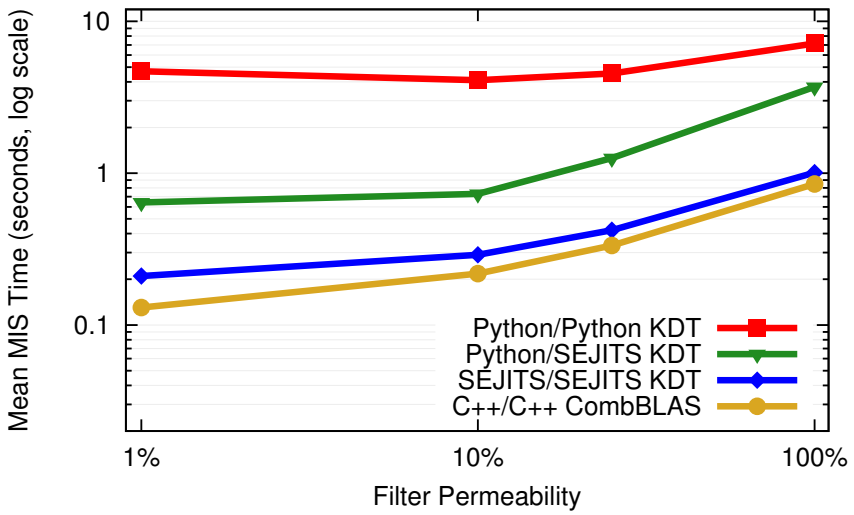

Figure 4.14: Relative maximal independent set performance of four methods on synthetic data (Erdős-Rényi scale 22). y-axis uses a log scale. The runs use 36 cores of Intel Xeon E7-8870 processors. Time is mean of 16 runs. Notation: [semiring implementation]/[filter implementation].

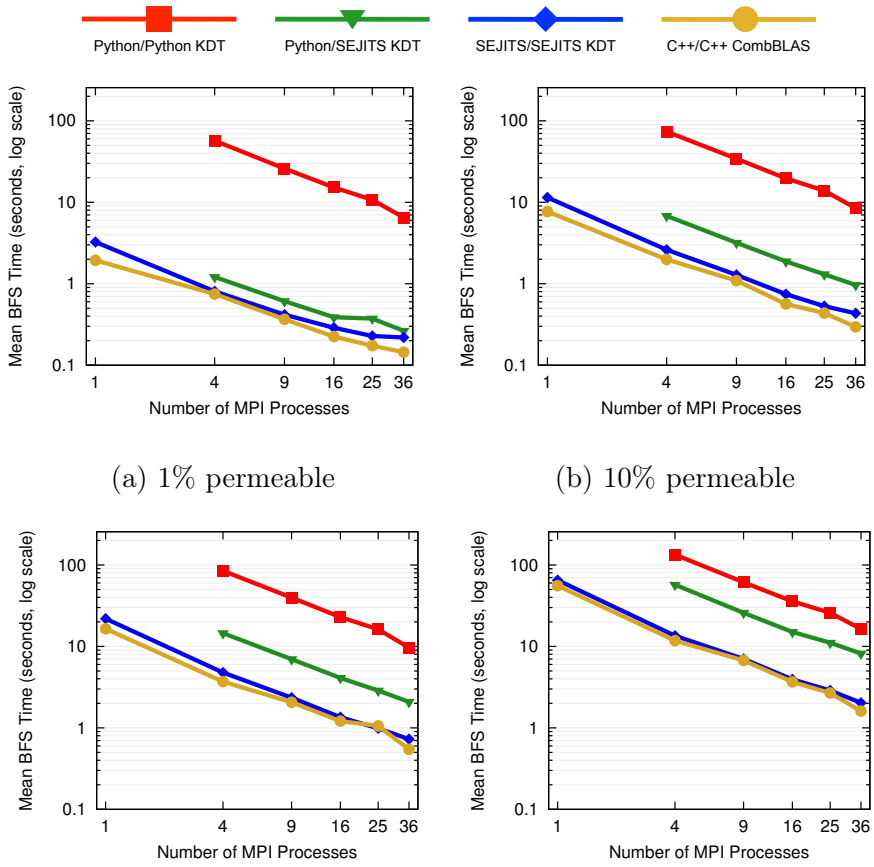

(a) 1% permeable

(b) 10% permeable

(c) 25% permeable

(d) 100% permeable

Figure 4.15: Parallel 'strong scaling' results of filtered BFS on Mirasol, with varying filter permeability on a synthetic data set (R-MAT scale 22). Both axes are in log-scale, time is in seconds (mean of 16 runs from different starting vertices). Single core Python/Python and Python/SEJITS runs did not finish in a reasonable time to report. Notation: [semiring implementation]/[filter implementation].

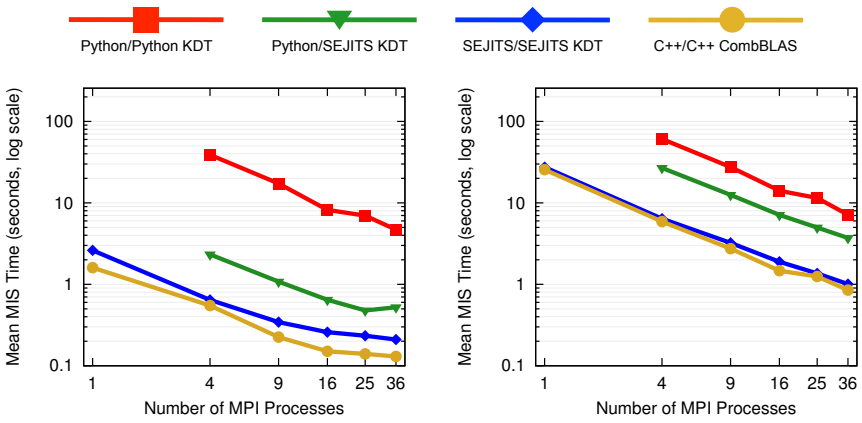

(a) 1% permeable (b) 100% permeable

Figure 4.16: Parallel 'strong scaling' results of filtered MIS on Mirasol, with varying filter permeability on a synthetic data set (Erdős-Rényi scale 22). Both axes are in log-scale, time is in seconds (mean of 16 runs). Notation: [semiring implementation]/[filter implementation].

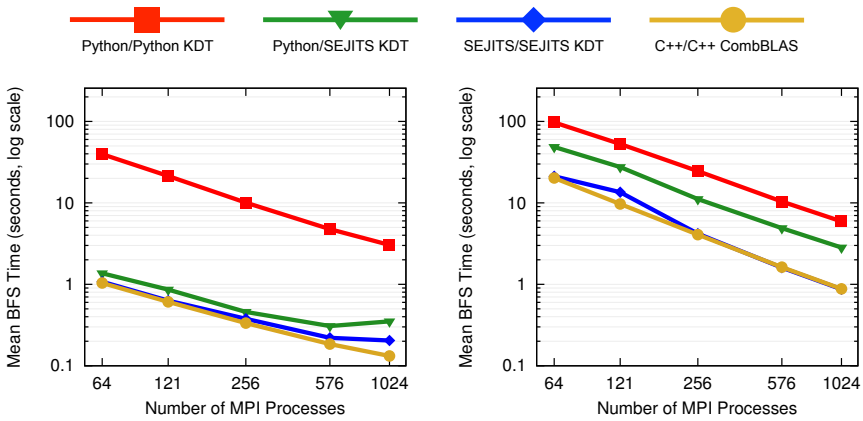

(a) 1% permeable (b) 100% permeable

Figure 4.17: Parallel 'strong scaling' results of filtered BFS on Hopper, with varying filter permeability on a synthetic data set (R-MAT scale 25). Both axes are in log-scale, time is in seconds (mean of 16 runs from different starting vertices). Notation: [semiring implementation]/[filter implementation].

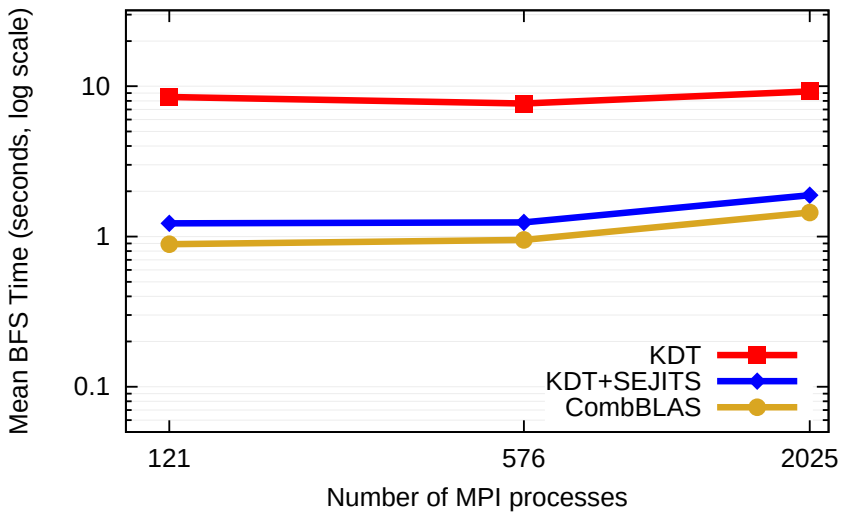

Figure 4.18: Parallel 'weak scaling' results of filtered BFS on Hopper, using 1% percent permeability. y-axis is in log scale, time is in seconds. From top to bottom, the methods are: high-level Python filters and semiring operations in KDT; high-level Python filters and semiring operations specialized at runtime by KDT+SEJITS; low-level C++ filters implemented as customized semiring operations and compiled into Combinatorial BLAS.

4.7.4 Performance on the Real Data Set

The filter used in the experiments with the Twitter data set considers only edges whose latest retweeting interaction happened before June 30, 2009, and is explained in detail in Section 4.5.1. Figure 4.19 shows the relative performance of three systems in performing breadth-first search on real graphs that represent the twitter interaction data on Mirasol. We chose to present 16-core results because that is the concurrency in which this application performs best, beyond which synchronization costs start to dominate due to the large diameter of the graph after the filter is applied. Since the filter-to-semiring-operations ratio is very high (on the order of 200 to 1000), SEJITS translation of the semiring operation does not change the running time. Therefore, we only include a single SEJITS line to avoid cluttering the plot. SEJITS/SEJITS performance is identical to the performance of CombBLAS in these data sets, showing that for real-world usage, our approach is as fast as the underlying high-performance library without forcing programmers to write low-level code.

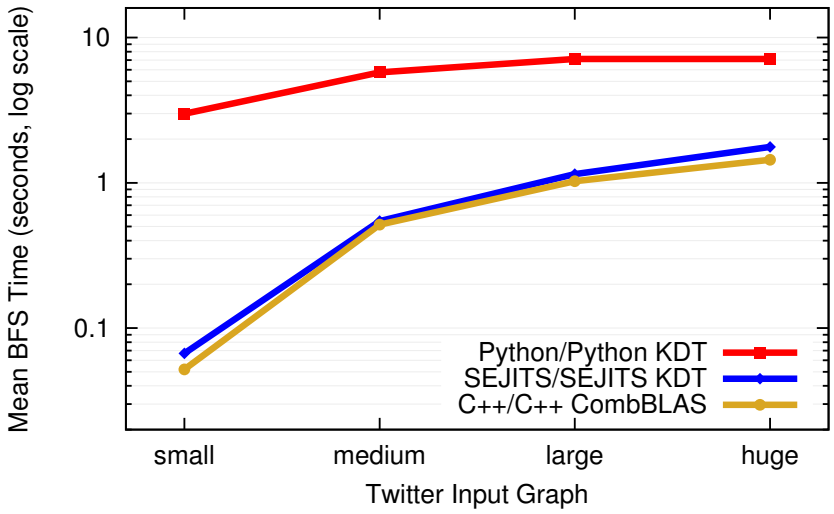

Figure 4.19: Relative filtered breadth-first search performance of three methods on real Twitter data. The y-axis is in seconds on a log scale. The runs use 16 cores of Intel Xeon E7-8870 processors.

4.8 Results From Hardware Performance Counters

The Performance Application Programming Interface (PAPI) library [4] provides direct access to low-level performance counters. These counters can measure performance attributes of a particular program execution. For example, PAPI counters can be used to measure the total number of instructions executed, or the total number of cache misses (L1 or L2, data or instruction).

Our study incorporates several PAPI performance counters to gain a detailed analysis of the performance benefits of KDT+SEJITS over Python KDT. We are particularly interested in the `PAPI_TOT_INS` (total instructions completed), `PAPI_L1_ICM` (number of L1 instruction cache misses), `PAPI_L1_DCM` (number of L1 data cache misses), and `PAPI_L2_TCM` (number of L2 total cache misses). Additional experiments with L3 cache misses did not provide any additional insights that were not already captured in the L2 cache analysis.

Performance counters were examined for our breadth-first search program on a scale 22 RMAT graph as described in Section 4.5, using both 10% and 100% permeable on-the-fly filters, repeating a BFS from a single starting vertex 16 times. These tests were conducted on Mirasol using 9 MPI processes, ensuring that all processes are placed on a single socket. Note that each part of each BFS iteration

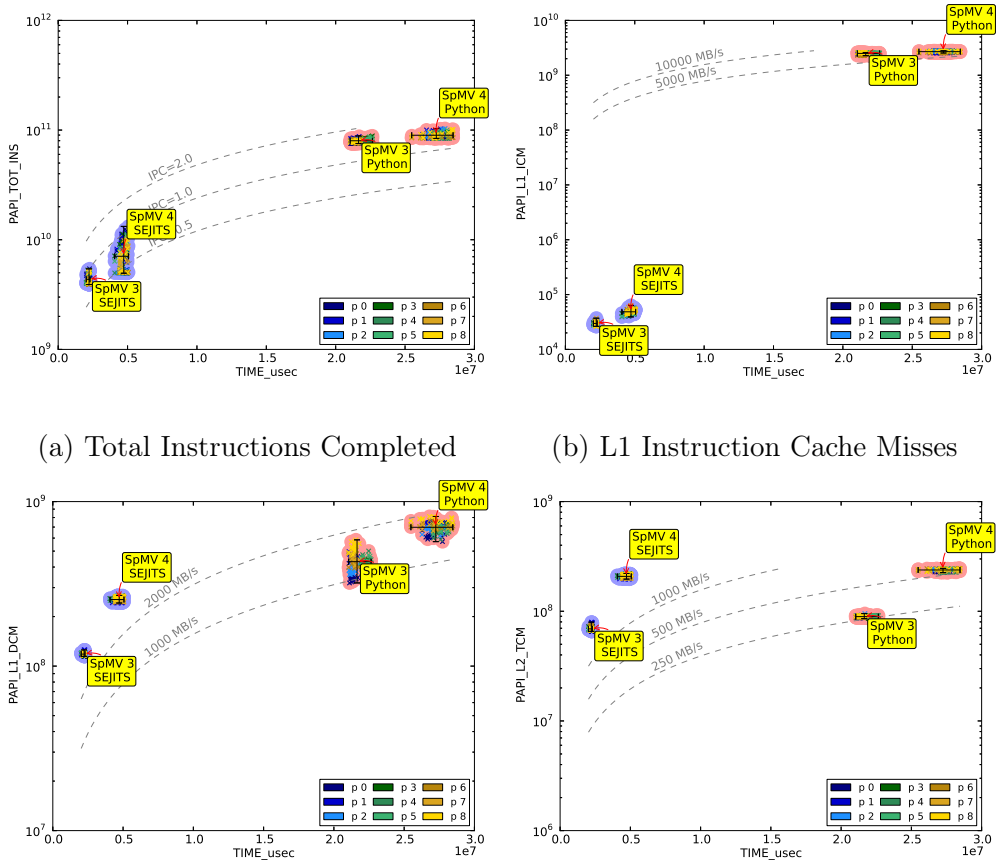

(a) Total Instructions Completed

(b) L1 Instruction Cache Misses

(c) L1 Data Cache Misses

(d) L2 Total Cache Misses

Figure 4.20: PAPI performance counters vs. time (in μs), showing (a) total instructions, (b) L1 instruction cache misses, (c) L1 data cache misses, and (d) total L2 misses. BFS on Scale 22 graph with 100% permeable filter, repeated 16 times from starting vertex 1726462. P=9 on Mirasol. Each point is a counter value for a single process in a single BFS iteration. Table 4.6 offers a summary of the same data in tabular form.

Table 4.6: PAPI measurements for 100% filter, showing (Time_usec) total time, (TOT_INS) total instructions, (L1_ICM) L1 instruction cache misses, (L1_DCM) L1 data cache misses, and (L2_TCM) total L2 misses. All values are the mean of 96 points (9 processes $\times$ 16 repeats). Figure 4.20 is a visual representation of this data.

	Time_usec	TOT_INS	L1_ICM	L1_DCM	L2_TCM
SpMV 3 Python	$2.16e+07$	$7.99e+10$	$2.50e+09$	$4.31e+08$	$8.94e+07$
SpMV 3 SEJITS	$2.22e+06$	$4.36e+09$	$2.98e+04$	$1.18e+08$	$6.91e+07$
SpMV 4 Python	$2.73e+07$	$8.97e+10$	$2.69e+09$	$6.98e+08$	$2.38e+08$
SpMV 4 SEJITS	$4.73e+06$	$7.07e+09$	$4.85e+04$	$2.54e+08$	$2.08e+08$
Other Python	$6.20e+04$	$3.13e+08$	$1.27e+06$	$2.90e+05$	$1.05e+05$
Other SEJITS	$4.39e+04$	$1.18e+08$	$3.93e+04$	$2.14e+05$	$1.00e+05$

is measured separately. The parts include the loop condition check, the SpMV, the frontier update and the parents vector update. Due to the small diameter of the input graph, nearly all the time is spent in two SpMV calls, during which the majority of the graph is explored.

Figures 4.20 and 4.21 present the performance counters data relative to runtime for the 100% and 10% filters, respectively. Only the most time-consuming SpMV calls are presented to keep from cluttering the plots. Each MPI process is represented by a different color as suggested by the legend. For a given colored dot, each occurrence in these plots correspond to a different BFS exploration

(out of 16 repeats), totaling 96 dots per operation. We clustered all the points corresponding to a particular operation into a point cloud for ease of visualization.

In addition, Table 4.6 and Table 4.7 provide the same information in tabular form for 100% and 10% filters, but only showing the mean of the 96 points. The tables also include an "Other" category that combines all overheads except the two SpMVs, which account for a small overall fraction of runtime (two orders of magnitude less time than SpMVs). Note that we shorten "KDT+SEJITS" to "SEJITS" and "Python/Python" to "Python" for brevity.

Table 4.7: PAPI measurements for 10% filter, showing (Time_usec) total time, (TOT_INS) total instructions, (L1_ICM) L1 instruction cache misses, (L1_DCM) L1 data cache misses, and (L2_TCM) total L2 misses. All values are the mean of 96 points (9 processes $\times$ 16 repeats). Figure 4.21 is a visual representation of this data.

	Time_usec	TOT_INS	L1_ICM	L1_DCM	L2_TCM
SpMV 3 Python	$1.63e+07$	$5.97e+10$	$1.86e+09$	$1.78e+08$	$2.01e+07$
SpMV 3 SEJITS	$6.58e+05$	$1.08e+09$	$2.46e+04$	$2.48e+07$	$1.66e+07$
SpMV 4 Python	$9.61e+06$	$3.59e+10$	$1.13e+09$	$1.14e+08$	$1.67e+07$
SpMV 4 SEJITS	$5.39e+05$	$8.13e+08$	$2.47e+04$	$2.09e+07$	$1.48e+07$
Other Python	$4.32e+04$	$1.73e+08$	$3.03e+06$	$3.68e+05$	$8.57e+04$
Other SEJITS	$3.96e+04$	$1.03e+08$	$3.60e+04$	$1.67e+05$	$8.75e+04$

These figures underscore the dramatic performance benefits of the SEJITS approach. In the 100% filter run (Figure 4.20), the SEJITS versions incur over

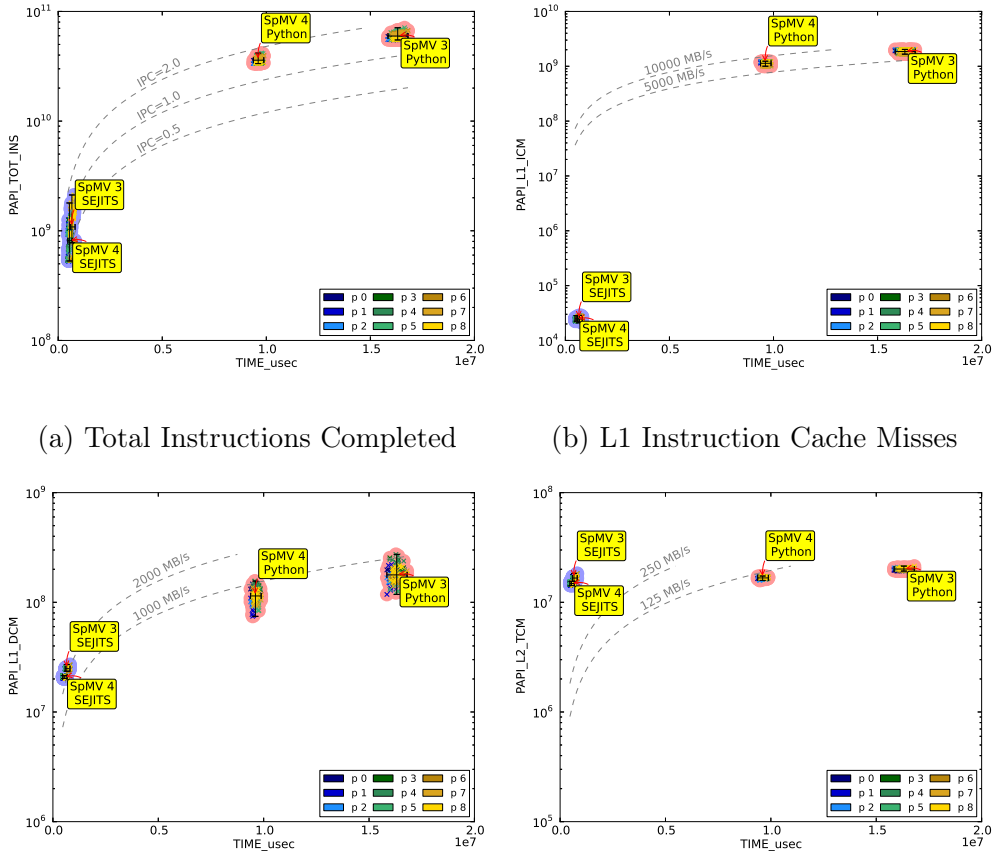

(a) Total Instructions Completed

(b) L1 Instruction Cache Misses

(c) L1 Data Cache Misses

(d) L2 Total Cache Misses

Figure 4.21: PAPI performance counters vs. time (in μs). BFS on Scale 22 graph with 10% permeable filter, repeated 16 times from starting vertex 1291427. P=9 on Mirasol. Each point is a counter value for a single process in a single BFS iteration. Table 4.7 offers a summary of the same data in tabular form.

an order of magnitude fewer total instruction completions, as well as four orders of magnitude fewer L1 instruction cache misses. The Python callbacks require a wrapper object, while their SEJITS counterparts do not. This results in a further half-order of magnitude fewer L1 data cache misses. The benefits are even larger for the 10% filter run, as shown in Figure 4.21. The L2 total cache misses are nearly same for both approaches, indicating that the majority of the performance impact between SEJITS and pure Python approaches is captured within the L1 cache. This can be visually observed in the L2 total cache misses (d) plots, where the SEJITS and Python clusters for SpMV 3 and SpMV 4 are on the same horizontal line.

The only performance cost for SEJITS is the JIT compilation, incurred on the first execution of a kernel which uses SEJITS callbacks. All our kernels use a SEJITS callback, which amounts to about 20 seconds for just the first iteration. Since the results of the JIT compilation are cached even between independent jobs, this cost is only paid the first time the script is run.

4.9 Related Work

Graph Algorithm Packages

Pegasus [55] is a graph-analysis package that uses MapReduce [31] in a distributed-computing setting. Other cloud-based graph analysis systems include GPS [94], and Apache Hama [3], and Giraph [2]. Redekopp et al. [93] recently studied performance optimizations for such cloud-based graph platforms.

Pegasus [55], uses a generalized matrix-vector multiplication primitive called `GIM-V`, much like KDT's `SpMV`, to express vertex-centered computations that combine data from neighboring edges and vertices. In Pegasus, the semiring multiply is referred to as combine2 and the semiring add is referred to as combineAll, followed by an assign operation.

Powergraph [48] advocates a similar GAS (gather-apply-scatter) abstraction for graph-parallel computations. This style of programming is called "think like a vertex" in Pregel [78], a distributed-computing graph API. In traditional scientific computing terminology, these are all BLAS-2 level operations; none of these aforementioned systems currently include KDT's BLAS-3 level `SpGEMM` "friends of friends" primitive. BLAS-3 operations are higher level primitives that enable more optimizations and generally deliver superior performance. Both Pegasus and

Powergraph require the application to be written in a relative low-level language (Java and C++, respectively) and neither supports filtering.

Other libraries for high-performance computation on large-scale graphs include the Parallel Boost Graph Library (PBGL) [50], the Combinatorial BLAS [24], Georgia Tech's SNAP [11], and the Multithreaded Graph Library (MTGL) [14]. These are all written in C/C++ and with the exception of the PBGL and MTGL do not include explicit filter support. The first two support distributed memory as well as shared memory while the latter two require a shared address space. PBGL and MTGL provides generic filter support via visitor functions. PBGL also supports an explicit FilteredGraph concept. Since PBGL and MTGL are written in C++ with heavy use of template mechanisms, they are not conceptually simple to use by domain scientists. By contrast, our approach targets usability by specializing algorithms from a high-productivity language.

SPARQL [91] is a query language for Resource Description Framework (RDF) [61], which supports semantic graph database queries. The existing database engines that implement SPARQL and RDF handle filtering based queries efficiently but they are not as effective for running traversal based tightly-coupled graph computations scalably in parallel environments.

The closest previous work is Green Marl [53], a domain specific language (DSL) for small-world graph exploration that runs on GPUs and multicore CPUs with-

out support for distributed machines (though such support is planned). Green Marl supports a very different programming model than KDT. In Green Marl, programmers iterate over nodes/edges or access them in specific traversal orders; work can be accomplished within a traversal or iteration step. KDT's underlying linear algebra abstraction allows graph algorithms to be implemented by customizing generic high-performance primitives of CombBLAS. In addition, the approach of Green Marl is to use an external DSL that has a different syntax and compiler than the rest of an application; KDT allows users to write their entire application in Python.

JIT Compilation of DSLs

Embedded DSLs [38] for domain-specific computations have a rich history, including DSLs that are compiled instead of interpreted [65]. Abstract Syntax Tree introspection for such DSLs has been used most prominently for database queries in ActiveRecord [1], part of the Ruby on Rails framework.

The approach applied here, which uses AST introspection combined with templates, was first applied to stencil algorithms and data parallel constructs [27], and subsequently to a number of domains including linear algebra and Gaussian mixture modeling [54].

Finally, general JIT approaches for Python such as PyPy [5] do not offer the advantages of embedded DSLs such as domain-specific optimizations and the lack of need to perform detailed domain analysis.

4.10 Conclusion

The KDT graph analytics system achieves customizability through user-defined filters, high performance through the use of a scalable parallel library, and conceptual simplicity through appropriate graph abstractions expressed in a high-level language.

We have shown that the performance impact of expressing filters in a high-level language like Python can be mitigated by Selective Embedded Just-in-Time Specialization. In particular, we have shown that our embedded DSLs for filters and semirings enable Python code to achieve comparable performance to a pure C++ implementation. In addition, we provide users with the ability to define new vertex and edge types from Python, yet still obtain the same high performance. A Roofline analysis shows that specialization enables filtering to move from being compute-bound to memory-bandwidth-bound. Further performance-counter-based analysis shows that the SEJITS performance gains are due to a combination of executing fewer instructions and the ability to avoid data move-

ment for object wrappers during computation. We demonstrated our approach on both real-world data and large synthetic datasets. Our approach scales to graphs on the order of hundreds of millions of edges, and to machines with thousands of processors, suggesting that our methodology can be applied to even more computationally intensive graph analysis tasks in the future. Ultimately, the ability to both attain high performance and scale to thousands of cores for most cases makes it possible for domain scientists to efficiently utilize large-scale clusters and supercomputers.

In future work we will further generalize our DSL to support a larger subset of Python, as well as expanding SEJITS support beyond filtering and semiring operations to cover more KDT primitives. An open question is whether CombBLAS performance can be pushed closer to the bandwidth limit by eliminating internal data structure overheads.

Chapter 5

Shared Memory Sparse Matrix-Sparse Matrix Multiplication

This chapter is based on a technical report [75] and an extended abstract published in CSC'14 [76].

5.1 Introduction

Sparse matrix-matrix multiplication (or *SpGEMM*) is a key primitive in some graph algorithms (using various semirings) [57] and in numeric problems such as algebraic multigrid [98]. Multicore shared memory systems can solve very large problems [99], or can be part of a hybrid shared/distributed memory high-performance architecture.

Two-dimensional decompositions are broadly used in state-of-the-art methods for both dense [104] and sparse [22, 24] matrices. Quadtree matrix decompositions and algorithms have a long history [40, 41, 95, 109, 110], including recursive matrix multiplication [108].

In this chapter we describe a new sparse matrix data structure and the first highly-parallel sparse matrix-matrix multiplication algorithm designed specifically for shared memory.

5.2 Quadtree Representation

Our basic data structure is a 2D quadtree matrix decomposition. Unlike previous work that continues the quadtree until elements become leaves, we instead terminate the quadtree early and store the elements in large leaf blocks. This arrangement brings the best of both worlds; the quadtree provides isolation and chunking, and the large leaf blocks provide locality and a way to amortize tree costs.

There are many answers to the question of when to stop subdivision. We use a simple strategy: subdivide until either leaf nnz or leaf size in bytes is below a threshold. This threshold can be fixed or dynamically chosen to provide sufficient parallelism for a particular matrix on a particular machine. The former approach

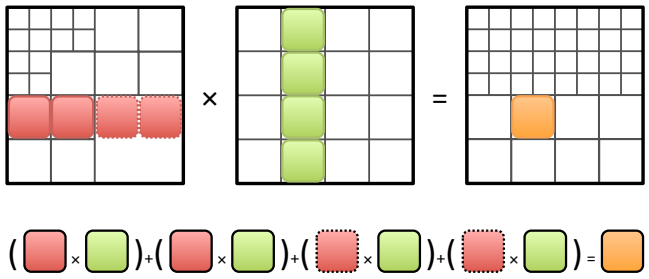

Figure 5.1: Computation of a result block using a list of pairwise block multiplications.

aims at efficient utilization of fixed resources such as caches, while the latter method aims to minimize the number of hypersparse blocks and total per-block overhead.

Inner blocks form the internal nodes of the quad tree. Each inner block is a container for four other blocks. Each child can be null, a leaf, or another inner block, and represents one quadrant of the parent inner block. Note that subdivisions always occur on powers of 2; hence, position in an inner block implies the high-order bits of row and column indices of the children. This allows the leaves to use smaller indices than the matrix dimensions appear to require. We do not, however require the matrix to have dimensions that are powers of 2.

The leaf blocks store the matrix elements in $(row, col, value)$ triples form. Row and column indices can be 8, 16, 32 or 64-bit unsigned integers, where the

minimum index size that fits the block dimensions is chosen at runtime. The type of the values is defined by the user.

A shadow block is a block that provides a view of a subset of a TriplesBlock's elements. This is useful when the blocks of two different quadtrees need to be matched. Depending on the two trees' decompositions, an inner block may be matched with a leaf block. If this is undesirable, we may perform a *shadow subdivision* of the leaf block.

In a shadow subdivision a new inner block is created and populated with four shadow blocks that together return the same data as the original TriplesBlock. The original TriplesBlock's elements are scanned once, and the shadow each one belongs to is determined with a simple bit comparison of its row and column indices. A shadow block doesn't own its data; rather it is a view of a part of another leaf block. Its data structure is a pointer to the original TriplesBlock and an array of offsets of each element. It and its parent inner block are considered temporary and are expected to be destroyed by the end of the operation that created them. For the purposes of read-only algorithms, a shadow block *is* a leaf block.

In our implementation, a shadow block with nnz nonzeros consists of an $O(nnz)$ space array of indices into the original TriplesBlock. Another possible scheme is to partially sort the TriplesBlock into four quadrants, which allows each

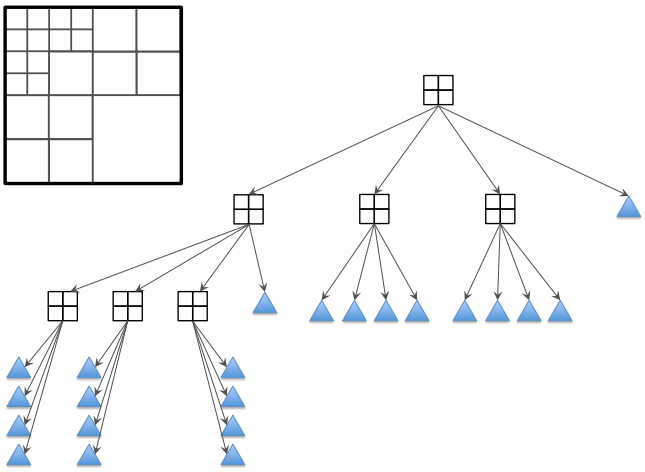

Figure 5.2: Quadtree of an adjacency matrix of a power law graph. This is matrix A in our running example in Figure 5.6.

shadow block to simply be an $O(1)$-space begin and end bound. This method has two problems. First, the partial sort is more expensive than a scan. Second, the original TriplesBlock is no longer in pure column order, which makes accessing its elements both more expensive and more complicated when this block is part of several tasks. Both problems can be solved by using Z-Morton order [85] instead of column order, which allows arbitrarily deep subdivisions. Z-Morton order, however, does not provide $O(1)$ lookups by row or column indices, which makes the sparse multiplication kernels asymptotically more expensive.

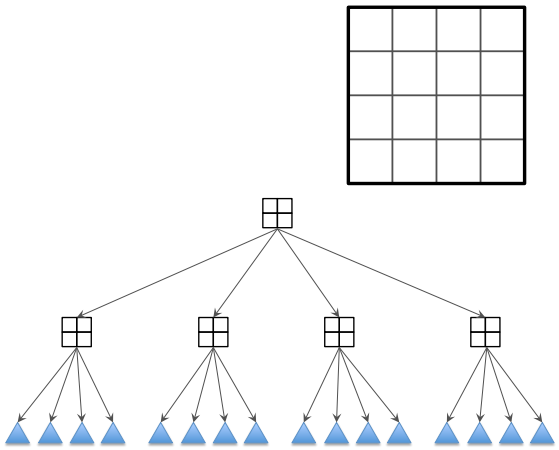

Figure 5.3: Quadtree of an adjacency matrix of an Erdős-Rényi graph. This is matrix B in our running example in Figure 5.6.

5.3 Pair-List Matrix Multiplication Algorithm

The quadtree decomposition suggests a natural recursive SpGEMM algorithm: recursively evaluate the following:

$$\begin{aligned} C_4 &= (A_1 \times B_1) + (A_2 \times B_3) \\ C_2 &= (A_1 \times B_2) + (A_2 \times B_4) \\ C_3 &= (A_3 \times B_1) + (A_4 \times B_3) \\ C_4 &= (A_3 \times B_2) + (A_4 \times B_4) \end{aligned} \tag{5.1}$$

This algorithm has a serious flaw, however. Each level of the recursion introduces a sparse matrix addition (SpAdd) operation in addition to the recursive multiplies. When thought of as a DAG of tasks, the multiplies are the leaves of a large tree of

SpAdds. The number of SpAdds each block is involved in is equal to its depth in the tree. Unfortunately, there is no known method to perform an SpAdd in time proportional to only the FLOPs required. Instead, the total time of all additions is proportional to total FLOPs plus the size of the operands times the height of the tree. The add tree therefore imposes an unwanted log factor and becomes a significant bottleneck. Our algorithm reformulates the operations such that the SpAdds can be inlined into the leaf multiplies.

The algorithm consists of a symbolic phase and a computational phase. The *symbolic phase* generates an execution strategy, and the computational phase carries out that strategy. Each phase is itself a set of parallel tasks. We are willing to temporarily reorganize data on-the-fly, and discard the changes after use. This extra work does not add to the asymptotic complexity.

The source of parallelism of both phases comes from the recursive structure of the quadtree of C. Each internal node yields a symbolic phase task, and each leaf yields a computational phase task.

We choose to formulate a DAG of tasks and let a scheduling framework map those tasks to threads. Our algorithm does not perform scheduling; rather, we use a standard scheduling framework such as TBB, Cilk, or OpenMP.

5.3.1 Symbolic Phase

The symbolic phase divides computation of $C = A \times B$ into compute tasks such that each compute task *owns* (is the only writer to) a particular block of C and is supplied with a list of all the operands it needs to perform the multiplication.

Let C_{own} be a leaf block in C, and *pairlist* be the list of pairs of leaf blocks from A and B whose block inner product is C_{own}:

$$C_{own} = \sum_{i=1}^{|pairlist|} A_i \times B_i \tag{5.2}$$

The blocks A_i and B_i may be original leaf blocks or shadow blocks. The symbolic phase recursively determines all the C_{own} and corresponding *pairlist*. Equation (5.2) still contains additions, but in Section 5.3.3 we describe a method to evaluate (5.2) without explicit SpAdd steps.

To provide intuition for what we wish to accomplish, consider a dense $\beta \times \beta$ grid of blocks instead of a quadtree. The result matrix will contain β^2 blocks, each one the result of a block inner product between the corresponding block row of A and block column of B. The i^{th} block in the block row of A is matched with the i^{th} block in the block column of B in this block inner product. Therefore, we describe this block inner product with a list, named *pairlist*, with length β of pairs of blocks.

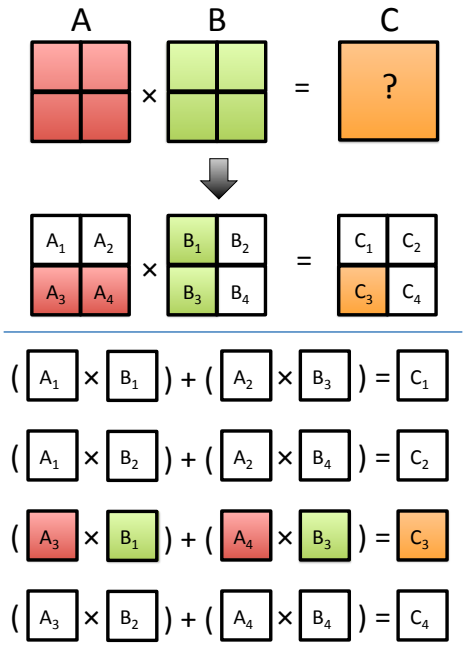

Figure 5.4: Illustration of Equation (5.3).

We now wish to accomplish the same task, but with two differently structured quadtrees of blocks instead of a dense grid. Different pairlists can have blocks of different sizes, though all the blocks in one pairlist are the same size. An element of an input matrix may participate in several pairlists with different block sizes, via shadow blocks.

The PairList algorithm's symbolic phase recursively determines all the C_{own} and corresponding *pairlist*. We begin with $C_{own} \leftarrow C$, and *pairlist* $\leftarrow [(A, B)]$.

If *pairlist* consists only of leaf blocks, spawn a compute task with C_{own} and *pairlist*.

If all the blocks in *pairlist* are divided, we divide C_{own} into four children with one quadrant each and recurse, rephrasing divided $C = A \times B$ using (5.2):

$$\begin{aligned} C_1 &= [(A_1, B_1), (A_2, B_3)] \\ C_2 &= [(A_1, B_2), (A_2, B_4)] \\ C_3 &= [(A_3, B_1), (A_4, B_3)] \\ C_4 &= [(A_3, B_2), (A_4, B_4)] \end{aligned} \tag{5.3}$$

In total, each recursive call receives a C_{own} and an entire list of pairs of blocks. For every pair in *pairlist*, insert two pairs into each child's *pairlist* according to the respective line in (5.3). Each child's *pairlist* is twice as long as the parent's *pairlist*, but totals only 4 sub-blocks to the parent's 8.

If *pairlist* includes both divided blocks and leaf blocks, we temporarily divide the leaves until all blocks in *pairlist* are equally divided. This temporary division creates shadow blocks as described in Section 5.2. Shadow subdivision resolves any differences in quadtree depth between the operands. It allows the symbolic phase to recurse until only leaves remain, which lets the compute phase only operate on leaves. See Figure 5.5 for an example. The shadow blocks persist only until the end of the SpGEMM.

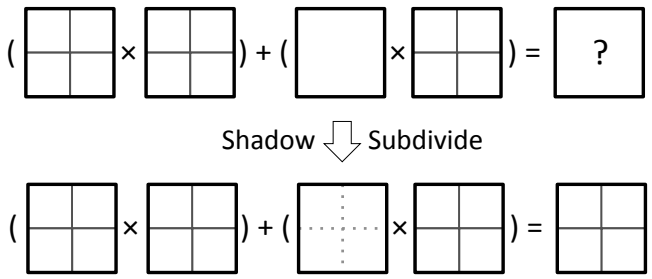

Figure 5.5: Division mismatch: a leaf block is paired with an inner block. A shadow subdivision of the leaf block yields an inner block that resolves the mismatch and allows another recursive step.

5.3.2 Symbolic Phase Example

We illustrate the symbolic phase of a multiplication of two matrices by tracing how two result blocks' pair lists are generated. We use the running example in Figure 5.6. Operand A is more dense in a corner as might appear in an adjacency matrix of a power law graph. Operand B shows a uniform subdivision, as might appear in an adjacency matrix of an Erdős-Rényi [36] graph. Their respective quadtrees are illustrated in Figures 5.2 and 5.3.

In the figures, leaf blocks and compute tasks are denoted with rounded corners; shadow blocks and shadow subdivisions are denoted with dotted lines.

Both traces share the same root symbolic task. This task is initialized with the full problem: $pairlist = [(A, B)]$ and $C_{own} = C$. It sees that all blocks in

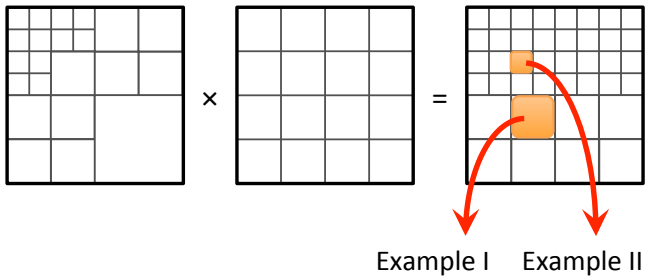

Figure 5.6: The running example. We wish to multiply an RMAT matrix with an adjacency matrix of an Erdős-Rényi graph. The quadtree for the RMAT is shown in Figure 5.2, and the ER in Figure 5.3.

pairlist are subdivided, so the recursive case applies. C_{own} is subdivided and a matching *pairlist* is generated according to (5.2) (as illustrated in Figure 5.4). Four new symbolic tasks are spawned, one for each newly divided C_{own} child. Our two traces diverge here; each one follows the recursive call on a different child.

Example Trace I follows the third (bottom left) child. It is fully illustrated in Figure 5.7. The second level symbolic task has a *pairlist* that consists of three inner blocks and one leaf. This requires a shadow subdivision of the leaf. The recursion then continues, spawning four more symbolic tasks. Each one of these four consists of only leaves, so they simply spawn compute tasks.

Example Trace II follows the first (top left) child of the root symbolic task. This trace is fully illustrated in Figure 5.8. The second level symbolic task has a *pairlist* that consists of all inner blocks, so the recursive case is trivially applied

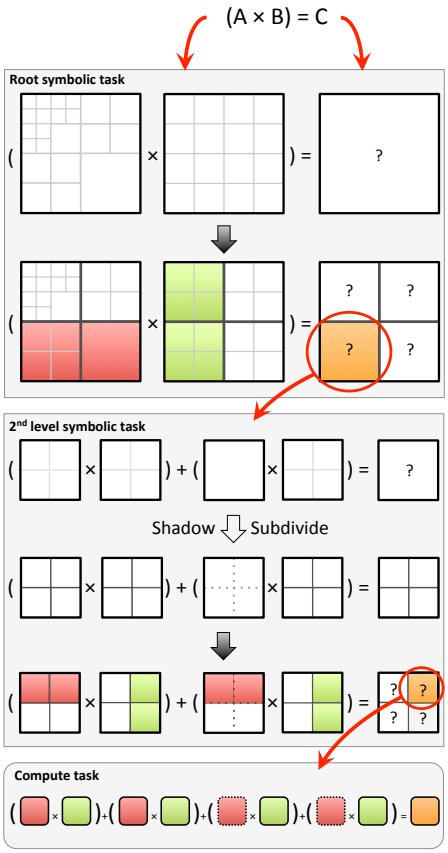

Figure 5.7: Example Trace I: The root symbolic task applies the recursive case. The next recursive symbolic task has a mix of inner block and leaves, so performs a shadow subdivide. The next recursion are all leaf tasks, so are turned into compute tasks.

again. This spawns four more symbolic tasks, and we choose to follow the fourth (bottom right) child. This third level symbolic task has a *pairlist* with one inner block and seven leaves. The leaves must be shadow subdivided so another recursive case can be applied. These recursive children contain only leaves. Some are

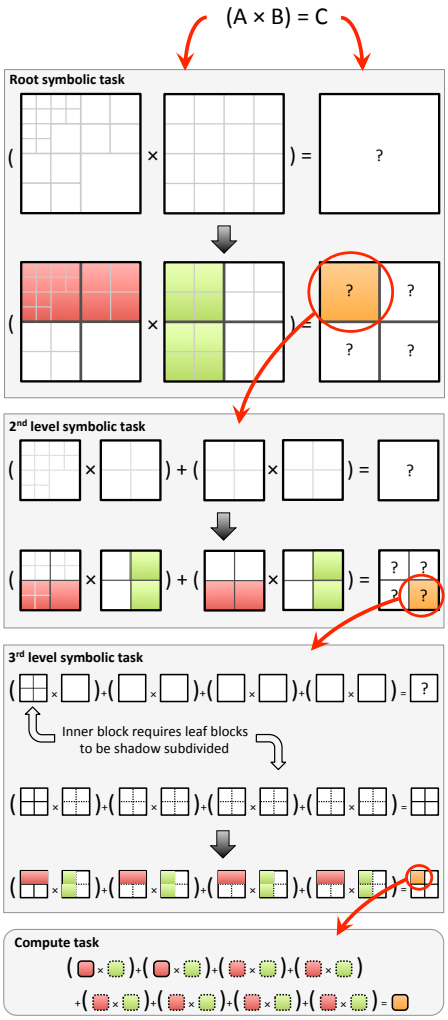

Figure 5.8: Example Trace II: Trace that requires 3 levels of symbolic tasks.

original leaves, corresponding to the most dense part of A. The rest are shadows, both from less dense parts of A, and from the generally less dense B. The final recursion, then, can spawn compute tasks.

5.3.3 Computational Phase

This phase consists of tasks that each compute one block inner product (5.2). We present the final approach in Algorithm 2 and describe it below. Observe that each compute task is lock-free because it only reads from the blocks in *pairlist* and only writes to C_{own}.

We extend Gustavson's sequential sparse matrix multiplication algorithm [51]. Gustavson computes the product of column j of B and A using a "sparse accumulator", or *SPA*. The SPA can be thought of as a dense auxiliary vector, or hash map, that efficiently accumulates sparse updates to a single column of C_{own}. Gustavson's algorithm reads both A and B column-by-column, but their columns are selected differently. The algorithm reads the non-empty columns of B in order, but performs random lookups of columns in A. To facilitate these access patterns for our $(row, col, value)$ triples storage, we *organize* the column-sorted triples. A *column organizer* is an auxiliary structure that allows quick access to particular columns of a block. Due to different access patterns for blocks A and B, we organize them differently.

Algorithm 2 Compute Task's Multi-Leaf Multiply

Require: C_{own} and $pairlist$
Ensure: Complete C_{own}
  for all (A_b, B_b) in $pairlist$ **do**
    organize A_b columns with hash map or CSC
    organize B_b columns into list
  end for
  merge all B organizers into $combined\_B\_org$
  for all (column j, $PairList_j$) in $combined\_B\_org$ **do**
    $SPA \leftarrow \{\}$
    for all (A_b, B_b) in $PairList_j$ **do**
      for all non-null k in column j in B_b **do**
        accumulate $B_b[k, j] \times A_b[:, k]$ into SPA
      end for
    end for
    copy contents of SPA to $C_{own}[:, j]$
  end for

The first type of column organizer is designed for constant-time lookup of a particular column i in A. We provide two methods to achieve this. The first is a hash map with an entry $i \rightarrow (\mathit{offset}_i, \mathit{length}_i)$ for each non-empty column i. The second is a CSC-like array of offsets of the first element of a column. Both offer $O(1)$ lookups of a particular column i, but the CSC-like method trades a faster constant for $O(n)$ space.

The second type of column organizer allows iteration over non-empty columns B. We generate a list of tuples $(j, \mathit{offset}_j, \mathit{length}_j)$.

All column organizers are generated with a single scan of only the column indices. Therefore each one takes linear time to generate. For maximum parallelism, the organizers can be generated in each compute task. This means each block is organized many times, once by each compute task it is used in. This cost is negligible for small to medium matrices, but can be greatly reduced by caching the organizers.

The column organizers allow us to efficiently use Gustavson's algorithm on our triples to evaluate the multiplies in (5.2). We show that if all pairwise block multiplies in a computational task are performed simultaneously then they can be interleaved in such a fashion that the addition step is inlined into the multiply step.

The key to this inlining is the SPA. Gustavson uses the SPA to accumulate the sparse updates to a single column j of C_{own}. Observe that in a blocked algorithm every non-null column j in any B in the pair list will lead to its own SPA for column j of that pair's partial result. The add step's only function is to accumulate all the partial column j results into one. Our key contribution is to do all updates to column j together, allowing us to use the same SPA for them all. Since there are no further updates to column j, no add step is necessary.

Another way to picture this process is to observe that the A blocks represent a short-and-fat slice of the matrix A, and the B blocks represent a tall-and-skinny

slice of the matrix B. C_{own} is the inner product of these two slices. When the slices are thought of as whole matrices, this inner product already handles the addition properly. Our contribution can be thought of as virtually merging the A and B blocks into such slices.

Our addition to Gustavson is a mechanism that combines columns j from all blocks B_i in *pairlist* to present a view of the entire column j from matrix B. This *organizer combiner* is like the second column organizer, but generalized to cover the non-empty columns in *all* blocks B instead of just one. We accomplish this with a structure that combines the B organizers with the property that all entries of column j are together.

We supply two ways to implement an organizer combiner. First is an ordered multi-map of $j \to (B_{source}, \mathit{offset})$. We fill the multimap from each B organizer. The second is a dense 2D array of the same entries as the multi-map values. This method escapes a $\log n$ insert time at the cost of higher space usage.

Our extensions to Gustavson therefore consist of column organizers, a column organizer combiner, and finally an interleaving of inner products of multiple block pairs.

We draw the reader's attention to a pattern in our auxiliary data structures: we provide two versions for each structure that requires random access. The traditional implementations of these structures use a dense array (like CSC column

pointers or a dense vector SPA), and are the only part of the QuadMat data structure and SpGEMM implementation that depend on the matrix dimensions m or n. This approach works superbly for matrices with dimensions small enough for these structures to fit in available memory. However, we wish to break this dependency in order to support huge matrix dimensions. We therefore always provide an alternative structure that has the same $O()$ time complexity (but with a higher constant) that does not depend on the matrix dimensions. The choice of which version to use is made at runtime.

Our dense SPA is similar to the traditional one [43]. It consists of two arrays of length m. The first, *vals* is the actual values (such as doubles). The second is an array of full/empty bits. Lastly, a *used_elements* array lists the i where $vals[i]$ is full. Our alternative SPA implementation uses a hashmap $i \rightarrow (val)$ instead of the dense arrays.

5.3.4 Post Processing

The symbolic and compute phases produce a valid result, but this result might not be subdivided appropriately. If this is undesirable, a *post-processing* phase can correct the problem.

If a resulting block is too dense, *i.e.* its $nnz > threshold$, it needs to be subdivided. A subdivision resembles a shadow subdivide, but the result is permanent.

This subdivision can be done by a single task as soon as the compute task finishes building the result.

If a resulting block is too sparse, *i.e.* the total nnz of it and its siblings $\leq threshold$, it needs to be coalesced with its siblings in the quadtree. Coalescing is the opposite of subdivision and can only be attempted after all children of a result inner block are computed. Coalescing also needs to be performed recursively up the quadtree; it is possible that the entire result matrix is nearly empty and needs to be coalesced into a single block.

5.4 Choice of Division Threshold

QuadMat has a tuning parameter in the form of the subdivision strategy. In this work it is the value of the division threshold as explained in Section 5.2.

In our experiments, we decided to avoid hand-tuning individual SpGEMM problems by using a one-size-fits-all algorithm to choose a threshold for a particular problem. We only allow ourselves to use information known at the start of the problem, namely the processing environment and the dimensions and nonzero count of the operands. An optimal algorithm is a matter of ongoing research, but for the purposes of these experiments we make an educated guess and choose a division threshold=$\max(50k, largest\_nnz/80)$.

The choice of division threshold has wide ramifications. The threshold determines the parallelism of the computation. At one extreme, if we set the threshold=nnz, the entire matrix is one single leaf block and potential parallelism is 1. At the other extreme we have a very small threshold with immense potential parallelism due to the fact that the compute blocks are independent. This, however, leads to an increase in the number of blocks and block overhead, mainly column organization, and an increase in the likelihood that each block is *hypersparse* ($nnz \ll n$).

The increased cost of column organization is mainly due to the fact that this preliminary work does not yet implement organizer caching. Observe that each block is used in many compute tasks. Without caching, each compute task performs its own organization of its operands. This leads to duplicate work, and becomes significant on some problems with small thresholds. This is the primary reason why we chose a relatively large threshold. When ongoing work in caching is complete we expect to be able to remove this restriction.

A smaller division threshold also leads to each block becoming less dense. To illustrate, assume that matrix M with dimensions n has an average of c nonzeros per column, or $nnz = cn$. As we divide each column into b blocks, each block owns c/b column nonzeros. As b increases with the division threshold, the nonzero count of each block approaches 0 and the block becomes hypersparse.

Hypersparse blocks have two important consequences. First, the dense structures (organizers, SPA) that depend on n and not on nnz become inefficient. CombBLAS solves this problem by using a *Doubly-Compressed Sparse Columns* (DCSC) datastructure, which is CSC with the column pointers compressed.

Second, hypersparse block inner products have lower utility for every lookup into A. Recall that the heart of the compute phase is "accumulate $B_b[k, j] \times A_b[:, k]$ into *SPA*". In an undivided M each nonzero with row k in B will look up column k in A once. This column may be empty (a miss), but assume it has c nonzeros. The algorithm then accumulates all c elements into the SPA. If we do the same on a divided M, column k is now in b parts. In total, there will now be b lookups instead of one, but the same number of accumulation operations to amortize the cost.

The hypersparse effect can be reduced with prevention and mitigation. Prevention means increasing the division threshold. In practice this likely means that the optimal division threshold is the maximum one that provides enough potential parallelism. This implies a threshold that depends on the number of threads used; we did not pursue this in our reported experiments. In qualitative experiments, however, we notice an increase in performance on low thread counts with higher thresholds.

The hypersparse effect can be mitigated by reducing the cost of a lookup miss. If the lookup is in cache then it can incur minimal penalty. Ongoing organizer work should address this with a hierarchal organizer (similar to DCSC) that allows many lookup misses to fail quickly using the same (cached) memory locations. A smaller threshold results in smaller blocks, and therefore a larger portion of the organizer can be in cache.

5.5 Experiments and Comparisons

5.5.1 Experimental Design

We implemented our algorithm in C++, using the Threading Building Blocks (TBB) framework [90] for task parallelism. We compare it to the fastest serial and parallel codes available. We use an Intel Westmere-EX machine with four E7-8870 @ 2.40GHz processors for a total of 40 physical cores and 80 threads. The machine has 256 GB RAM.

Codes

We compare against the leading serial code, CSparse [30], and the parallel code Combinatorial BLAS [24]. For this paper, we only consider SpGEMM kernels.

CSparse is a small sparse matrix package written in C. It includes implementations for a wide range of sparse matrix algorithms that are either asymptotically optimal or fast in practice. The primary drawback to CSparse is that it is single threaded. Nevertheless, it is considered a leading sparse matrix code and offers a strong benchmark.

The Combinatorial BLAS (CombBLAS) is a library written in highly-templated C++ and MPI that offers a small set of linear algebraic kernels that can be used as building blocks for the most common graph-analytic algorithms. Graph abstractions can be built on top of its sparse matrices, taking advantage of its existing best practices for handling parallelism in sparse linear algebra. The main data structures are sparse matrices and vectors which are distributed in a two-dimensional processor grid for scalability. This means that the CombBLAS requires a square number of processes. CombBLAS is written for distributed memory, but we compare our shared-memory code with it as it is a leading parallel SpGEMM code.

Datasets

We present a set of problems that consist of a single sparse matrix multiplication $A \times B$ or a triple product $A \times B \times C$. We generate three types of matrices, and two randomly permuted variants, to serve as the base of our problem set as described in Table 5.1.

Kronecker product (RMAT) matrices [66] approximate a power-law degree distribution among vertices. We use quadrant edge probabilities of $[.57, .19, .19, .05]$ and a fill factor of 16. We also symmetrize the matrix to model an undirected graph. Each RMAT is labeled with its *scale*, where the dimensions of the matrix are $n = 2^{scale}$. The maximum possible nnz is $32n$; however due to a large number of collisions in the dense regions the actual number can be substantially less.

We generate adjacency matrices for Erdős-Rényi graphs with similar vertex and edge counts to our RMAT graphs. Each ER graph has $n = 2^{scale}$ vertices and about $32n$ edges.

A 3D torus mesh serves to represent 3D geometic mesh applications. A mesh size of d contains d^3 vertices, each with a connection to its six neighbors and itself. Therefore, the sparse matrix has dimension d^3 with $7d^3$ nonzeros.

Finally we consider a simple algebraic multigrid application. We consider a 3D rectahedral mesh of dimension d, with d^3 cells, which performs a linear combination of its 27 neighbors.

Each dataset has a scale parameter as described. For the RMAT and torus datasets we also include a randomly-permuted variant, denoted with a *RP* suffix. This variant shows the effect of nonzero distribution. To ensure compatibility with all codes, all datasets only contain numeric elements of type *double*.

Table 5.1: Dataset categories. Each SpGEMM problem's name specifies the matrix used and the operation. The matrix name is a concatenation of *Base*, *Scale*, and *RP* from this table. The operation is denoted by a *suffix* from Section 5.5.1.

Base	Scale	Randomly Permuted	Matrix Dim.	Approx. nnz
Flat random:				
ER	18 or 20		2^{scale}	$32 * 2^{scale}$
Power law random:				
rmat	16 or 18		2^{scale}	$32 * 2^{scale}$
Power law random (randomly permuted):				
rmat	16 or 18	RP	2^{scale}	$32 * 2^{scale}$
3D structured mesh:				
torus3D	150 or 200		$scale^3$	$7 * scale^3$
3D structured mesh (randomly permuted):				
torus3D	150 or 200	RP	$scale^3$	$7 * scale^3$
Algebraic multigrid:				
AMG	150 or 200		$scale^3$	$27 * scale^3$

Problems

We generate SpGEMM problems from the datasets in several ways, each marked by a distinct suffix to the dataset name:

1. Suffix `_sq`: We square the matrix.

2. Suffix `_perm`: We randomly permute the matrix rows by left multiplying it by a generated random permutation matrix.

3. Suffix `_sub`: We select half the rows and half the columns of the matrix by a triple product. This operation is also called SpRef.

4. Suffix `_cont`: Finally, we generate a set of three matrices that approximate the contraction step of algebraic multigrid. We contract a dimension d matrix with d^3 cells to a dimension $d/2$ matrix with $d^3/8$ cells. This entails a $R \times A \times P$ triple product.

The complete set of problems is described in Tables A.1 and A.2 in Appendix A.

Measurements

For each problem we calculate the number of non-zero arithmetic operations (floating-point multiplies and additions) that occur. We then run each code/number of cores combination and record the elapsed time.

This data allows us to make a variety of comparisons. We can determine serial efficiency by looking at the $p = 1$ results. We can determine strong scaling by comparing increasing processor counts on the same problem, or weak scaling by comparing larger generated problems on the same number of processors. We can also compare to the serial CSparse code to determine when parallelism becomes profitable.

Additionally, we probe QuadMat by profiling its behavior on one core.

5.5.2 Results

We ran QuadMat with blocksize threshold=max($50k, \mathit{largest\_nnz}/80$), with a naïve index caching implementation, no post-processing phase, and only dense versions of auxiliary data structures. The raw elapsed times for each problem are listed in Tables A.3 and A.4 in Appendix A.

We analyze QuadMat's performance from several angles. First, we get a broad overview of the performance of all codes by comparing them to each other. We then explore the effect of nonzero distribution on the runtimes, and the effect of threshold choice on scalability. Finally we profile QuadMat execution.

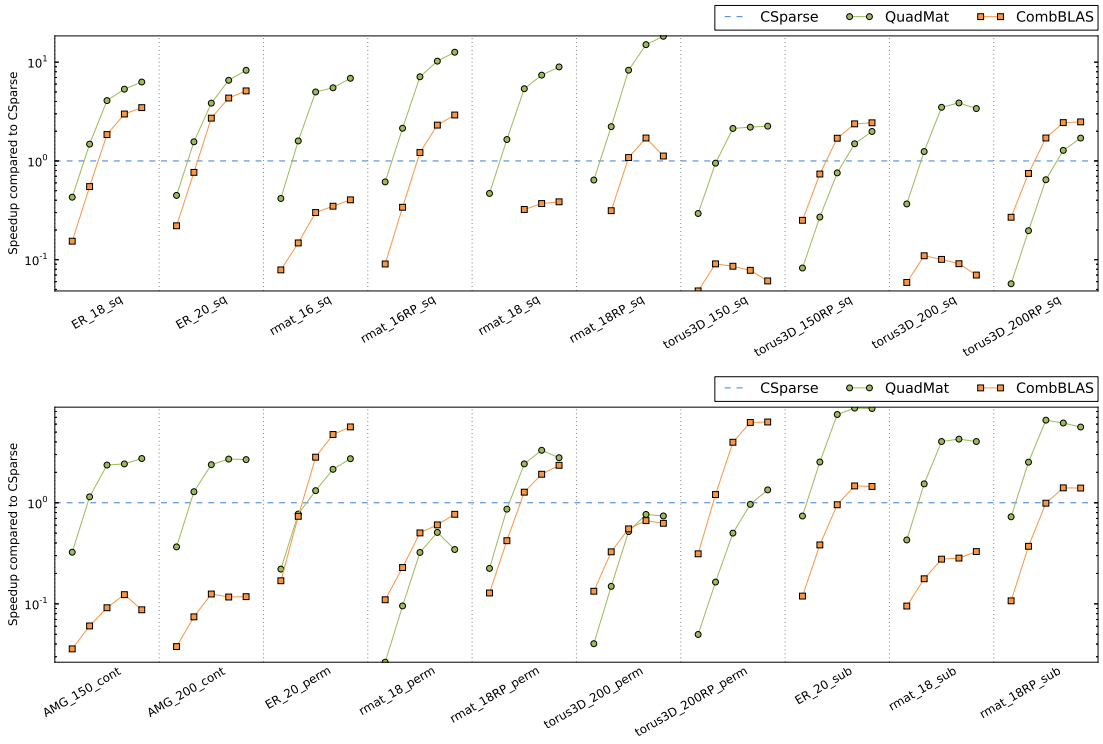

Figure 5.9: Speedup compared to CSparse for CombBLAS and QuadMat on 1, 4, 16, 36, and 64 threads. Y-axis is in log scale. Note that the machine has 40 cores, so the 64 thread results are using multiple threads per core.

5.5.3 Code Comparisons

The purpose of a shared-memory parallel code is to perform a task faster than a sequential code. In this vein we get a broad performance overview of both parallel codes by comparing the speedup each offers compared to CSparse. In Figure 5.9 we plot the speedup (or slowdown) of 1, 4, 16, 36, and 64-thread runs compared to single-threaded CSparse on each problem in our set.

We see many strengths of QuadMat and some weaknesses. QuadMat's strongest performance is on ER and RMAT matrix squares, and the AMG contraction and submatrix extraction triple products. In 13 out of 20 problems QuadMat matches CSparse performance with four cores or fewer. QuadMat shows good speedup on the remaining problems, and does not match the CSparse sequential time on only two out of 20 problems. This shows that there are clearly some significant bottlenecks remaining.

We plot the same data as absolute values, namely FLOPS (or nonzero arithmetic operations per second) achieved. Figure A.1 plots the same 1, 4, 16, 36, and 64-thread runs for CombBLAS and QuadMat, but they can now be directly compared to the FLOPS achieved by single-threaded CSparse. We observe that on some problems all codes suffer reduced FLOPS, while all are faster on others. The gap is large, two orders of magnitude.

Effects of Nonzero Distribution

We compare the effect of nonzero distribution on the various codes. This is most evident when the same problem is available in a highly structured and a randomly permuted form, namely torus squares. CSparse and QuadMat both perform better on the structured version, CombBLAS on the randomized version. There are two primary reasons for this.

Both CSparse and QuadMat use a dense lookup table for the columns (CSC and CSC-like dense organizer, respectively). This makes sequential reads of the columns very efficient. This locality is lost when the matrix is randomly permuted, and FLOPS performance approaches that of the ER squares.

The hypersparse algorithm used by CombBLAS does not allow it to benefit from this locality as much, so it is less affected by its loss. On the other hand, CombBLAS uses a uniform block decomposition so the narrow-banded torus gives a very unbalanced computational load. The random permutation provides a nearly uniform nonzero distribution which allows CombBLAS to scale very well. Indeed we see this effect in all problems; CombBLAS performs well on problems that offer good load balancing and less well on ones that do not.

While load balance has a much weaker effect on QuadMat, we observe that QuadMat struggles when the left factor is much more sparse and random than the right factor, such as the permutation problems.

To help explain why sparse left factors are a performance bottleneck, we measure the observed utility of A organizer lookups. As described in Section 5.4, our inner product computation performs lookups into A's column organizer. The cost of each miss (empty column) is amortized by the number of nonzero elements discovered by hits. Each hit discovers at least one element.

We instrumented QuadMat to measure the total number of organizer lookups, the number of hits, and the number of nonzeros discovered through each hit. Dividing the latter by the total number of lookups gives us the lookup utility. Note that these measured numbers are specific to each particular block decomposition and will change with a different division threshold. See Table A.5 in Appendix A.

We quickly observe a pattern. QuadMat has good computational performance on problems with high lookup utility and poor performance on problems with low lookup utility. Indeed the worst performing permutation problems have terrible lookup utility because nearly all lookups miss (due to the sparseness of the permutation matrix) and the hits discover the minimum one element. This is the hypersparse block effect.

CombBLAS is not affected by poor lookup utility because its hypersparse sequential kernel does not perform lookups. In ongoing work we try to get the best of both worlds. We mitigate the cost of the misses by switching to a DCSC-like organizer on hypersparse blocks. Our design also permits us to selectively perform the hypersparse algorithm on some block pairs then combine that result with results using our Gustavson-derived kernel.

Strong Scaling

We are interested in what our code does on the same problem when it is given more resources. In Figure 5.10 we plot the speedup of QuadMat on two to 36 cores. On a single socket laptop with 4 cores and 8 threads we see excellent scaling even with two threads per core, but on our larger machine we see much less benefit from multiple threads per core.

We observe excellent scaling with 2 and 4 threads on all problems, and good scaling with 9 threads on most problems. Thread counts above 9 bring mixed performance; most problems continue scaling; some stay about the same. We hypothesize two reasons: insufficient parallelism and memory effects.

Our profile statistics in Table A.5 include the total compute task work (total number of seconds) and the span (longest individual task). The ratio of those two times is our potential parallelism. We see that for our chosen division threshold, some problems (particularly AMG contraction) are indeed constrained by insufficient potential parallelism.

To explore memory effects, we performed a set of runs in which we artificially inflated the cost of arithmetic operations by looping them 5,000 times. This drastically reduces the effects of memory latency, bandwidth, and caches. Figure 5.11 shows the results for three problems, comparing the speedup of the normal code with the one with inflated arithmetic.

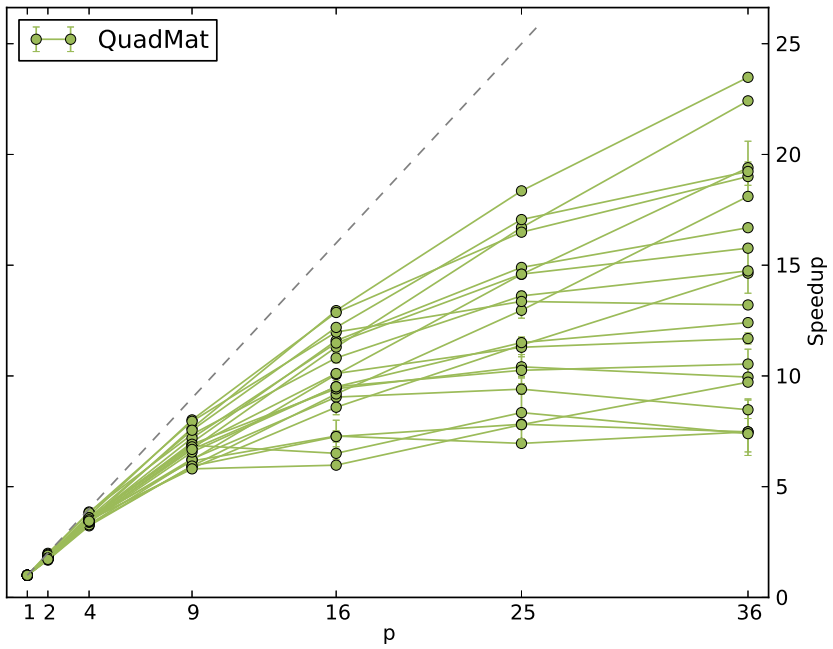

Figure 5.10: Strong scaling of normal QuadMat. Each line shows the speedup for a particular problem when more threads are used.

The vastly improved scaling of the code with inflated arithmetic shows that memory effects have a significant impact on strong scaling.

We wish to bring the reader's attention to a hidden pitfall of shared memory algorithms that perform memory allocation in threaded kernels. Main memory is a shared resource, therefore its allocation must be done in a thread-safe manner. The naïve approach, locking, introduces a serialization hidden to the algorithm designer. One solution is an allocator based on thread-private heaps. TBB provides such an allocator [59].

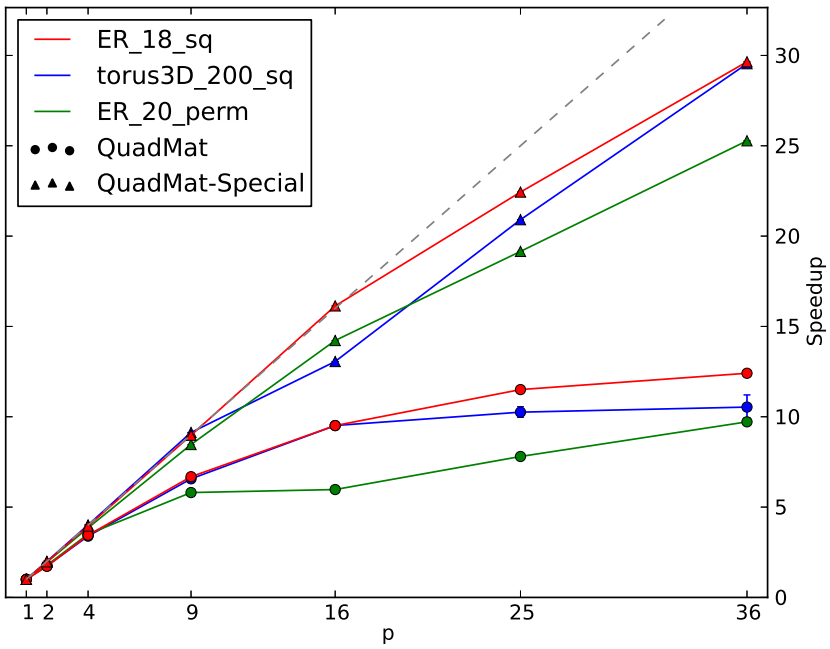

Figure 5.11: Strong scaling comparison of normal QuadMat with a special version with increased arithmetic intensity to show impact of memory effects.

Profiling

We explore the efficiency of our algorithm and implementation through profiling. We compiled a special profiled binary which records the time spent in each phase of the algorithm. We are particularly interested in the amount of time taken by overhead in our design: the symbolic phase (dominated by shadow block creation) and column organization. We profile every problem in our problem set on one core in Figure 5.12.

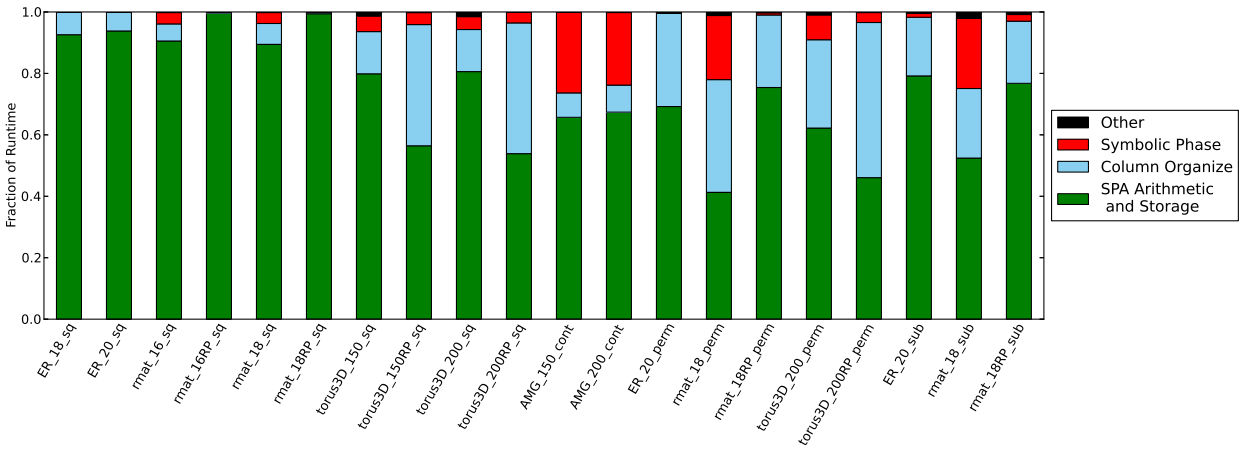

Figure 5.12: Breakdown of time spent in each part of the algorithm on a single core. The green 'SPA Arithmetic & Storage' portion represents the inner block product computation. The blue 'Column Organize' proportion accounts for the time to generate and combine column organizers. The red 'Symbolic Phase' is dominated by shadow block creation. Miscellaneous code such as destructors and TBB overhead go into the black 'Other' portion.

The profile data shows that the symbolic phase, dominated by shadow block creation, is not a significant portion of the runtime. The time spent in the symbolic phase is less than 5% of runtime in all but four problems; the maximum is 25%.

Recall that this preliminary implementation includes only a naïve implementation of organizer caching. The need for efficient organization and organizer reuse is suggested by the profile data; column organization accounts for between 15 and 45% of runtime for all but ER and RMAT square problems.

5.6 Discussion and Future Work

Our results show that, despite room for improvement, our algorithm has excellent performance and scaling. It offers significant speedup on some problems, and we have strong leads on how to improve the cases where it does not.

Interestingly, the problems that QuadMat excels on are also the ones that are sometimes considered the most difficult in the graph community: ones with a small number of high-degree vertices.

Our continuing work includes two main improvements that should significantly reduce or eliminate QuadMat's weaknesses: organizer caching and a hierarchical A-side organizer. These improvements should provide more latitude in automatically choosing a good division threshold.

Our algorithm has potential to be extended in several ways.

We envision a triple product primitive that does not materialize the entire intermediate product at any one time. This can be accomplished by merging the two SpGEMMs' symbolic phases. When done carefully with added destructor tasks, the portions of the intermediate product needed for a portion of the second SpGEMM can be materialized, used, and destroyed.

We also believe that the quadtree intermediate structure and triples leaf storage enables computing $A^T \times B$ with similar complexity to $A \times B$.

Additionally, we plan to take advantage of the block decomposition to use serialization coupled with compression algorithms for savings in both memory and memory bandwidth.

We may be able to save extra post-processing work by merging the subdivide or coalesce step with the compute phase. This is a great application for autotuning, as the appropriate choice needs to be made at runtime and according to the actual workload.

We also emphasize that our leaf blocks provide a triples *interface*, but do not mandate triples storage as an implementation. This enables features such as dense blocks or generator blocks that emit triples but do not store them.

5.7 Conclusion

In conclusion, we summarize the key contributions of the design of our quadtree sparse matrix multiplication algorithm:

- A method for elimination of explicit SpAdd operations that offers a significant reduction in work for block-based SpGEMM.
- A split between symbolic and computational phases with temporary on-the-fly data reorganization for simpler operations.
- An algorithm description that divides work into small tasks that can be scheduled on any number of threads by third-party frameworks.
- A quadtree of triples blocks datastructure that has significant flexibility with manageable overhead.
- A preliminary implementation that demonstrates these benefits.

Chapter 6

Complex Graph Algorithms in a Database Query Language

This chapter is based on a (second-place winning) entry to the YarcData Graph Analytics Challenge [6]. An abridged version is published in SIAM Workshop on Network Science [32]. A paper published in EBT/ICT Workshops [102] also contains portions of this work.

6.1 Introduction

SPARQL is a powerful query language similar to SQL that operates on graphs specified in the RDF format. RDF graphs are composed of triples, where each triple consists of a *subject*, *predicate*, and *object* and specifies a directed edge from *subject* to *object* with attribute *predicate*.

SPARQL provides a rich way to query local neighborhoods. Our motivation is to find a way to combine this with a global graph metric: clustering.

The driving application is clustering large clinical datasets, to help identify potential disease causes. Autism researchers need to understand the underlying causes of autism spectrum disorders, based on data from genetic (e.g., SNPs in the GABA and glutamate pathways), medical history (diagnoses, prescriptions, provider visits, including pre-natal/infant, esp. infant brain MRIs), environmental (e.g., carcinogens, household chemicals), family medical history (i.e., parental psychiatric history), and early-childhood intervention-strategy domains. In practice, the patient base consists of thousands of individuals, with roughly 1M relationships per patient [**?**].

6.2 Our Selected Clustering Algorithm

Peer Pressure [57, pp. 59-68] [97] is a clustering algorithm based on the observation that for a given graph clustering the cluster assignment of a vertex will be the same as that of most of its neighbors.

The algorithm starts with an initial cluster assignment, such as each vertex being in its own cluster. Each iteration performs an election at each vertex to select which cluster that vertex should belong to at the end of the iteration. The

votes are the cluster assignments of its neighbors. Ties are settled by selecting the lowest cluster ID to maintain determinism, but could be settled arbitrarily. The algorithm converges when two consecutive iterations have a (tunably) small difference between them. Typically this leads to five to ten iterations on well-clustered graphs.

This algorithm is also known by the name *Label Propagation* [92] in the physics literature. Boldi et. al. [16] extend that work with *Layered Label Propagation*, which accepts a parameter γ that selects between large relatively sparse clusters and small relatively dense clusters.

6.3 Clustering Application

The design of the queries we use to implement Peer Pressure in SPARQL is informed by the layout of the data we wish to cluster. We therefore first describe our dataset, then the algorithm implementation.

6.3.1 Datasets

Clinical autism datasets are in general proprietary and protected by privacy laws. Therefore, as a surrogate, we target our code for a dataset from the Mayo

Clinic "Smackdown" project [101]. This dataset was synthesized by combining data from various real-world sources to represent the nature of health-care records.

Despite being synthetic, this data was not freely available to outside researchers such as ourselves for the majority of the project duration. We therefore chose to benchmark our code using the cluster-realistic synthesis work of Pinar et al. [96]. We tailored our generator to produce data in a similar format to Smackdown. Once we gained access to Smackdown data we were able to tailor our code to work with it.

Smackdown data

The Smackdown data is a collection of database tables taken from public sources (such as data.gov) which are then linked together to form a structure that is subjectively similar to the clinical Autism data. The tables chosen have no particular meaning; they range from timezone information to air traffic networks and botanical datasets. Their semantics are not important, in fact they are artificially augmented with foreign keys that link tables together in an arbitrary way. While a US Post Office location may have nothing to do with a flower, in aggregate these links make the whole structure resemble the clinical Autism data such that it is useful for testing.

The overall organization of the tables is as follows.

- The data itself is all public, and comes from data.gov.
- There are on the order of 200-300 different SQL tables.
- Tables have between 15 and 60 columns.
- Tables have row counts anywhere from hundreds of thousands to tens of millions.
- Each table has between 1 and 15 foreign keys.

The primary dataset is called `dogdb-2G`, as its size is about 2GB when stored in a SQL database. The team at Mayo found this too small compared to their real dataset, so they decided to augment the data with random rows generated using a scheme that maintains the value distribution of the original dataset. Using this method they have generated 20GB, 50GB, 80GB and 100GB datasets.

These SQL tables are converted to RDF to work on uRiKA. The 2G dataset has 39M triples. The 100GB dataset has 5.6B triples with an uncompressed RDF filesize size of 850GB.

The RDF is structured as follows:

- Each table is identified by a URI, with links to a `Class`.
- Each table column (identified by URI) contains two triples that declare the column and link it to its table:

  - `?colURI <rdf:type> <rdf:Property> .`
  - `?colURI <rdf:label> "Table label" .`

- Each table row has a URI (primary key).
- Each value in the table consists of a triple with a literal value: `?rowID ?colURI value .`
- The foreign keys link two rows from different tables: `?rowID_tbl1 <xxx_Key_n> ?rowID_tbl2`
- The column URI contains the string "`Col`" and foreign key URI "`Key`".

Our goal is to cluster rows within a table but to also follow the foreign keys to find clusters that span multiple tables. These clusters would show links between multiple tables, helping the scientist link multiple potential factors for Autism.

6.3.2 Peer Pressure in SPARQL

The SPARQL implementation of Peer Pressure is relatively straight forward. The algorithm maintains the clustering assignment of each vertex as its only state. We store this state by creating RDF triples to represent an "inCluster" relationship. We reuse names of existing vertices in the graph as cluster IDs, as the IDs themselves are arbitrary and only have to be unique. A graph vertex would

then be said to be in a particular cluster if there is an RDF triple specifying an "inCluster" edge between the vertex and the cluster ID.

The cluster election at a vertex is equivalent to counting the number of length-two paths between that vertex, one of its neighbors, and that neighbor's cluster ID (via an "inCluster" edge). The winner of the election is found by grouping these paths by cluster ID, counting them, and selecting the cluster ID with the maximum count.

Once the election is complete, we construct new edges between vertices and their new clusters.

Since Peer Pressure is an iterative algorithm, the election and assignment need to be performed multiple times to reach convergence. Our approach is to construct actual RDF triples for each cluster assignment, then store them in a named graph for retrieval by the election query of the next iteration. Once convergence is reached the clustering can be read from the final named graph.

The query in Figure 6.1 is what one iteration's election query looks like in SPARQL. The query uses nested subqueries which tally the votes using a `GROUP BY` and `COUNT`, and find the winner using a `MAX`.

This particular query only clusters edges with a "hasLink" relationship. This relationship marks edges that passed the similarity metric, as embodied in the initialization query mentioned earlier. The "hasLink" edges are stored in a separate

```
"
DROP GRAPH <http://ga.org/g/" + graphName + (i+1) + ">
CREATE GRAPH <http://ga.org/g/" + graphName + (i+1) + ">
INSERT
{
  GRAPH <http://ga.org/g/" + graphName + (i+1) + ">
      { ?s <http://ga.org/p/inCluster> ?clus3 }
}
WHERE
{
  {
    SELECT ?s (SAMPLE(?clus) AS ?clus3)
    {
      {
        SELECT ?s (MAX(?clusCt) AS ?clus2)
        {
          SELECT ?s ?clus (COUNT(?clus) AS ?clusCt)
          WHERE
          {
            GRAPH <http://ga.org/g/" + graphName + "Links>
                  {?s <http://ga.org/p/hasLink> ?o . }
            GRAPH <http://ga.org/g/" + graphName + i + ">
                  { ?o <http://ga.org/p/inCluster> ?clus }
          } GROUP BY ?s ?clus
        } GROUP BY ?s
      }
      {
        SELECT ?s ?clus (COUNT(?clus) AS ?clusCt)
        WHERE
        {
          GRAPH <http://ga.org/g/" + graphName + "Links>
                 {?s <http://ga.org/p/hasLink> ?o .}
          GRAPH <http://ga.org/g/" + graphName + i + ">
                 { ?o <http://ga.org/p/inCluster> ?clus }
        } GROUP BY ?s ?clus
      } FILTER (?clusCt = ?clus2)
    } GROUP BY ?s
  }
}
"
```

Figure 6.1: One iteration of the PeerPressure clustering algorithm. We have included JavaScript references to *graphName* and i variables, which denote the user's choice of graph name and algorithm iteration, respectively.

named graph, and the result of each iteration of the algorithm is stored in its own named graph as well. Each stored iteration consists of only the "inCluster" edges, and there is only one such edge per vertex. Therefore, depending on average degree, each stored iteration is small compared to the total number of triples in the original graph. We compare results of consecutive iterations with each other to determine convergence.

Note that our driver code is written in JavaScript to run queries remotely (see Section 6.4). We kept references to our JavaScript variables, $graphName$ and i, which denote the name of the graph and the iteration count, respectively.

6.3.3 Discussion

We believe that Peer Pressure is a good fit for a SPARQL-based implementation because its inherently local nature fits well with the SPARQL paradigm. The heart of the algorithm, the election, has natural analogues in SPARQL aggregate functions. We also observe that our queries are highly dependent on large joins, which give uRiKA an advantage over its competition (See Section 6.5).

We note that our approach to the Peer Pressure algorithm, i.e. keeping algorithm state and iterating, makes possible a wide variety of other graph algorithms to be performed using SPARQL queries. For example, breadth-first search could be implemented using a similar approach, with state maintained by adding links

to "`nFrontier`" and "`discovered`" edges as the queries traverse the graph. More complex state schemes could enable algorithms such as PageRank and Betweenness Centrality.

6.4 Workflow and Implementation

We have divided our workflow into three distinct steps: Conversion, Cluster Algorithm, Results. Each is described below. SPARQL backends typically have an interface similar to SQL: individual queries are sent to the engine and results returned. This can occur at a manual administration console, or it can be scripted using a database connection interface. We chose to implement our workflow in an HTML+JavaScript webpage which guides the user through the steps and can automate query execution.

6.4.1 Implementation in HTML/JavaScript

Our Peer Pressure implementation consists of several queries per iteration. We chose to combine all these queries into a JavaScript function whose only logic is a loop.

The script is pointed at a SPARQL endpoint such as uRiKA or Apache Fuseki. A single click of a button automatically runs all the Peer Pressure queries in the right order and stops upon convergence.

We found it useful to automate some of the other steps of the workflow as well. A large portion of the data preparation is also be done via this webpage. The results can be fetched through several pre-made aggregation queries.

Apart from user friendliness, a benefit of using HTML/JavaScript is that it allows easy formatting and visualization. A screenshot of our (admittedly crude and developer-oriented) interface is in Figure 6.5.

6.4.2 Conversion Stage

Our Peer Pressure clustering implementation does not work on the data directly, instead it follows explicit "hasLink" relationships as denoted by a triple with a "hasLink" predicate. As such, we need a step which converts the raw data into these relationships.

The conversion means that edges are created between table rows that are similar "enough". In fact, this means that this step is one of the main ways that the scientist influences the computation. The scientist must find specify what they deem to be a good similarity metric for a particular table or even a particular

```
INSERT {
    GRAPH <http://ga.org/g/sprLinks> {?rowID1
       <http://ga.org/p/hasLink> ?rowID2 }
    GRAPH <http://ga.org/g/sprLinks> {?rowID2
       <http://ga.org/p/hasLink> ?rowID1 }
}
WHERE {
    SELECT ?rowID1 ?rowID2 ?value1 ?value2
    WHERE {
        ?rowID1
           <http://localhost:2020/vocab/tblfee6_c2rk_209_table13_Col_11>
           ?value1 .
        ?rowID2
           <http://localhost:2020/vocab/tblfee6_c2rk_209_table13_Col_11>
           ?value2 .
        FILTER(?rowID1 != ?rowID2)
        FILTER(abs(?value1 - ?value2) < 5)
    }
}
```

Figure 6.2: A query which creates "hasLink" edges between two rows of a table if their Column 11 values are within 5 of each other.

column, then write a query which creates a `?rowID1 <hasLink> ?rowID2` triple (and its inverse).

To aid the scientist in this manner we have created a set of example queries that are useful for examining the data as well as doing the conversion. For example, one click will emit a query which dumps all values in a certain column, another takes the user's chosen column and emits a query which will link all values that are within a user-specified threshold from each other (see Figure 6.2).

6.4.3 Algorithm Stage

This step runs the Peer Pressure iteration query as well as a convergence check query. We limit the number of iterations to 20. The SPARQL engine considers each query to be independent, therefore it is easy to allow restarting the algorithm from an arbitrary iteration if it has been interrupted for any reason.

6.4.4 Results Stage

Our results consist of a set of queries which provides aggregate information about the clusters such as size, average in-cluster degree, average inter-cluster degree, etc. We may also fetch the individual cluster data; however, that becomes unwieldly on large datasets.

We have implemented a way to visualize the clusters using a Sankey diagram [18]. This implementation uses D3.js [17], a JavaScript-based framework for creating visualizations. Sankey diagrams show how particular components are split among entities in a large system. In our visualization, each cluster ID and table name are a node, with a link between a cluster and a table if there are any table rows in that cluster. Link line thickness is proportional to the number of table rows represented by the link. A example is presented in Figure 6.3, and its corresponding query is in Figure 6.4. Note that this diagram clearly illustrates clusters that span multiple tables, as well as clustering within a table.

Our web-based approach opens the possibility of using compute-intensive visualization since it may be done on the server side.

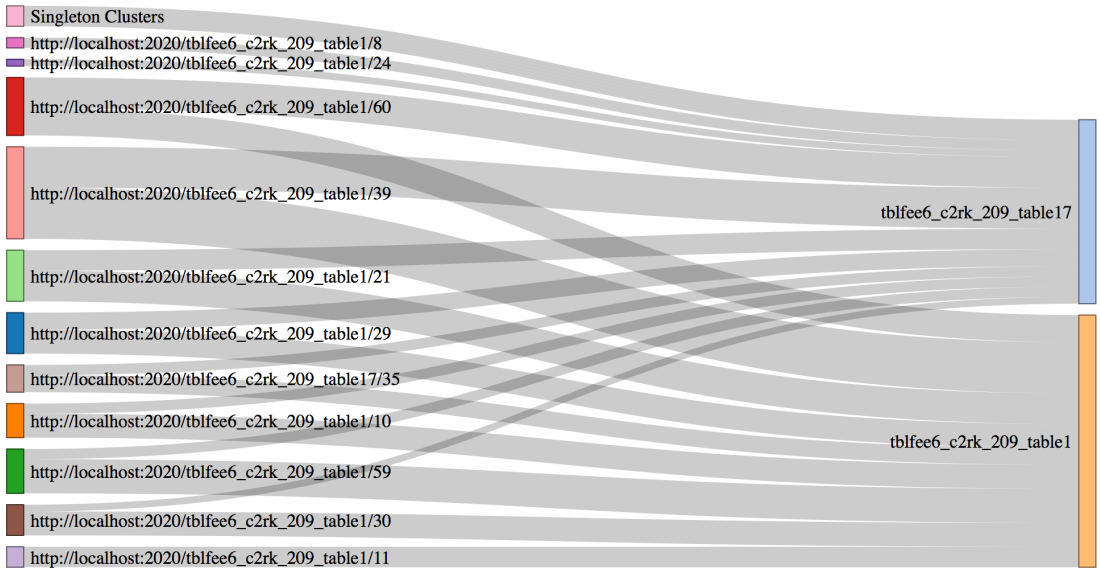

Figure 6.3: Sankey diagram visualization of clustering. Nodes on the left are individual clusters (labeled with cluster ID, which is derived from a rowID), nodes on the right are tables. The thickness of a link between a cluster and a table is proportional to the number of rows of that table in that cluster.

6.5 Results

Here we describe the various datasets used and their results using 64-processor uRiKA. For cross comparison we also used one of our machines called Neumann, a 32 core Opteron (2.4 GHz) machine with 128 Gb of RAM, running Apache Fuseki

```
SELECT ?clus (?tableNameFromRowid as ?tableName) (COUNT(*) as
   ?ct)
WHERE {
    GRAPH <http://ga.org/g/graphName> {?rowid
       <http://ga.org/p/inCluster> ?clus}
    BIND(REPLACE(str(?rowid), "^(.*)/([^/]*)/([^/]*)$", "$2")
       AS ?tableNameFromRowid)
} GROUP BY ?clus ?tableNameFromRowid
```

Figure 6.4: Query used for Sankey diagram.

v. 0.2.5. Note that unfortunately Fuseki is single-threaded within an individual query; it only makes use of multiple cores if there are multiple concurrent queries. We were unable find a usable alternative that would use multiple threads per query.

We tested our implementation on three different datasets. We generated datasets in two different ways to test scalability and to compare uRiKA to an x86 machine. We also tested on Smackdown data.

6.5.1 Test Data

In order to test the algorithm beyond small test cases we needed to synthesize data with a predictable clustering. To do this, our test script uses a stochastic blockmodel [106] that determines the size and number of clusters in advance. We set the number of clusters to $numclus = (\log_2 n)^{1.5}$ where n is the number

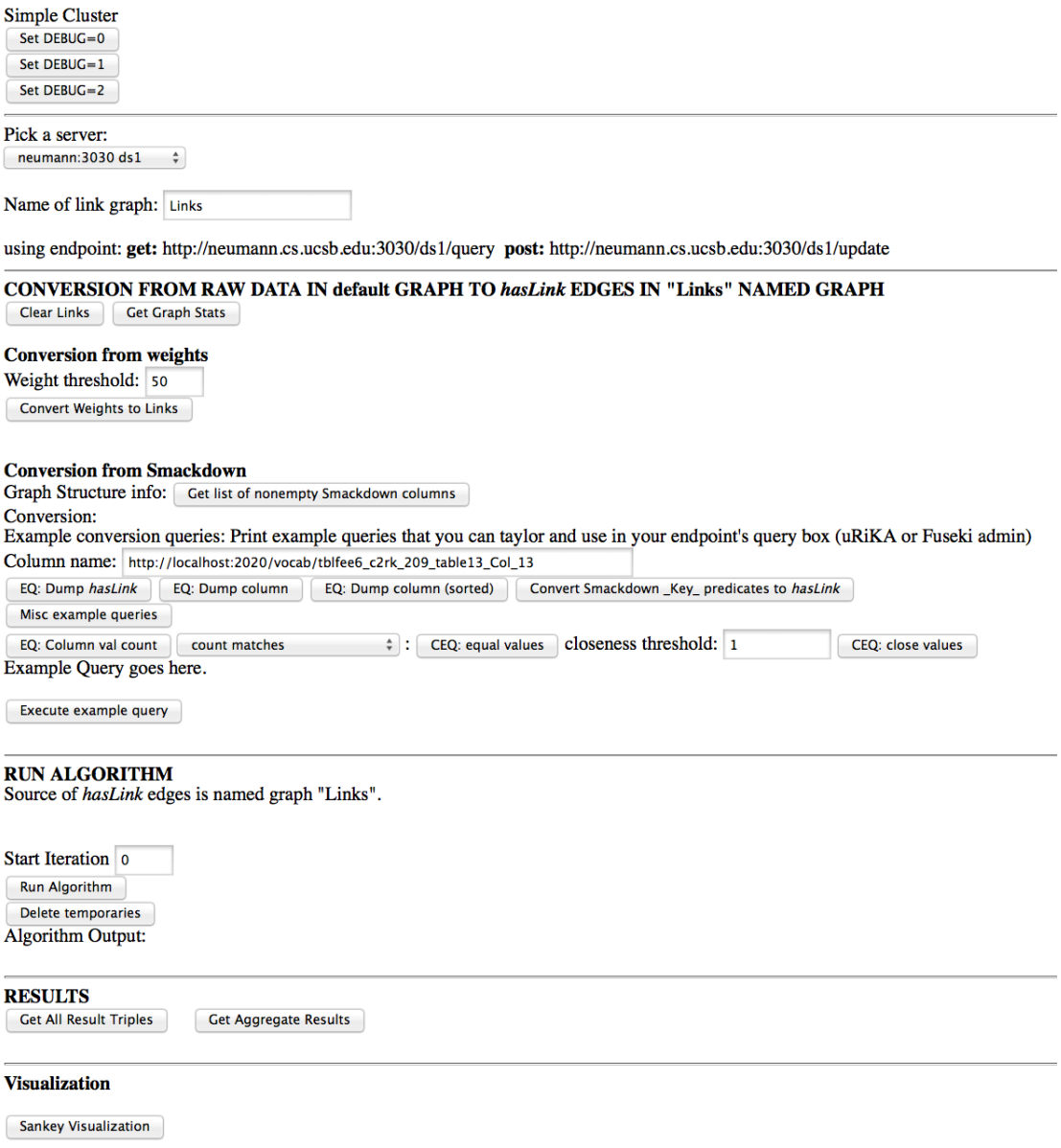

Figure 6.5: A screenshot of our SPARQL over HTTP webpage. Output for each section is printed above each horizontal line.

of vertices. The generator then considers all edge pairs and adds intercluster edges with probability 0.02 and intracluster edges with probability 0.1. Thus the clustering algorithm should find the desired clusters with high probability. The data we generated contained 100,000 vertices and 15,736,484 triples. The triples were assigned a random similarity measure as described above to test the threshold conversion query. On uRiKA the clustering converged in 5 iterations after 200.2 seconds. On Neumann the first update alone took about 9 hours with the first iteration completing in just under 12 hours. The whole algorithm did not finish.

6.5.2 BTER Data

The BTER data was generated using the Matlab generator written by Pinar et al. [96]. We then wrote a script to convert the result of this generator into RDF triples. The parameters we used in the generator along with specifying a power-law degree distribution are $\gamma = 2$, $maxdegree = 100$, $\rho_{init} = 0.99$, $\rho_{decay} = 0.8$. The BTER dataset we used contained 1,643,915 vertices and 7,332,102 triples. On uRiKA this graph did not converge as the maximum number of iterations is 20, but it did complete these iterations in 3 hours, 9 minutes.

6.5.3 Smackdown Data

Working with the full Smackdown data posed a challenge. The amount of data is vast, and we only had access to it for a relatively short time. We loaded a small (100,000 triple) subset of the 2G dataset on our Fuseki machine and were able to debug our script with it. We discovered that this made debugging our queries and driver script much easier, as uRiKA does not provide a way to kill a query that's unexpectedly too slow (at least to end users).

We experimented with the 20G dataset (1.3B triples) on uRiKA. We discovered several difficulties that are not clear on smaller datasets.

First, every query takes a very long time, no matter how simple it is. We discovered that this is largely due to the fact that even though our queries narrow down their operands to a relatively small subset of the entire graph, the entire graph is still traversed. We came up with several potential solutions, such as using named graphs to shard the data into chunks. For example, each table or even column can have its own named graph. This would mean that the conversion queries would operate on a very small subset of the graph.

Second, the need for "hasLink" edges between similar rows results in a potential quadratic expansion. While this was obvious from the start, this property began to pose significant problems on the large dataset. Specifically, even if the result has been narrowed down, the computation is still very expensive. We are exploring

ways to alleviate this problem, such as using explicit groups and intermediate links to reduce the amount of "hasLink" edges. This requires changing the PeerPressure queries to support groups, which is ongoing work.

6.6 Conclusion

We have managed to create an entire workflow solution for clustering RDF graphs using SPARQL. This is an important result because it shows that a global graph metric like clustering can be implemented in SPARQL. We also propose that our method is easily extendible to other graph algorithms not previously available to SPARQL users.

We've also shown that uRiKA really shines on a variety of queries as compared to x86 servers. This has allowed us to cluster very large RDF graphs, something not possible on lesser hardware.

We've also shown that an HTML/JavaScript driver has multiple advantages. It allows automation of boilerplate tasks, makes data exploration simpler, and allows for easy visualization. It makes a scientist's life easier.

Chapter 7

Conclusions

This thesis advances the state of the art in computation on very large graphs by enabling efficient implementations of interfaces to algebraic primitives.

We have put non-HPC expert graph analysts at the forefront. We bring them flexible primitives and algorithms exposed in a high productivity language, without compromising on performance or scalability.

We also contribute a new sparse matrix datastructure and sparse matrix multiplication algorithm to better take advantage of large shared memory machines or nodes in hybrid clusters.

Bibliography

[1] Active Record - Object-Relation Mapping Put on Rails. http://ar.rubyonrails.org, 2012.

[2] Apache Gigraph. http://giraph.apache.org, 2013.

[3] Apache Hama. http://hama.apache.org, 2013.

[4] Performance Application Programming Interface (PAPI). http://icl.cs.utk.edu/papi/, 2013.

[5] PyPy. http://pypy.org, 2013.

[6] YarcData Graph Analytics Challenge, April 2013.

[7] C. Avery. Giraph: large-scale graph processing infrastructure on hadoop. *Proceedings of Hadoop Summit. Santa Clara, USA*, 2011.

[8] D. Bader, J. Berry, A. Amos-Binks, D. Chavarría-Miranda, C. Hastings, K. Madduri, and S. Poulos. STINGER: Spatio-Temporal Interaction Networks and Graphs (STING) extensible representation. *Georgia Institute of Technology, Tech. Rep*, 2009.

[9] D. Bader, J. Gilbert, J. Kepner, D. Koester, E. Loh, K. Madduri, B. Mann, and T. Meuse. HPCS Scalable Synthetic Compact Applications #2. http://graphanalysis.org/benchmark.

[10] D. Bader, S. Kintali, K. Madduri, and M. Mihail. Approximating Betweenness Centrality. In A. Bonato and F. Chung, editors, *Algorithms and Models for the Web-Graph*, volume 4863 of *Lecture Notes in Computer Science*, pages 124–137. Springer Berlin/Heidelberg, 2007.

[11] D. A. Bader and K. Madduri. SNAP, small-world network analysis and partitioning: An open-source parallel graph framework for the exploration of

large-scale networks. In *Proc. IEEE Int. Symposium on Parallel&Distributed Processing*, pages 1–12, 2008.

[12] S. Beamer, K. Asanović, and D. Patterson. Direction-optimizing breadth-first search. *Scientific Programming*, 21(3):137–148, 2013.

[13] S. Beamer, A. Buluç, K. Asanovic, and D. Patterson. Distributed memory breadth-first search revisited: Enabling bottom-up search. In *Proceedings of the 2013 IEEE 27th International Symposium on Parallel and Distributed Processing Workshops and PhD Forum*, pages 1618–1627. IEEE Computer Society, 2013.

[14] J. Berry, B. Hendrickson, S. Kahan, and P. Konecny. Software and Algorithms for Graph Queries on Multithreaded Architectures. In *Proc. Workshop on Multithreaded Architectures and Applications*. IEEE Press, 2007.

[15] D. Bickson. Gaussian Belief Propagation: Theory and Application. *CoRR*, abs/0811.2518, 2008.

[16] P. Boldi, M. Rosa, M. Santini, and S. Vigna. Layered label propagation: a multiresolution coordinate-free ordering for compressing social networks. In *Proceedings of the 20th international conference on World wide web - WWW '11*, pages 587–596, New York, New York, USA, 2011. ACM Press.

[17] M. Bostock. Data-driven documents (d3.js), a visualization framework for internet browsers running javascript, 2012.

[18] M. Bostock. Sankey diagrams, May 2012. http://bost.ocks.org/mike/sankey/.

[19] U. Brandes. A Faster Algorithm for Betweenness Centrality. *J. Math. Sociol.*, 25(2):163–177, 2001.

[20] S. Brohée and J. van Helden. Evaluation of clustering algorithms for protein-protein interaction networks. *BMC Bioinformatics*, 7:488, 2006.

[21] A. Buluç, E. Duriakova, A. Fox, J. R. Gilbert, S. Kamil, A. Lugowski, L. Oliker, and S. Williams. High-productivity and high-performance analysis of filtered semantic graphs. In *27th IEEE International Symposium on Parallel and Distributed Processing (IPDPS 2013)*, May 2013.

[22] A. Buluç, J. T. Fineman, M. Frigo, J. R. Gilbert, and C. E. Leiserson. Parallel sparse matrix-vector and matrix-transpose-vector multiplication using

compressed sparse blocks. In *Proc. 21st Symp. on Parallelism in Algorithms and Arch.*, 2009.

[23] A. Buluç, A. Fox, J. R. Gilbert, S. Kamil, A. Lugowski, L. Oliker, and S. Williams. High-performance analysis of filtered semantic graphs. In *Proceedings of the 21st international conference on Parallel architectures and compilation techniques*, PACT '12, pages 463–464, New York, NY, USA, 2012. ACM. extended abstract.

[24] A. Buluç and J. Gilbert. The Combinatorial BLAS: Design, implementation, and applications. *The International Journal of High Performance Computing Applications*, 25(4):496–509, 2011.

[25] A. Buluç and J. R. Gilbert. On the Representation and Multiplication of Hypersparse Matrices. In *Proc. IPDPS*, April 2008.

[26] A. Buluç and K. Madduri. Parallel breadth-first search on distributed memory systems. In *Proc. Supercomputing*, 2011.

[27] B. Catanzaro, S. Kamil, Y. Lee, K. Asanović, J. Demmel, K. Keutzer, J. Shalf, K. Yelick, and A. Fox. SEJITS: Getting Productivity and Performance With Selective Embedded JIT Specialization. In *PMEA*, 2009.

[28] T. Davis. *Direct Methods for Sparse Linear Systems (Fundamentals of Algorithms 2)*. Society for Industrial and Applied Mathematics, Philadelphia, PA, 2006.

[29] T. Davis and Y. Hu. The University of Florida Sparse Matrix Collection. *ACM Transactions on Mathematical Software*, to appear, 2011.

[30] T. A. Davis. *Direct Methods for Sparse Linear Systems*. SIAM, Philadelphia, Sept 2006.

[31] J. Dean and S. Ghemawat. MapReduce: simplified data processing on large clusters. In *Proc. 6th Symposium on Operating System Design and Implementation*, pages 137–149, Berkeley, CA, USA, 2004. USENIX Association.

[32] K. Deweese, J. R. Gilbert, A. Lugowski, and S. Reinhardt. Graph clustering in sparql. In *SIAM Workshop on Network Science*, 2013.

[33] B. Dezső, A. Jüttner, and P. Kovács. Lemon–an open source c++ graph template library. *Electronic Notes in Theoretical Computer Science*, 264(5):23–45, 2011.

[34] B. Dorow. *A Graph Model for Words and their Meanings*. PhD thesis, Universität Stuttgart, 2006.

[35] A. Enright, S. Van Dongen, and C. Ouzounis. An efficient algorithm for large-scale detection of protein families. *Nucl. Acids Res.*, 30(7):1575–1584, 2002.

[36] P. Erdős and A. Rényi. On the evolution of random graphs. In *Publication of the Mathematical Institute of the Hungarian Academy of Sciences*, pages 17–61, 1960.

[37] P. Erdős and A. Rényi. On random graphs. *Publicationes Mathematicae*, 6(1):290–297, 1959.

[38] M. Fowler. *Domain Specific Languages*. Addison-Wesley Professional, 2010.

[39] L. Freeman. A Set of Measures of Centrality Based on Betweenness. *Sociometry*, 40(1):35–41, 1977.

[40] J. D. Frens and D. S. Wise. Auto-blocking matrix-multiplication or tracking BLAS3 performance from source code. *SIGPLAN Not.*, 32(7):206–216, June 1997.

[41] J. D. Frens and D. S. Wise. QR factorization with Morton-ordered quadtree matrices for memory re-use and parallelism. In *Proceedings of the Ninth ACM SIGPLAN Symposium on Principles and Practice of Parallel Programming*, PPoPP '03, pages 144–154, New York, NY, USA, 2003. ACM.

[42] J. Gilbert, C. Moler, and R. Schreiber. Sparse matrices in MATLAB: Design and implementation. *SIAM J. Matrix Anal. Appl*, 13:333–356, 1992.

[43] J. Gilbert, C. Moler, and R. Schreiber. Sparse matrices in MATLAB: Design and implementation. *SIAM Journal on Matrix Analysis and Applications*, 13(1):333–356, 1992.

[44] J. R. Gilbert. Sparse matrices and graphs: There and back again. Talk given at SVG 70, Stanford, 1 2014.

[45] J. R. Gilbert. xxxxxxx. Talk given at Graph Algorithms Building Blocks Workshop (GABB'14) in conjunction with IPDPS'14, 5 2014.

[46] J. S. Golan. *Semirings and their Applications*. Springer, 1999.

[47] A. Goldberg and R. Werneck. Computing Point-to-Point Shortest Paths from External Memory. In *Proc. 7th Workshop on Algorithm Engineering and Experiments (ALENEX05)*, pages 26–40, 2005.

[48] J. E. Gonzalez, Y. Low, H. Gu, D. Bickson, and C. Guestrin. PowerGraph: Distributed graph-parallel computation on natural graphs. In *Proceedings of the 10th USENIX Symposium on Operating Systems Design and Implementation (OSDI)*, pages 17–30, 2012.

[49] Graph500. http://www.graph500.org.

[50] D. Gregor and A. Lumsdaine. The Parallel BGL: A Generic Library for Distributed Graph Computations. In *Proc. Workshop on Parallel/High-Performance Object-Oriented Scientific Computing (POOSC'05)*, 2005.

[51] F. G. Gustavson. Two fast algorithms for sparse matrices: Multiplication and permuted transposition. *ACM Trans. Math. Softw.*, 4(3):250–269, 1978.

[52] M. A. Heroux, R. A. Bartlett, V. E. Howle, R. J. Hoekstra, J. J. Hu, T. G. Kolda, R. B. Lehoucq, K. R. Long, R. P. Pawlowski, E. T. Phipps, A. G. Salinger, H. K. Thornquist, R. S. Tuminaro, J. M. Willenbring, A. Williams, and K. S. Stanley. An Overview of the Trilinos Project. *ACM Trans. Math. Softw.*, 31:397–423, September 2005.

[53] S. Hong, H. Chafi, E. Sedlar, and K. Olukotun. Green-Marl: a DSL for easy and efficient graph analysis. In *Proceedings of the seventeenth international conference on Architectural Support for Programming Languages and Operating Systems*, ASPLOS '12, pages 349–362, New York, NY, 2012. ACM.

[54] S. Kamil, D. Coetzee, S. Beamer, H. Cook, E. Gonina, J. Harper, J. Morlan, and A. Fox. Portable parallel performance from sequential, productive, embedded domain specific languages. In *PPoPP'12*, 2012.

[55] U. Kang, C. Tsourakakis, and C. Faloutsos. PEGASUS: A Peta-Scale Graph Mining System - Implementation and Observations. In *Data Mining, 2009. ICDM'09. Ninth IEEE International Conference on*, pages 229–238. IEEE, 2009.

[56] G. Karypis, K. Schloegel, and V. Kumar. ParMETIS: Parallel Graph Partitioning and Sparse Matrix Ordering Library. Technical report, Dept. of Computer Science, University of Minnesota, 1997.

[57] J. Kepner and J. R. Gilbert, editors. *Graph Algorithms in the Language of Linear Algebra*. Society for Industrial and Applied Mathematics, 2011.

[58] P. Konecny. Introducing the Cray XMT. *Cray User Group meeting (CUG)*, 2007.

[59] A. Kukanov and M. J. Voss. The foundations for scalable multi-core software in Intel Threading Building Blocks. *Intel Technology Journal*, 11(4):309 – 322, 2007.

[60] H. Kwak, C. Lee, H. Park, and S. Moon. What is Twitter, a social network or a news media? In *WWW '10: Proceedings of the 19th international conference on World wide web*, pages 591–600, New York, NY, USA, 2010. ACM.

[61] O. Lassila and R. Swick. Resource Description Framework (RDF) Model and Syntax Specification. W3c recommendation, W3C, Feb 1999.

[62] L. Lee, A. Lumsdaine, and J. Siek. The Boost Graph Library: User Guide and Reference Manual, 2002. www.osl.iu.edu/publications/Year/2002.complete.php.

[63] R. Lehoucq, D. Sorensen, and C. Yang. *ARPACK Users' Guide: Solution of Large Scale Eigenvalue Problems with Implicitly Restarted Arnoldi Methods*. SIAM, 1998.

[64] X. Lei, X. Ostwald, J. Hu, C. Qiu, C. Porcaro, A. P. Bagshaw, and D. Yao. Multimodal functional network connectivity: an EEG-fMRI fusion in network space. *PloS one*, 6(9):e24642, 2011.

[65] D. Leijen and E. Meijer. Domain specific embedded compilers. In *Proc. Conference on Domain-Specific Languages*, DSL'99, pages 9–9, Berkeley, CA, 1999. USENIX.

[66] J. Leskovec, D. Chakrabarti, J. Kleinberg, and C. Faloutsos. Realistic, Mathematically Tractable Graph Generation and Evolution, Using Kronecker Multiplication. In *PKDD*, pages 133–145. Springer, 2005.

[67] J. Leskovec, D. Chakrabarti, J. Kleinberg, and C. Faloutsos. Realistic, Mathematically Tractable Graph Generation and Evolution, Using Kronecker Multiplication. In *PKDD*, pages 133–145, 2005.

[68] X. Li, J. Demmel, J. Gilbert, L. Grigori, and M. Shao. *SuperLU Users' Guide*, 2010.

[69] Y. Low, J. Gonzalez, A. Kyrola, D. Bickson, C. Guestrin, and J. Hellerstein. GraphLab: A New Parallel Framework for Machine Learning. In *Conference on Uncertainty in Artificial Intelligence (UAI)*, Catalina Island, California, July 2010.

[70] M. Luby. A simple parallel algorithm for the maximal independent set problem. In *Proc. ACM symposium on Theory of computing*, STOC '85, pages 1–10, New York, NY, 1985. ACM.

[71] M. Luby. A simple parallel algorithm for the maximal independent set problem. *SIAM journal on computing*, 15(4):1036–1053, 1986.

[72] A. Lugowski, D. Alber, A. Buluç, J. R. Gilbert, S. Reinhardt, Y. Teng, and A. Waranis. A flexible open-source toolbox for scalable complex graph analysis. In *Proceedings of the Twelfth SIAM International Conference on Data Mining (SDM12)*, pages 930–941, April 2012.

[73] A. Lugowski, A. Buluç, J. Gilbert, and S. Reinhardt. Scalable complex graph analysis with the knowledge discovery toolbox. In *International Conference on Acoustics, Speech, and Signal Processing (ICASSP)*, 2012.

[74] A. Lugowski, A. Buluç, J. Gilbert, and S. Reinhardt. Scalable Complex Graph Analysis with the Knowledge Discovery Toolbox. In *Int. Conference on Acoustics, Speech, and Signal Processing*, 2012.

[75] A. Lugowski and J. R. Gilbert. Efficient sparse matrix-matrix multiplication on multicore architectures. Technical Report UCSB/CS-2014-04, Computer Science Dept., University of California, Santa Barbara, May 2014.

[76] A. Lugowski and J. R. Gilbert. Efficient sparse matrix-matrix multiplication on multicore architectures. In *SIAM Workshop on Combinatorial Scientific Computing (CSC14)*, July 2014.

[77] A. Lugowski, S. Kamil, A. Buluç, S. Williams, E. Duriakova, L. Oliker, A. Fox, and J. R. Gilbert. Parallel processing of filtered queries in attributed semantic graphs. *Journal of Parallel and Distributed Computing (JPDC)*, Accepted.

[78] G. Malewicz, M. Austern, A. Bik, J. Dehnert, I. Horn, N. Leiser, and G. Czajkowski. Pregel: A System for Large-Scale Graph Processing. In *Proceedings of the 2010 International Conference on Management of Data*, SIGMOD '10, pages 135–146, New York, NY, USA, 2010. ACM.

[79] K. Maschho and D. Sorensen. A portable implementation of ARPACK for distributed memory parallel architectures. In *Proceedings of the Copper Mountain Conference on Iterative Methods*, pages 9–13, April 1996.

[80] M. Matsumoto and T. Nishimura. Mersenne twister: a 623-dimensionally equidistributed uniform pseudo-random number generator. *ACM Transactions on Modeling and Computer Simulation (TOMACS)*, 8(1):3–30, 1998.

[81] J. D. McCalpin. STREAM: Sustainable Memory Bandwidth in High Performance Computers. http://www.cs.virginia.edu/stream/.

[82] J. McPherson, K.-L. Ma, and M. Ogawa. Discovering Parametric Clusters in Social Small-World Graphs. In *Proceedings of the 2005 ACM symposium on Applied computing*, SAC '05, pages 1231–1238, New York, NY, USA, 2005. ACM.

[83] H. Meuer, E. Strohmaier, J. Dongarra, and H. Simon. Top500 supercomputer sites. In *Proc. SC2001*, pages 10–16, 2001. http://www.top500.org.

[84] A. Meyer-Lindenberg. From maps to mechanisms through neuroimaging of schizophrenia. *Nature*, 468(7321):194–202, 2010.

[85] G. M. Morton. A computer oriented geodetic data base and a new technique in file sequencing. Technical report, IBM, Ottawa, Canada, 1966.

[86] M. Najork and J. L. Wiener. Breadth-First Search Crawling Yields High-Quality Pages. In *Proceedings of the 10th International Conference on World Wide Web*, WWW '01, pages 114–118, New York, NY, USA, 2001. ACM.

[87] J. O'Madadhain, D. Fisher, P. Smyth, S. White, and Y.-B. Boey. Analysis and visualization of network data using jung. *Journal of Statistical Software*, 10(2):1–35, 2005.

[88] L. Page, S. Brin, R. Motwani, and T. Winograd. The PageRank Citation Ranking: Bringing Order to the Web. Technical Report 1999-66, Stanford InfoLab, November 1999. Previous number = SIDL-WP-1999-0120.

[89] A. Petróczi, T. Nepusz, and F. Bazsó. Measuring tie-strength in virtual social networks. *CONNECTIONS - the official journal of the International Network for Social Network Analysis*, 27(2):49–57, 2006.

[90] C. Pheatt. Intel threading building blocks. *J. Comput. Sci. Coll.*, 23(4):298–298, Apr. 2008.

[91] E. Prud'hommeaux and A. Seaborne. SPARQL query language for RDF (working draft). Technical report, W3C, March 2007.

[92] U. N. Raghavan, R. Albert, and S. Kumara. Near linear time algorithm to detect community structures in large-scale networks. *Physical Review E - Statistical, Nonlinear and Soft Matter Physics*, 76(3 Pt 2):036106, 2007.

[93] M. Redekopp, Y. Simmhan, and V. Prasanna. Optimizations and analysis of bsp graph processing models on public clouds. In *27th IEEE International Symposium on Parallel Distributed Processing (IPDPS)*, pages 203–214, 2013.

[94] S. Salihoglu and J. Widom. Gps: a graph processing system. In *SSDBM*, page 22, 2013.

[95] H. Samet. The quadtree and related hierarchical data structures. *Computing Surveys*, 16(2):187–260, 1984.

[96] C. Seshadhri, T. G. Kolda, and A. Pinar. Community Structure and Scale-Free Collections of Erdös-Rényi Graphs. *Phys. Rev. E*, 85:056109, May 2012.

[97] V. B. Shah. *An Interactive System for Combinatorial Scientific Computing with an Emphasis on Programmer Productivity.* PhD thesis, University of California, Santa Barbara, June 2007.

[98] Y. Shapira. *Matrix-based Multigrid: Theory and Applications.* Springer, 2003.

[99] J. Shun and G. E. Blelloch. Ligra: A lightweight graph processing framework for shared memory. *SIGPLAN Not.*, 48(8):135–146, Feb. 2013.

[100] J. Siek, A. Lumsdaine, and L. Lee. Boost Graph Library, 2001. http://www.boost.org/libs/graph/doc/index.html.

[101] R. Techentin, D. Foti, S. Al-Saffar, P. Li, E. Daniel, B. Gilbert, and D. Holmes. Characterization of a semi-synthetic dataset for big-data semantic analysis. In *18th IEEE High Performance Extreme Computing Conference (HPEC 2014) (to appear)*, 2014.

[102] R. W. Techentin, B. K. Gilbert, A. Lugowski, K. Deweese, J. R. Gilbert, E. Dull, M. Hinchey, and S. P. Reinhardt. Implementing iterative algorithms with sparql. In *EDBT/ICDT Workshops*, pages 216–223, 2014.

[103] Titan Informatics Toolkit. http://titan.sandia.gov.

[104] R. A. Van De Geijn and J. Watts. Summa: Scalable universal matrix multiplication algorithm. *Concurrency: Practice and Experience*, 9(4):255–274, 1997.

[105] S. van Dongen. Graph Clustering via a Discrete Uncoupling Process. *SIAM J. Matrix Anal. Appl*, 30(1):121–141, 2008.

[106] Y. J. Wang and G. Y. Wong. Stochastic blockmodels for directed graphs. *Journal of the American Statistical Association*, 82(397):8–19, 1987.

[107] S. Williams, A. Waterman, and D. Patterson. Roofline: an insightful visual performance model for multicore architectures. *Communications of the ACM*, 52(4):65–76, 2009.

[108] D. S. Wise. Representing matrices as quadtrees for parallel processors: Extended abstract. *SIGSAM Bull.*, 18(3):24–25, Aug. 1984.

[109] D. S. Wise and J. Franco. Costs of quadtree representation of nondense matrices. *Journal of Parallel and Distributed Computing*, 9(3):282 – 296, 1990.

[110] D. S. Wise, J. D. Frens, Y. Gu, and G. A. Alexander. Language support for Morton-order matrices. *SIGPLAN Not.*, 36(7):24–33, June 2001.

[111] J. Yang and J. Leskovec. Patterns of temporal variation in online media. In *Proc. ACM Int. Conference on Web search and Data Mining*, WSDM '11, pages 177–186, New York, NY, USA, 2011. ACM.

[112] YarcData LLC, a Cray Company. Urika graph-analytic appliance, 2014.

[113] J. Yedidia, W. Freeman, and Y. Weiss. Understanding Belief Propagation and its Generalizations. *Exploring artificial intelligence in the new millennium*, 8:236–239, 2003.

Appendices

Appendix A

QuadMat Experimental Data

...

Table A.1: The Problems - Matrix Squares. Colors in the visual representation of nonzero distribution indicate density. Green and red hues represent more nonzeros. All matrices here and in Table A.2 share the same color scale.

Name	Factors	Product	Non-Zero Arithmetic Ops.
ER_18_sq	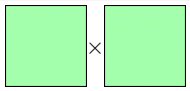 $262K \times 262K$, $nnz = 8.39M$ $262K \times 262K$, $nnz = 8.39M$	$262K \times 262K$ $nnz = 268M$	$269M$
ER_20_sq	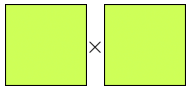 $1.05M \times 1.05M$, $nnz = 33.6M$ $1.05M \times 1.05M$, $nnz = 33.6M$	$1.05M \times 1.05M$ $nnz = 1.07G$	$1.07G$
rmat_16_sq	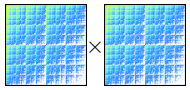 $65.5K \times 65.5K$, $nnz = 1.83M$ $65.5K \times 65.5K$, $nnz = 1.83M$	$65.5K \times 65.5K$ $nnz = 365M$	$2.15G$
rmat_16RP_sq	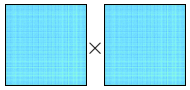 $65.5K \times 65.5K$, $nnz = 1.83M$ $65.5K \times 65.5K$, $nnz = 1.83M$	$65.5K \times 65.5K$ $nnz = 365M$	$2.15G$
rmat_18_sq	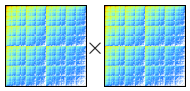 $262K \times 262K$, $nnz = 7.65M$ $262K \times 262K$, $nnz = 7.65M$	$262K \times 262K$ $nnz = 3.04G$	$16.1G$
rmat_18RP_sq	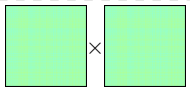 $262K \times 262K$, $nnz = 7.65M$ $262K \times 262K$, $nnz = 7.65M$	$262K \times 262K$ $nnz = 3.04G$	$16.1G$
torus3D_150_sq	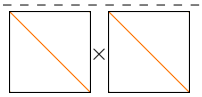 $3.38M \times 3.38M$, $nnz = 23.6M$ $3.38M \times 3.38M$, $nnz = 23.6M$	$3.38M \times 3.38M$ $nnz = 84.4M$	$246M$
torus3D_150RP_sq	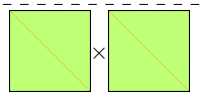 $3.38M \times 3.38M$, $nnz = 23.6M$ $3.38M \times 3.38M$, $nnz = 23.6M$	$3.38M \times 3.38M$ $nnz = 84.4M$	$246M$
torus3D_200_sq	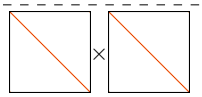 $8.00M \times 8.00M$, $nnz = 56.0M$ $8.00M \times 8.00M$, $nnz = 56.0M$	$8.00M \times 8.00M$ $nnz = 200M$	$584M$
torus3D_200RP_sq	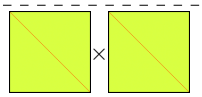 $8.00M \times 8.00M$, $nnz = 56.0M$ $8.00M \times 8.00M$, $nnz = 56.0M$	$8.00M \times 8.00M$ $nnz = 200M$	$584M$

Table A.2: The Problems - Algebraic Multigrid Contractions, Permutations, and Submatrix Extractions. Colors in the visual representation of nonzero distribution indicate density. Green and red hues represent more nonzeros. All matrices here and in Table A.1 share the same color scale.

Name	Factors	Product	Non-Zero Arithmetic Ops.
AMG_150_cont	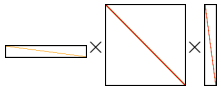 $422K \times 3.38M$, $nnz = 3.38M$ $3.38M \times 3.38M$, $nnz = 90.7M$ $3.38M \times 422K$, $nnz = 26.8M$	$422K \times 422K$ $nnz = 11.4M$	$571M$
AMG_200_cont	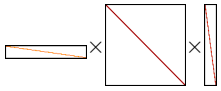 $1.00M \times 8.00M$, $nnz = 8.00M$ $8.00M \times 8.00M$, $nnz = 215M$ $8.00M \times 1.00M$, $nnz = 63.7M$	$1.00M \times 1.00M$ $nnz = 27.1M$	$1.36G$
ER_20_perm	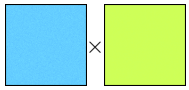 $1.05M \times 1.05M$, $nnz = 1.05M$ $1.05M \times 1.05M$, $nnz = 33.6M$	$1.05M \times 1.05M$ $nnz = 33.6M$	$33.6M$
rmat_18_perm	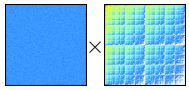 $262K \times 262K$, $nnz = 262K$ $262K \times 262K$, $nnz = 7.65M$	$262K \times 262K$ $nnz = 7.65M$	$7.65M$
rmat_18RP_perm	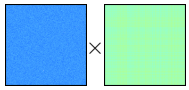 $262K \times 262K$, $nnz = 262K$ $262K \times 262K$, $nnz = 7.65M$	$262K \times 262K$ $nnz = 7.65M$	$7.65M$
torus3D_200_perm	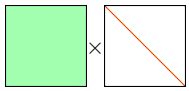 $8.00M \times 8.00M$, $nnz = 8.00M$ $8.00M \times 8.00M$, $nnz = 56.0M$	$8.00M \times 8.00M$ $nnz = 56.0M$	$56.0M$
torus3D_200RP_perm	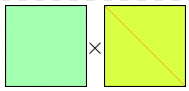 $8.00M \times 8.00M$, $nnz = 8.00M$ $8.00M \times 8.00M$, $nnz = 56.0M$	$8.00M \times 8.00M$ $nnz = 56.0M$	$56.0M$
ER_20_sub	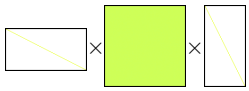 $524K \times 1.05M$, $nnz = 524K$ $1.05M \times 1.05M$, $nnz = 33.6M$ $1.05M \times 524K$, $nnz = 524K$	$524K \times 524K$ $nnz = 8.39M$	$25.2M$
rmat_18_sub	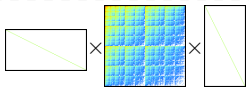 $131K \times 262K$, $nnz = 131K$ $262K \times 262K$, $nnz = 7.65M$ $262K \times 131K$, $nnz = 131K$	$131K \times 131K$ $nnz = 4.24M$	$9.98M$
rmat_18RP_sub	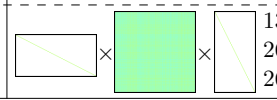 $131K \times 262K$, $nnz = 131K$ $262K \times 262K$, $nnz = 7.65M$ $262K \times 131K$, $nnz = 131K$	$131K \times 131K$ $nnz = 1.88M$	$5.67M$

Table A.3: Matrix Square elapsed time in seconds, mean of 5 runs. The machine has 40 cores capable of 80 concurrent threads.

		ER_18_sq	ER_20_sq	rmat_16_sq	rmat_16RP_sq	rmat_18_sq	rmat_18RP_sq	torus3D_150_sq	torus3D_150RP_sq	torus3D_200_sq	torus3D_200RP_sq
CSparse	1p	9.20	56.2	12.4	14.6	115.	131.	1.43	11.4	4.37	29.4
CombBLAS	1p	59.7	255.	158.	161.			29.6	45.5	74.2	109.
	4p	16.7	73.4	84.1	42.9		418.	15.8	15.5	39.8	39.4
	9p	8.39	35.0	65.4	20.0	577.	161.	10.6	9.16	27.2	23.8
	16p	4.97	20.7	41.4	12.0	355.	121.	16.7	6.71	43.4	17.2
	25p	3.82	15.9	40.2	8.23	342.	67.9	6.73	5.55	18.2	14.0
	36p	3.08	13.0	35.7	6.32	309.	76.8	18.3	4.80	47.9	12.0
	64p	2.65	11.0	30.8	4.99	297.	117.	23.5	4.68	62.5	11.8
QuadMat	1p	21.4	126.	29.8	23.7	244.	204.	4.88	138.	11.9	516.
	2p	12.5	73.1	15.3	13.3	138.	117.	2.89	80.6	6.82	282.
	4p	6.21	36.0	7.80	6.80	69.5	58.9	1.51	42.2	3.51	150.
	9p	3.20	21.5	3.75	3.40	34.0	26.8	.823	23.3	1.81	76.8
	16p	2.25	14.6	2.49	2.05	21.3	15.8	.672	15.1	1.25	45.6
	25p	1.86	11.0	2.23	1.59	16.7	11.1	.624	10.7	1.16	30.9
	36p	1.73	8.57	2.26	1.42	15.5	8.71	.652	7.64	1.13	23.0
	64p	1.46	6.79	1.81	1.15	12.8	7.17	.636	5.74	1.29	17.3
	80p	1.40	6.55	1.61	1.22	11.0	7.31	.653	5.12	1.08	16.5

Table A.4: Algebraic Multigrid Contraction, Permutation, and Submatrix Extraction elapsed time in seconds, mean of 5 runs. The machine has 40 cores capable of 80 concurrent threads.

		AMG_150_cont	AMG_200_cont	ER_20_perm	rmat_18_perm	rmat_18RP_perm	torus3D_200_perm	torus3D_200RP_perm	ER_20_sub	rmat_18_sub	rmat_18RP_sub
CSparse	1p	2.69	6.99	5.40	.583	.681	3.99	17.3	2.69	.503	.452
CombBLAS	1p	75.1	185.	31.9	5.31	5.32	30.0	55.3	22.5	5.29	4.22
	4p	44.5	94.0	7.35	2.55	1.62	12.2	14.3	7.02	2.84	1.22
	9p	29.3	74.3	3.25	1.86	.873	8.83	6.98	3.93	2.61	.686
	16p	29.4	55.9	1.91	1.16	.535	7.24	4.35	2.81	1.82	.456
	25p	21.8	53.5	1.41	1.09	.435	6.51	3.29	2.21	1.85	.382
	36p	21.8	59.8	1.14	.965	.356	6.00	2.77	1.83	1.77	.322
	64p	30.8	59.3	.958	.758	.290	6.37	2.74	1.85	1.53	.323
QuadMat	1p	8.30	19.1	24.5	22.0	3.04	99.0	347.	3.63	1.17	.622
	2p	4.45	10.7	13.7	11.7	1.53	52.8	203.	2.06	.616	.331
	4p	2.35	5.44	6.97	6.11	.788	26.8	105.	1.06	.327	.179
	9p	1.35	2.78	4.21	2.92	.413	12.4	55.9	.535	.170	.0996
	16p	1.14	2.94	4.09	1.81	.281	7.70	34.5	.359	.125	.0688
	25p	1.19	2.29	3.13	1.29	.223	6.01	23.8	.322	.113	.0662
	36p	1.11	2.58	2.52	1.14	.206	5.21	17.9	.311	.118	.0734
	64p	.982	2.61	1.98	1.69	.244	5.39	12.9	.314	.125	.0805
	80p	1.25	2.64	1.90	2.11	.241	5.53	12.2	.342	.134	.0896

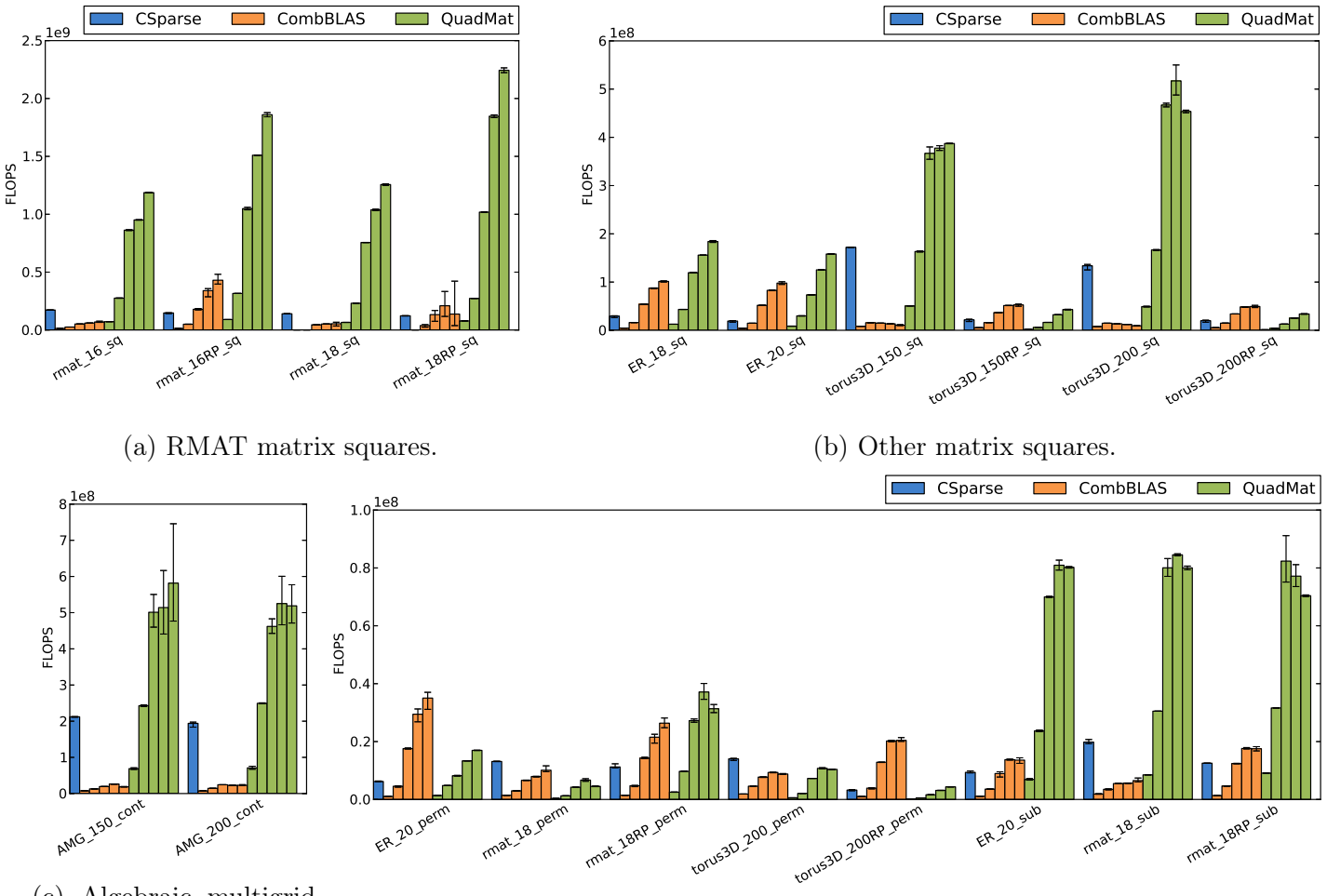

(a) RMAT matrix squares.

(b) Other matrix squares.

(c) Algebraic multigrid contractions.

(d) Permutations and submatrix extractions.

Figure A.1: FLOPS, or nonzero arithmetic operations per second, for each of the problems listed in Tables A.1 and A.2. Each set of five CombBLAS and QuadMat bars correspond to 1, 4, 16, 36 and 64 threads, while the CSparse bar is a single thread. The machine has 40 cores capable of 80 concurrent threads. The height of each bar indicates the mean of 5 runs; the error bars mark the fastest and slowest runs.

Table A.5: Problem statistics extracted using an instrumented build of QuadMat run with one thread. Detailed analysis of this data is in Sections 5.5.3 and 5.5.3. The division threshold is chosen to balance parallelism with minimization of total block count (reduce hypersparse blocks). The same *very preliminary* choice algorithm is used for all problems. Relatively poor QuadMat performance on some problems is explained by two factors. Poor scaling can be due to insufficient potential parallelism (threshold too large). Poor computational performance (torus squares, all permutations and submatrix extractions) is due to low A organizer lookup utility (threshold too small).

	ER_18_sq	ER_20_sq	rmat_16_sq	rmat_16RP_sq	rmat_18_sq	rmat_18RP_sq	torus3D_150_sq	torus3D_150RP_sq	torus3D_200_sq	torus3D_200RP_sq
Block Division Threshold	104850	419424	50000	50000	95639	95639	295312	295312	700000	700000
Total Comp. Tasks (Work)	21.7s	122s	26.1s	25.2s	236s	202s	4.85s	133s	11.6s	471s
Max Comp. Task (Span)	0.0971s	0.634s	0.224s	0.437s	0.867s	0.948s	0.031s	0.315s	0.0621s	0.893s
Potential Parallelism	223.7	191.8	116.3	57.8	271.8	213.2	156.3	423.2	186.0	527.1
A Organizer Lookups	1.34×10^8	5.37×10^8	8.06×10^7	1.46×10^7	6.33×10^8	1.22×10^8	7.53×10^7	6.14×10^8	1.78×10^8	1.74×10^9
Hits	86.5%	86.5%	69.6%	96.3%	63.4%	93.7%	74.5%	24%	69.7%	20.5%
A nnz / Hit	2.31	2.31	22.4	89.1	23.9	83.3	2.95	1.12	3.15	1.1
A nnz / Lookup	2	2	15.6	85.7	15.1	78.1	2.2	0.269	2.2	0.226

	AMG_150_cont	AMG_200_cont	ER_20_perm	rmat_18_perm	rmat_18RP_perm	torus3D_200_perm	torus3D_200RP_perm	ER_20_sub	rmat_18_sub	rmat_18RP_sub
Block Division Threshold	1133988	2690984	419424	95639	95639	700000	700000	419424	95639	95639
Total Comp. Tasks (Work)	6.29s	15.3s	23s	17.6s	2.9s	86.6s	339s	3.34s	0.912s	0.615s
Max Comp. Task (Span)	0.215s	0.45s	0.114s	0.0226s	0.0284s	0.0177s	0.401s	0.0108s	0.0045s	0.00319s
Potential Parallelism	29.2	33.9	201.1	780.7	102.1	4906.9	846.7	310.0	202.8	192.6
A Organizer Lookups	3.94×10^7	9.5×10^7	5.37×10^8	6.09×10^8	1.22×10^8	6.89×10^9	1.73×10^9	4.19×10^6	4.65×10^6	1.05×10^6
Hits	79.3%	77.3%	6.25%	1.26%	6.25%	0.813%	3.23%	86.5%	18%	28.3%
A nnz / Hit	6.85	6.92	1	1	1	1	1	2.31	5.08	6.32
A nnz / Lookup	5.43	5.35	0.0625	0.0126	0.0625	0.00813	0.0323	2	0.912	1.79

Appendix B

Systems

The experimental results presented in this work have been conducted on several machines. They are described here.

B.1 Neumann

Neumann is a shared memory machine composed of eight quad-core AMD Opteron 8378 processors. 16 GB of DRAM is attached to each socket, for a total of 128 GB in a NUMA arrangement.

Neumann is the CSC lab machine and is located at UCSB.

B.2 Mirasol

Mirasol is a single node platform composed of four Intel Xeon E7-8870 processors. Each socket has ten cores running at 2.4 GHz, and supports two-way simultaneous multithreading (20 thread contexts per socket). The cores are connected to a 30 MB L3 cache via a ring architecture. The sustained stream bandwidth is about 30 GB/s per socket. The machine has 256 GB 1067 MHz DDR3 RAM.

Mirasol is located at Georgia Tech.

B.3 Hopper

Hopper is a Cray XE6 massively parallel processing (MPP) system, built from dual-socket 12-core "Magny-Cours" Opteron compute nodes. In reality, each socket (multichip module) has two 6-core chips, and so a node can be viewed as a four-chip compute configuration with strong NUMA properties. Each Opteron

chip contains six super-scalar, out-of-order cores capable of completing one (dual-slot) SIMD add and one SIMD multiply per cycle. Additionally, each core has private 64 KB L1 and 512 KB low-latency L2 caches. The six cores on a chip share a 6MB L3 cache and dual DDR3-1333 memory controllers capable of providing an average STREAM[81] bandwidth of 12GB/s per chip. Each pair of compute nodes shares one Gemini network chip, which collectively form a 3D torus.

Hopper is located at NERSC.

B.4 Carver

Carver is an IBM iDataPlex system with 400 compute nodes, each node having two quad-core Intel Nehalem processors. The interconnect is Infiniband.

Carver is located at NERSC.